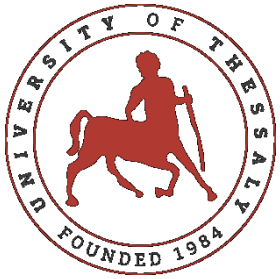

University of Thessaly

School of Engineering

Department of Mechanical Engineering

Experimental Investigation of Spray Characteristics in Crossflow

Charalampous Konstantinos

Submitted in partial fulfilment of the requirements for the Diploma of Mechanical Engineering

Volos 2021

Thesis Committee

1st Examiner (Supervisor): Assistant Professor Charalampous Georgios

Department of Mechanical Engineering, University of Thessaly

2nd Examiner: Professor Pelekasis Nikolaos

Department of Mechanical Engineering, University of Thessaly

3rd Examiner: Professor Stamatelos Anastasios

Department of Mechanical Engineering, University of Thessaly

Abstract

In the current experimental investigation, an effort was made to study the behaviour of a spray which was produced by a twin-fluid air assist atomizer. The spray is injected into a uniform crossflow airstream. The dominant parameters are the liquid Reynolds number Re, the aerodynamic Weber We, the gas to liquid momentum ratio Q and the gas to liquid mass flow ratio q. These parameters ranged Re=1082-2235, We=0-0.66, $Q=4.24\cdot10^{-4}$-$163\cdot10^{-4}$ and q=0.22-0.51. The images were captured by a camera and shadowgraphy method is employed to characterize the atomization process and measure the main characteristics of a liquid jet/spray. The main characteristics that are of interest are the trajectory of a jet and the column break-up location. A power law function is good approach to predict the trajectory of a jet at low aerodynamic Weber numbers. Moreover, the spray cone angles were measured. In this study is shown that a power law function can effectively describe the behaviour of spray cone angle under various conditions.

Acknowledgements

The following thesis was elaborated in the scope of partial fulfilment of the requirements for the Diploma of the Mechanical Engineer at the University of Thessaly. It is worth mentioning that the aid and support of some people during this work was remarkable.

First and foremost, I would like to express my sincere gratitude to my supervisor Assistant Professor Dr. Georgios Charalampous for giving me this opportunity to do the current project on the topic of liquid injection into a crossflow airstream. His continuous support, patience, motivation and suggestions not only helped me overcome every difficulty that has come up during the experimental investigation but also his constant guidance through the experimental techniques and the proper writing of this thesis was of immense significance. During this thesis, my supervisor helped me learn so many new things and I am really grateful to him for the extensive amount of knowledge that he has transmitted to me.

Besides my supervisor, I would also like to thank the members of the Thesis committee, Professor Dr. Pelekasis Nikolaos and Professor Dr. Stamatelos Anastasios for their valuable advice and inspiring discussions.

Last but not the least, I would like to thank my family for supporting me during the whole period of my studies. I am really thankful to them for their spiritual support throughout writing this thesis.

Charalampous Konstantinos

July 2021, Volos

Table of Contents

List of Figures

List of Tables

Nomenclature

D	Droplet diameter	m
Re	Reynolds number	$-$
We	Weber number	$-$
Oh	Ohnesorge number	$-$
Q	Momentum Ratio	$-$
MFR	Momentum Flux Ratio	$-$
G	Mass Flux	$\frac{kg}{m^2 s}$
U	Average Velocity	$\frac{m}{s}$
V_D	Drop volume	m^3
ΔP	Pressure Differential	$-$
m_D	Mass of drop	kg
g	Gravity	$\frac{m}{s^2}$
σ	Surface tension	$\frac{N}{m}$
ρ_i	Density	$\frac{kg}{m^3}$
μ	Dynamic Viscosity	$\frac{kg}{m*s}$
p_I	Internal pressure of drop	$\frac{N}{m^2}$
p_a	External aerodynamic pressure	$\frac{N}{m^2}$
p_σ	Surface tension pressure	$\frac{N}{m^2}$
C_D	Drag Coefficient of Drop	$-$
L	Characteristic Length	m

$\dot{v}, \dot{Q}$	Flowrate	$\frac{m^3}{s}$
d_o	Orifice Diameter	m
θ	Angular location of the sampling tubes	rad
y	Liquid volume within the Sampling Tube	m^3
$\dot{m}_i$	Mass flow	$\frac{kg}{s}$
q	Mass flow Ratio	$-$

Subscripts

a, g	air, gas
l	liquid
R	Relative
k	Left or Right angle

1. Introduction

1.1 General Considerations and Applications

Atomization refers to the transformation process of a liquid bulk into a multiplicity of small drops in a gaseous atmosphere, where a spray can be formed. In this process, the liquid bulk (it can be a liquid jet or sheet) can be disintegrated by the kinetic energy of the liquid or when the liquid bulk is exposed to a gas of high-velocity. Several industrial processes use the concept of atomization. Atomization is found to be applicable in many applications such as agriculture, medicine and meteorology. For example, atomization is commonly used when chemicals are applied to crops, paint spraying or spray drying of wet solids applications. Moreover, the atomization process can be useful in many applications such as cooling of various systems including nuclear cores, gas-liquid mass transfer applications or by injecting fuels for combustion, consumer sprays (including medical sprays). There is large variety of apparatuses used in atomization which are mainly called as nozzles or atomizers. Each atomizer produces different spray characteristics that may be important or not, depending on the application. Typical characteristics of a spray are illustrated in Figure 1.1. Effective atomization is necessary in combustion applications such as the fuel injection in internal combustion engines, gas turbines or even rocket engines. For example, in combustion systems when the mean fuel drop size is reduced, then is likely to lead to higher volumetric heat release rates, easier light up, wider burning range and emit less pollutants (Sharma, Bachalo and Agarwal, 2020).

A spray can be produced with several methods. Numerous basic processes are related with the methods of atomization, for instance, the flow within the atomizer that controls the turbulence properties of the liquid that flows through the outer orifice. The development of the jet and the growth of small disturbances that lead to the disintegration of the jet should be also considered when the shape and penetration of the spray are to be determined. Additionally, spray characteristics such as drop size, velocity, number density are also crucial parameters for determining the spray structure (Dumouchel, 2008). Moreover, several parameters influence the spray characteristics such as the internal geometry of the atomizer, the properties of the gaseous atmosphere where the liquid discharges and the properties of the liquid Figure 1.1. Most commonly, a spray includes a wide spread of drop sizes and the knowledge of drop size distribution may be supportive enough to evaluate the process in spray applications. However, specifying drop size distributions and mean drop size can be difficult. These parameters can be predicted though with empirical correlations as a complete theory hasn't been developed yet to describe precisely the hydrodynamic and aerodynamic processes that are involved. The atomization process divides in two main processes which are referred as the primary

and secondary atomization. During primary atomization, the emerging liquid bulk is broken up into shreds and ligaments, while in secondary atomization, these ligaments are further disintegrated to drops of smaller size. The detailed characteristics of a liquid spray can be determined by these two processes.(Lefebvre and Ballal, 1988, p. 221).

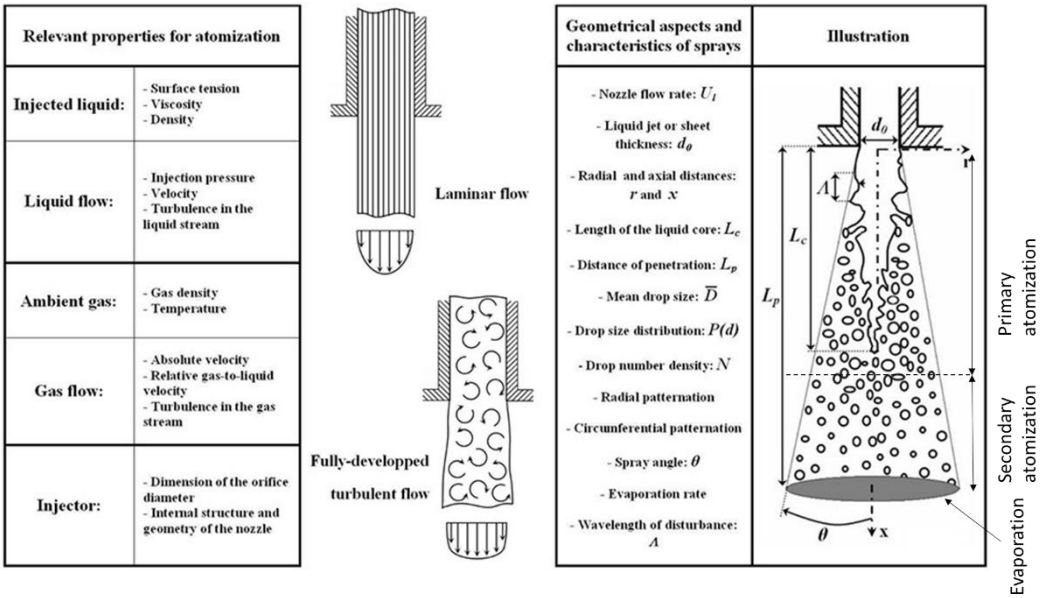

Figure 1.1 Simple spray and features that need to be characterized https://spray-imaging.com/spray-description.html

1.2 Atomizers

An atomizer is an apparatus that reduces a liquid to a fine spray and this can be accomplished if the relative velocity between the dispersed and the continuous phase is high enough. Dispersed phase refers to the liquid to be atomized, while continuous phase to the ambient gas. Each atomizer produces a spray in a unique way. Several forms of pressure and rotary atomizers atomize a liquid by discharging it at high-velocity into a relatively slow-moving airstream. On the other hand, atomization can be also accomplished by discharging the liquid in relative slow velocity to a high-velocity gas stream. The latter method, is also known as twin-fluid air-assist or air-blast atomization. An ideal atomizer possesses some specific features. First, the ability to provide the necessary atomization in a wide range of operating conditions, a variety of liquid flowrates, quick response in liquid flow rate change (e.g. ICE-large fuel flowrate at high rpms) and low power requirements (Lefebvre and Ballal, 1988). The design of an atomizer varies on application, as each one of them requires different spray characteristics (e.g. specific flow pattern, uniform drop size distribution and drop-velocity distribution) (Dumouchel, 2008; Ashgriz, 2011). The most commonly used atomizers are pressure, rotary and twin-fluid atomizers Figure 1.2. Each atomizer generates drops of a different size and therefore the atomization quality, can be described in the matter of mean drop size. Usually, mean drop size can be described with empirical correlations (most widespread is Sauter mean diameter) which relate the mean drop size and the variables of the atomization such as the liquid and gas properties, flow condition, atomizer geometry. It could be very handy, if for each atomizer to be able to provide an estimation of atomization quality for varying operating conditions and liquid properties. The liquid properties that are of prime importance in atomization are surface tension, viscosity and density while for the gas phase dominant property is gas density. The important flow variables of the dispersed phase are the velocity of the jet but also the turbulence within. For the gas flow, the important flow variables are its absolute velocity and the relative velocity between the gas and liquid. Last but not least, geometric variables of each atomizer affect the mean drop size and therefore atomization quality. For example, length and orifice diameter of plain-orifice injector are the main variables that are of concern, or final orifice diameter for pressure-swirl atomizers. For the pre-filming type air-blast atomizers mean drop size is mainly influenced from the pre-filmer diameter and the hydraulic diameter of the outer orifice. With rotary atomizers the rotating disk or cup diameter is mainly the most important dimension. Generally, for twin-fluid injectors the mass ratio of liquid to gas flows is a relevant parameter too.

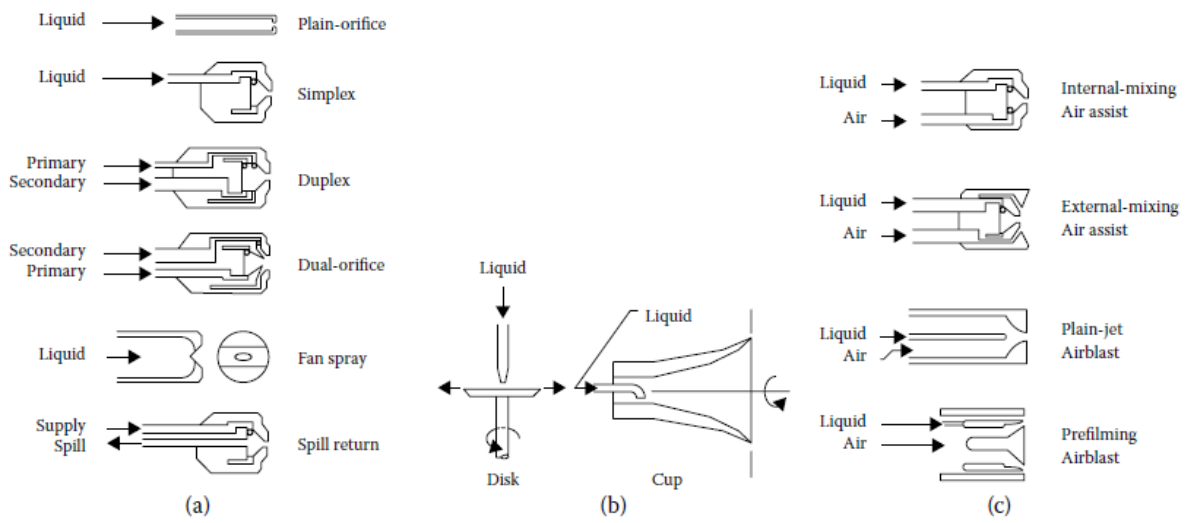

Figure 1.2 Types of atomizers: (a) Pressure atomizers, (b) rotary atomizers, (c) twin-fluid atomizers (Lefebvre and Mcdonell, 2017)

1.2.1 Pressure atomizers

There is a variety of pressure atomizers. The dominant atomizers in this category are the plain-orifice, simplex, duplex, dual orifice and spill return atomizers which took their name mainly from their geometry Figure 1.3 (Lefebvre and Ballal, 1988). By definition, pressure atomizers discharge the liquid under high pressures, therefore the pressure energy is converted to kinetic energy $\Delta P \sim U^2$ (Lefebvre and Mcdonell, 2017; Sun, Guan and Hooman, 2019).

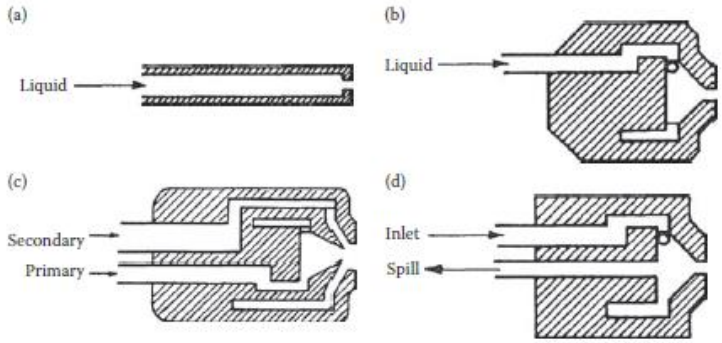

Figure 1.3 Pressure-swirl atomizers (a)plain orifice (b) simplex (c) dual orifice (d) spill return (Lefebvre and Ballal, 1988)

Plain orifice atomizer

A plain orifice atomizer, consists of a circular orifice through which liquid is ejected. It is commonly used in combustion applications. When the injection velocity is low, the liquid emerges as a thin solid jet. In order to obtain a spray, the pressure differential across the nozzle needs to exceed about

ΔP=150kPa (Lefebvre and Mcdonell, 2017, p. 72), otherwise a solid liquid jet will emerge. Atomization is facilitated by increased injection velocity which increases the turbulence of the jet, promoting aerodynamic drag while increased liquid viscosity and surface tension oppose atomization. Plain orifice atomizers produce a spray with a cone angle $5° - 15°$ where geometry slightly affects spray angle. The liquid properties and the flow state are variables that strongly affect the spray angle are viscosity, surface tension and the turbulence of the jet. Flow within this type of atomizer is similar with a pipe and its directly related with Reynolds number. Moreover, as function of Reynolds number, the discharge coefficient can be described as it is different for low and high Reynolds number (Lefebvre and Mcdonell, 2017, p. 106). The dispersion of a spray is observed when the Reynolds number reaches a certain value and this may attribute to the flow transition from laminar to turbulent within the atomizer. As a result, jet was disrupted rapidly (Schweitzer, 1937). The critical Reynolds number lies between 2000-3000 and relates the transition of the flow from laminar to turbulent. The flow tends to be laminar for values lower than 2000 and turbulent if a critical value is exceeded. In general, Reynolds number is associated with many parameters and the critical value cannot be precisely defined. Parameters that affect flow condition are shown below.

In general, laminar flow is promoted by the following:

1. A rounded entrance to the orifice
2. Smooth passage walls
3. Absence of bends
4. High liquid viscosity
5. Low liquid velocity

Turbulent flow is promoted by the following:

1. Large passage diameters
2. Changes in flow velocity and direction
3. Abrupt changes in cross-sectional area
4. Surface roughness
5. Imperfections in atomizer geometry
6. Mechanical vibrations
7. Low liquid viscosity
8. High liquid velocity

Generally, the good atomization is promoted by turbulent flow but inevitability this leads to an increased loss of pressure. In fact, the performance of the plain-orifice atomizer is a function of several parameters.

Another parameter that should be also concerned is the discharge coefficient. The discharge coefficient describes the ratio of the actual flowrate to the theoretical Equation 1. Factors that affect this coefficient are the Reynolds number, length to diameter ratio, injection pressure differential, gaseous medium pressure, inlet chamfer and cavitation.

$$C_d = \frac{\dot{m}_l}{2\rho_l \Delta P} \quad \text{Equation 1}$$

Generally, if the flow within the atomizer is laminar, then the discharge coefficient increases proportionally with Reynolds number. As the flow passes from laminar to the semi-turbulent region, this coefficient reaches a peak and then declines. As far as the turbulent region is concerned, the discharge coefficient remains steady. In Figure 1.4 the influence of the Reynolds number on the discharge coefficient is described. The length to diameter ratio Figure 1.5 is another parameter that influences the discharge coefficient. If this ratio is sufficiently low then the coefficient is also low because the vena contracta effect takes place. In this situation the distance within the atomizer is too short and has not enough time to re-expand and fully fill that distance, which leads to decreased flowrate. However, large values of this parameter may also reduce the discharge coefficient because the frictional losses within that distance have been increased. Typical values of this parameter usually are between 1-4.

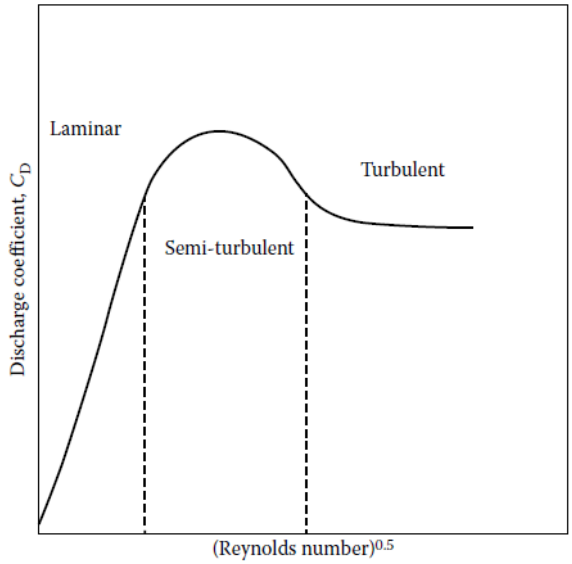

Figure 1.4 Reynolds number influence (Lefebvre and Mcdonell, 2017)

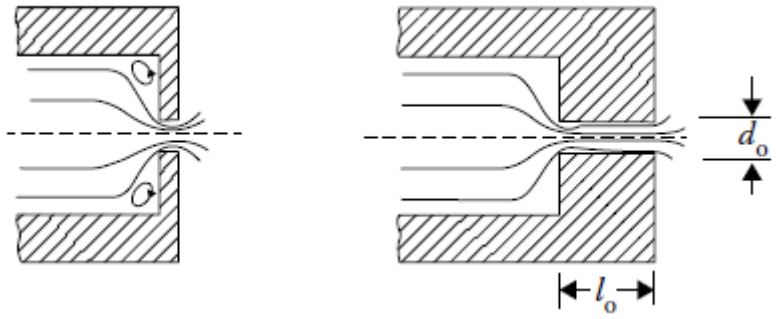

Figure 1.5 Length/diameter ratio influence on the final flow pattern (Lefebvre and Mcdonell, 2017)

The injection pressure possesses minor impact on the discharge coefficient. A study (Gelalles, 1931) showed that for a length to diameter ratio of 3, the discharge coefficient was increased from 0.91 to 0.93 when the injection pressure was increased by five times. Nonetheless, for higher length to diameter ratio, the discharge coefficient decreases with an increase in injection because the frictional losses are growing with the square of the flow velocity. Another study, (Hiroyasu, Arai and Shimizu, 1991) showed that, for a length to diameter ratio of 4 at ambient pressure, the discharge coefficient can reach a value of around 0.8 at Re=3000, while at Reynolds numbers that exceed 15000 the coefficient remains constant at 0.7. In general, this coefficient remained unchanged with ambient pressure variations. More specifically, this study showed that this coefficient remains constant of about 0.8 for a range of Re 2000-20000 while at sufficiently high Reynolds numbers this coefficient settles in 0.72. Also, many tests have been carried out to further study the influence of the inlet chamfer on the discharge coefficient. In fact, the smoother the inlet chamfer is the higher the discharge coefficient. Common angles for the inlet chamfer range from 20° to 60°. When the inlet chamfer angle is sharp this may result in regions where the velocity is extremely high and low static pressure. At low static pressures, cavitation may occur which also affects the discharge coefficient. The release of bubbles in regions where the static pressure is lower than the liquid local vapor pressure can cause serious erosion into the internal flow passages and accelerate the jet break-up process.

Probably the most well-known application of plain-orifice atomizers is the diesel injector. The main purpose of a diesel injector is to provide an intermittent supply of fuel within the combustion chamber of an engine. The high injection pressure is essential because the desired characteristics of a spray such as high-quality atomization and spray penetration have to be reached. Initially the fuel jet is moving at a high velocity into the highly compressed air within the combustion chamber. The core of the jet persists as a solid fuel jet surrounded by finely atomized fuel drops mixed with air at the outer edges of the spray. The solid fuel jet has the highest velocity at its core, while the droplets at the outer edges of the spray have almost zero velocity. As the jet disintegrates, concentration of fuel ranges

from 100% at core to almost 0% at the outer edge of the spray. Therefore, the fuel vaporization begins and self-ignition occurs in a region between the injector and the tip of the spray. The flame is rapidly spread along the spray while the burning occurs as a mixture of air, fuel vapor and evaporated fuel drops. Under these conditions, the combustion process takes place under turbulent and fuel-rich conditions as the more fuel is injected into the spreading flame. Parameters such as the spray aerodynamic motion and the fuel-air mixing rate, strongly affect exhaust gas concentrations of unburned fuel, NO_X, SO_X, and particulates.

Another application that Plain-orifice atomizers can be also used is in rocket engines and other applications. Generally, this type of nozzle is widely used, as introduces a liquid into a flowing gas stream. Important practical cases are co-flow, contra-flow and cross-flow injection into a flowing gas stream. The gas stream velocity is also important because the atomization process is not fully completed when the liquid exits the outer orifice of nozzle. Atomization is ongoing until a critical drop size is reached where, beyond that limit no further disintegration can occur. The drop size is depended on the relative velocity of the liquid jet to the surrounding gas. For co-flow applications (liquid and gas moving to same direction), mean drop diameter and penetration increases but atomization decreases. For contra-flow (liquid and gas move to opposite direction), penetration is decreased but quality of atomization improves and therefore cone angle is wider. The gas motion effects on the spray characteristics of plain orifice atomizers are considered significant only when the gas velocity is not high enough to affect and change the basic atomization process, but when the gas stream velocity is sufficient enough, then the disintegration of jet changes and corresponds to air-blast atomization.

Pressure-swirl-Simplex atomizers

Many types of pressure-swirl or simplex atomizers have been developed for a variety of applications. With Simplex atomizers a much wider cone angle is possible to be achieved (a range from $30°$ to $180°$ can be achieved) over the plain-orifice atomizers which are suitable for the most practical applications. The finest atomization can be obtained if high injection pressures and wide spray angles are reached. The performance of the atomization obtained from simplex atomizers is generally good. A simplex swirl atomizer has a simple geometry design but the hydrodynamic processes involved within the nozzle are quite complex. Various investigators tried to enrich the knowledge of the pressure swirl atomizers by extracting correlations between liquid properties, nozzle dimensions with the produced mean drop size. The correlations obtained though are of doubtful validity because the atomization process in Simplex atomizers is quite complex. With Simplex atomizers, factors that affect the atomization quality are the liquid properties and its injection pressure, the gas properties in which the liquid is injected and the atomizer size used. The internal flow characteristics have a strong influence on the final spray as the spray thickness and its uniformity are greatly affected by any flow changes

within the atomizer. With simplex atomizers, the flowing liquid within the flow chamber, experiences a swirling motion and therefore centrifugal forces are developed. As the liquid is ejected through the outlet orifice, a conical sheet is formed due to the act of these forces. The Simplex nozzles mainly produce two types of spray pattern. For instance, they are able to produce a solid cone spray or hollow cone spray as illustrated in Figure 1.6. Inviscid theory analysis can be applied for low-viscosity liquids to provide a basic understanding of the flow characteristics, but also, to provide a lead of how the discharge coefficient and the cone angle of the final spray is affected in Simplex atomizers.

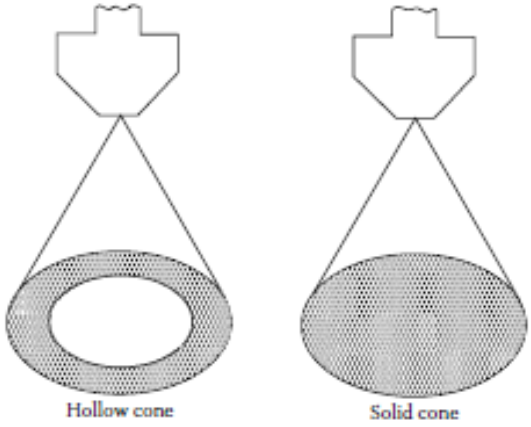

Figure 1.6 Spray patterns produced from Simplex atomizers (Lefebvre and Mcdonell, 2017)

First type of simplex atomizers comprises that drop distribution is even and uniform throughout its volume and the latter that drops are mainly concentrated at the outer edges of the spray Figure 1.6. Solid cone atomizers are mainly consisting of a main body with a core of a removable vane-type. The purpose of the core is to provide drops at the center in order to form a spray of a conical pattern (Delavan solid cone atomizer). Main drawback of solid cone atomizers is that they produce a coarse spray where drop size is larger at the center than its outer edges. Atomizers that form a solid-cone spray are preferred in chemical processing, drenching operations, scrubbers and coke quenching. On the other hand, hollow cone atomizers provide better atomization, as distribution of liquid is radial and this makes them suitable for applications such as combustion, gas washing, fire protection, foam breaking, gravel washing. The most common method to produce a hollow-cone spray pattern is to feed the liquid in a swirling chamber within the atomizer. As the liquid flows through the tangential ports within the atomizer, high angular velocity is developed and as a result a core of gas is emerged at the center. The ejected liquid emerges from an outer orifice and flows radially outward, thereby, a hollow conical spray is formed. The actual spray cone of the emerging liquid is a function of the relative magnitude of the velocity components and it is strongly affected by any flow changes within the atomizer. The resulting spray passes through five stages in total starting from the point that the

differential pressure is zero and rises until the desired atomization is achieved. The five main stages are indicated in the Figure 1.7.

The five stages of development are the following:

1. Dripping liquid from the orifice

2. Liquid forms a thin distorted pencil

3. A cone starts to form but the cone is confined by the action of surface tension forces into a closed bubble

4. When the bubble opens it forms a hollow tulip shape that results in a ragged edge, where the liquid disintegrates into fairly large drops

5. The curved surface straightens and forms a conical sheet. Further disintegration leads to a well-defined hollow-cone spray

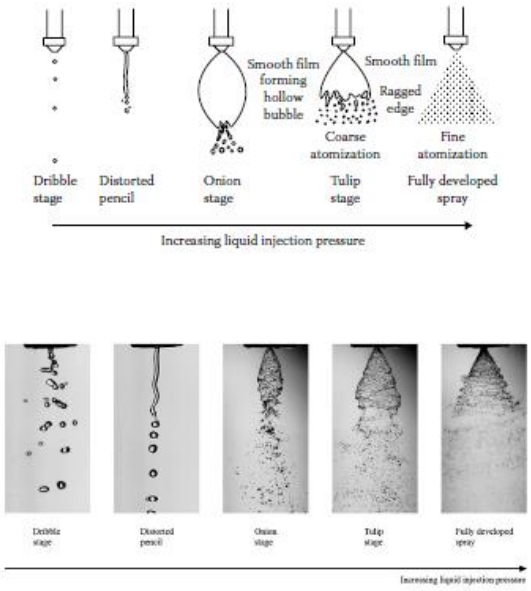

Figure 1.7 Stages of spray development (Lefebvre and Mcdonell, 2017)

A major drawback of simplex atomizers is that flowrate is proportional to the square root of injection pressure. Therefore, if double flowrate is needed then the required injection pressure is quadrupled. For low viscosity liquids, atomization can be achieved when the differential pressure is more than 100kPa (Lefebvre and Mcdonell, 2017, p. 79). Even for low viscosity liquids, high delivery pressures are necessary to achieve fine atomization. The high-pressure demand is a basic drawback of simplex atomizers which has led to the development of the Wide range atomizers. The category of wide range

atomizers consists of atomizers which are named as duplex, dual orifice, spill return atomizers. These atomizers were developed in order to provide an alternative method to achieve better atomization quality with less injection pressure demands.

Wide range atomizers

Wide-range atomizers have been developed with common design objective, to provide good atomization in a range of flowrates without the demand of extremely high pressures. The atomizers of prime importance are discussed in the following sub-sections.

Duplex atomizer

The Simplex and Duplex atomizers are very similar, but their main difference is that the latter has a swirl chamber with a set of two tangential swirl slots, each one having separate liquid supply. In the cross-sectional area, primary slots are smaller than secondary slots. The liquid to be atomized flows from primary slots at low flow rates which are supplied first with the liquid during operation, while at higher flow rates the liquid flows from both primary and secondary slots. As the injection pressure rises, the flowrate is increased and a pressurizing valve that blocks the liquid from entering the secondary manifold opens at predetermined injection pressures. Therefore, the liquid flows through both primary and secondary slots.

The performance of the Duplex atomizer is superior to the Simplex atomizer, as for the same flowrate the injection pressures demands are sufficiently lower as shown in Figure 1.8. To be more precise, Duplex atomizers have much higher injection pressure at low flowrates than Simplex atomizers (injection pressure is 8 times greater at 10% of maximum flowrate). The Duplex atomizers achieve good atomization at low flowrates (applies equally for dual-orifice atomizers), without extremely high delivery pressures demands.

The main drawback of duplex atomizers is that spray cone angle is not constant and varies on flowrate. More specifically, when the pressurizing valve opens and the secondary liquid enters the swirl chamber, the atomization quality is relatively poor for a small flowrate range. Additionally, the cone angle is wider at low flowrates while at higher flowrates cone angle is narrower. To sum up, in the combined flow range spray cone tends to be smaller than in the primary flow range. In the combined flow, a reduced spray cone angle is associated with an increase of the atomizer's internal geometry ratio, therefore the resulting spray cone angle is smaller. This problem is likely to be prevented in some designs by setting the primary swirl slots on a smaller tangent circle than the secondary slots. As a result, swirl component is reduced and therefore this leads to a reduced spray cone angle at low flowrates.

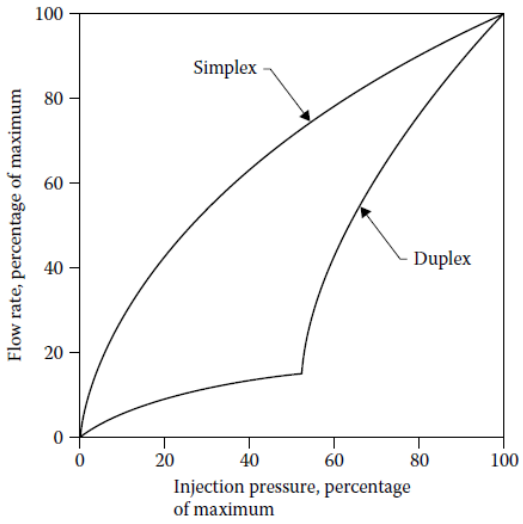

Figure 1.8 Function of maximum percent flowrate and injection pressure for simplex and duplex atomizers (Lefebvre and Mcdonell, 2017)

Dual orifice

The Dual orifice atomizer has many similarities with Duplex atomizer. The Dual atomizer has been extensively used on aircraft and industrial engines. It consists of two separate swirl chambers each one for primary and secondary flow. The primary and secondary swirl chamber have a common axis and they can be considered as two Simplex nozzles the one inside the other. The primary nozzle is arranged to be on the inside in way that primary spray doesn't impinge or interfere with the other orifice or to the secondary spray what is inside the orifice. At the lower flowrates, the liquid entirely flows through the inner primary nozzle while at higher flowrates a large proportion of the liquid supply passes through the secondary nozzle. Demands of high liquid pressure are necessary to force the liquid through the small slots of the primary swirl chamber, therefore higher atomization quality is likely to be promoted. When the flowrate is progressively increased, it leads to an increased fuel pressure. As the injection pressure rises, a pressurizing valve opens at predetermined pressures and the liquid passes through both chambers. As far as the valve opens, the pressure of the secondary liquid is low and this leads to a decreased atomization quality. As flowrate is further increased, the injection pressure of the secondary liquid rises and the atomization quality gets better. To sum up, for a certain range of liquid flowrates the atomization quality is unavoidably low. This occurs when the pressurizing valve opens until sufficient injection pressure is reached. In order to avoid the poor quality of atomization for this range of flowrates, the primary spray cone angle is set to be slightly wider than secondary cone angle as the two sprays merge within a short distance from atomizer. This advantage of Dual orifice atomizers provides more flexibility over the Duplex atomizers. The atomization quality can be improved but still may be relatively poor. Another aspect that the designers should consider is

that when the engine runs at a certain operating point and the pressurizing valve opens, the combustion efficiency must remain high when low pollutant emissions are considered of prime importance.

Spill return

The Spill return atomizer is much the same as Simplex atomizer but they differ as the Spill return atomizer has a return line at the back of the swirl chamber. This return flow line is useful because quantity of liquid is spilled or returned back to the main supply. Therefore, this method results in constantly maximum pressure supply and flowrate of liquid within the swirl chamber. A pressurizing valve that is located in the spill line controls the quantity of liquid that returns back to supply. At the maximum flowrate that can be reached, the valve is closed so the liquid doesn't return back to the main supply. Therefore, the liquid ejects from the nozzle as a well atomized spray. however, when the valve is opened, the liquid is diverted back to the main supply while less liquid is ejected from the outer orifice of the nozzle. Generally, this type of atomizer comprises high injection pressure that is consistently kept constant. The Spill return atomizer provides a hollow-cone spray pattern and high-quality atomization for a wide range of flowrates which makes it suitable for a variety of applications. The Spill-return atomizer possesses some good features such as the absence of moving parts. Moreover, the design of the return flow lines continually handling large flows it may be quite difficult to be blocked by any contaminants in the liquid.

However though, the Spill-return atomizer has a drawback, the spray cone angle varies on any flowrate changes. The spray angle tends to be wider at low flowrates because the axial velocity component within the swirl chamber is decreased and the tangential velocity remains unchanged. Furthermore, others drawbacks of the Spill-return atomizer are the demands of a pump of large capacity for handling the flows that are diverted back to main supply and the extensive complexity of metering the flowrate.

Currently, the main application of Spill-return atomizer is in large industrial furnaces. Nowadays, fuels for gas turbines application comprise high aromatic content which causes gum formation to the conventional pressure atomizers and are likely that blockage problems to be appeared. The Spill return atomizer may be able enough to deal with this situation as it provides good atomization, is free of blockage problems and it can be suitable when it comes to the future alternative fuels which have high aromaticity and high viscosity.

Fan spray

The Fan spray atomizers have been widely used in many applications. For instance, they are very handy in the coating industry, small annular gas turbines combustors and other applications such as aerial

spraying and agricultural applications. In these applications, a narrow elliptical pattern is more desirable over a normal circular pattern. Also, with the small annular combustors the Fan spray atomizers can provide good lateral spread of the fuel and thus injection can be minimized. A flat or fan shaped spray can be produced with several different concepts. One method comprises that a jet will collide on a curved surface, therefore, a flat coarse spray with a uniform drop distribution will be produced. Wide spray angle and high flowrates can be obtained with this type of nozzle. Also, the risk of plugging problem is minimized as it contains relatively large flow passages. Another method that a Fan spray can be produced is shown in Figure 1.9. This atomizer consists of a V groove intersection with a hemispheric surface that communicates with the cylindrical liquid inlet. A liquid sheet can be produced which has the same parallel direction as the orifice's major diameter. Then, after further disintegration the liquid sheets turns into a narrow elliptical spray. With this method, viscous and Non-Newtonian fluids can be successfully atomized.

Investigations of the behaviour of flat sprays (Dombrowski, Hasson and Ward, 1960) suggested that mean drop diameter increases as surrounding pressure increases. On the other hand, for fan spray injectors, the spray angle seems to be slightly affected by pressure variations. Moreover, investigators (Dombrowski, Hasson and Ward, 1960) showed that the liquid sheet trajectories is function of several parameters and that the sheet thickness as moving away from the orifice is reduced. For example, the variables that govern the trajectory are the injection pressure, sheet thickness, surface tension. Drops of larger size can be obtained from a fan spray atomizer than swirl spray atomizers for an equal amount of flowrate. Liquids with high viscosity can be atomized successfully as Fan spray can produce very fine sprays.

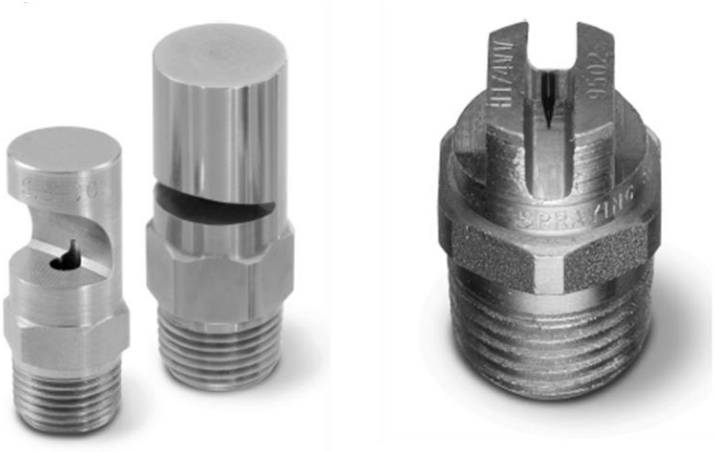

Figure 1.9 Flat spray flood nozzle(left) and Flat spray nozzle (right) (Lefebvre and Mcdonell, 2017) (Courtesy of Spraying Systems Co.)

1.2.2 Rotary atomizers

The basic concept of the Rotary atomizers is that liquid supply is fed to the centre of a cup or disk which rotates at high angular velocity. As a result of friction, liquid rotates roughly at the same velocity as the disk, therefore, the liquid is spread radially and uniformly outwards across the disk and the liquid leaves from the periphery of the rotating disk at high velocity. The rotating disk is likely to be smooth or to have guiding vanes or slots, guiding the liquid more efficiently to the periphery of the disk. The rotating disks have a variety of diameters 25-450mm. The smaller rotating disks can spin up to $1000rps$ while the larger can rotate up to 200rps. When the small rotating disks spin at high angular velocities and the liquid flowrate is low, then, the spray produced has drops of uniform size. With this method, the capacity of atomization can reach up to 1.4 kg/s. Moreover, in order to assist atomization and minimize the angular velocity of the order of $50rps$, a coaxial air jet can be used. This system can be easily regulated in order to successfully atomize liquids which widely vary in their viscosity. Also, the liquid sheet thickness and its uniformity can be adjusted by properly regulating the liquid flowrate and the angular velocity of the rotating disk to the desired flow characteristics. A major advantage of the rotary atomizers is that the independence variation of the flowrate and the rotational velocity of the disk, that leads to wide flexibility in operations over the pressure nozzles. Generally, for a rotating flat disk, the atomization mechanisms are a function of liquid flowrate and the angular velocity of the disk. At low flowrates, the liquid discharges from the periphery of the disk and drops of uniform size are formed which draw behind them fine ligaments. This phenomenon can be called the direct drop formation. Increasing the flowrate, the atomization process still may remain the same but the ligaments are now larger in diameter and they are formed down the edges where they are further disintegrated to drops. The thickness of the ligaments is increased as the flowrate is higher and the ligaments disintegrate further to drops at some distance from the outer edge of the disk. This process is generally known as the atomization by ligament formation. For higher flowrates, ligaments can't follow any more the liquid flow and a thin sheet forms that is extended from the lip until an equilibrium point is reached. The number of the ligaments increases as the flow is increased and they remain constant until their maximum number and size is reached that is regardless of the flowrate. At the equilibrium point, the surface tension causes a contraction force at the free edge, equals the kinetic energy of the sheet that is being developed. The thick rim that is produced disintegrates further to ligaments and drops that have considerable size variations. This process is commonly known as atomization by film formation. The mean drop size though is diminished as the rotational velocity increases and it becomes greater when the flowrate and viscosity are increased. Parameters that affect the way that this film is disintegrated are the size and the geometry of the rotating disk, the rotational velocity, the liquid flowrate and the liquid properties. To avoid this, the rotating disks are

serrated, therefore the transition from ligament formation to sheet formation is delayed. Moreover, serrated disks promote a spray that has a uniform drop size distribution. Eventually, when the rotating disk reaches a very high peripheral velocity, at the disk edge the liquid can be instantly atomized by the ambient air. To sum up several factors contribute to the achievement of better atomization quality. First and foremost, atomization is significantly improved as the rotational speed is high, the flowrate and the viscosity of the liquid is decreased and the outer edges of the rotating disk to be serrated. If a uniform film thickness and with a uniform drop size distribution is desired, some conditions are necessary to be reached. The factors that affect the film thickness are a) the centrifugal forces should be greater in magnitude than gravitational forces, b) the vibrations must be absent as the disk rotates, c) constant supply of liquid to the rotating disk and d) the cup should have smooth surfaces.

One disadvantage of the flat disk atomizer is that the liquid may slips from the rotating disk. This is very common at the high rotational speeds. When slippage occurs, results in the liquid ejection from the edge of the disk at velocities that are lower that the peripheral velocity of the disk, thus atomization quality is affected. A possible solution to the slippage problem in commercial atomizers is to use radial vanes Figure 1.10. The vaned disk is supplied with liquid that flows over its surface until it is contained by a rotating vane. Then the liquid experiences centrifugal forces and flows radially outwards as a thin film over the vane surface. These vanes prevent the slippage of the liquid at the periphery of the rotating disk and tend to eject the liquid almost at the same peripheral velocity as the rotating disk.

The vaned atomizer disks are mainly used in industrial applications while the rotational velocity controls the mean drop size of any liquid to be atomized. Usually, this type of atomizer is made of metals or alloys that are resisting corrosion, thus corrosive liquids can be successfully handled. In addition, rotary atomizers are found that they are useful in industrial spray drying applications. The drive system and the operation of the wheel in the newer designs of the rotary atomizers has made them more reliable and able enough to reach higher supplies of liquid at higher peripheral velocities which eventually lead to fine atomization.

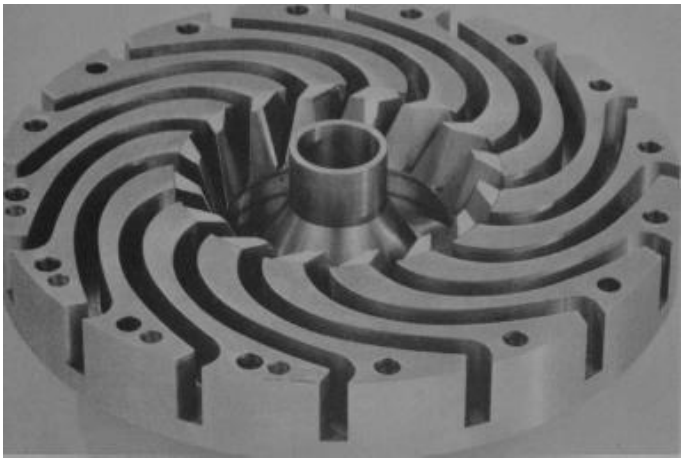

Figure 1.10 Rotating Disk with curved vanes (Lefebvre and Mcdonell, 2017) (Courtesy of NIRO Atomizer.)

1.2.3 Twin fluid atomizers

Air-assist atomizers

Air-assist atomizers are an alternative method in order to achieve good atomization at low injection pressures. Various designs of the Air-assist atomizers are extensively used in industrial gas turbines and oil-fired furnaces applications. In all designs, a liquid of low velocity is being discharged to a relatively high velocity gas stream, therefore atomization is accomplished. The two main types of twin-fluid atomizers are Air-assist and Air-blast atomizers. These two types are very similar as they almost have similar geometric features and both employ a high-velocity airstream to successfully atomize a liquid. The main difference between them is that they expose the liquid to be atomized at different air velocity. For instance, Air-assist nozzles use extremely high velocities of air >200 m/s and often an external supply of pressurized air is required. The latter has lower air velocities requirements 50-100 m/s where can be reached by the utilization of pressure differential across the combustor liner. Generally, Air-assist atomizers utilize smaller amounts of air than Air-blast atomizers and makes them suitable to be used in atomizing systems that need to be operated with the minimum mass airflow.

The main configurations of the Air-assist atomizers are the internal and external mixing atomizers Figure 1.11. The internal mixing atomizers, mix the two phases within the nozzle before being discharged from the outer orifice. The liquid can be supplied through slots in order to promote a conical discharge pattern. The spray cone angle in this configuration has its minimum value as the airflow is maximum and as the airflow decreases the spray widens. The maximum spray angle that can be reached is about 60°. Internal mixing nozzles are very flexible and they are notably effective for atomizing liquids with high viscosity and liquid slurries. Within the mixing chamber, the mixing of the two phases is quite intense, therefore the aerodynamic and fluid dynamic flow patterns involved are

to be quite complex. The Internal mixing atomizer may be energy inefficient but it can successfully produce finer sprays over a simple pressure atomizer. The latter configuration implies that the same principle is applied but they differ as the liquid and a high velocity gas impinge at or outside the liquid discharge orifice. Major advantage is that both liquid and air flowrate can be individually controlled in order to achieve the desired atomization quality. Various designs of external mixing atomizers have the ability to produce a constant spray angle over a wide range of flowrates. When the flowrate is low, both configurations can provide good atomization even if the liquid has high viscosity. Generally, this configuration lacks back pressures effects over the internal mixing configuration as the two fluids (the liquid to be atomized and the gas stream) are isolated until collision. However, the first configuration is more effective than the latter, as in the external mixing atomizers higher gas flowrates are necessary to achieve the same degree of atomization, thus the power requirements are of higher demand.

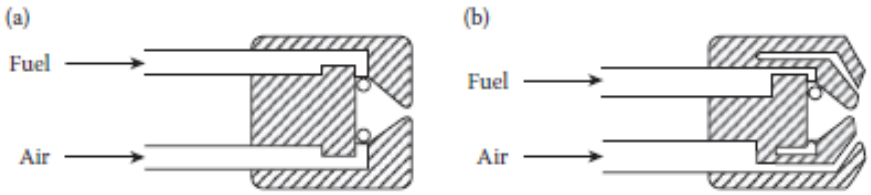

Figure 1.11 (a)Internal Mixing (b)External Mixing Atomizers (Lefebvre and Ballal, 1988)

The major disadvantage of these atomizers is that an external supply of highly pressurized air is needed, thus, air-assist atomizers are excluded from aircraft applications. However, they can be suitable in industrial engines applications. The Air-assist atomizers are found to be very handy when it comes to applications that require fine droplets, such as material manufacturing, fire suppression systems, emulsions and atomization of high viscosity liquids.

The pressure atomizing component of the air assist atomizers is able enough to provide a fair atomization quality for the most of the operating range. The air assistance can be used as supplement to enrich atomization process at conditions where the liquid flowrate is low and the nozzle pressure differential is not high enough to provide sufficient pressure atomization. For some other nozzle designs, the liquid injectors alone have the tendency to produce low quality of atomization, so air assistance is unavoidably necessary for the whole operating range. Also, in some applications such as coal-water slurries, the conventional means are not able enough to successfully atomize the liquid so some other more complicated nozzles were designed Figure 1.12. A more complicated nozzle is designed for such occasions that comprises the two configurations of internal and external mixing into one to achieve the desired atomization. The both airstreams, the inner and outer are used to

accomplish a shearing action on the annular liquid sheet that is formed at the nozzle tip. The airflows are swirled clockwise, while the liquid sheet swirls anticlockwise in this configuration.

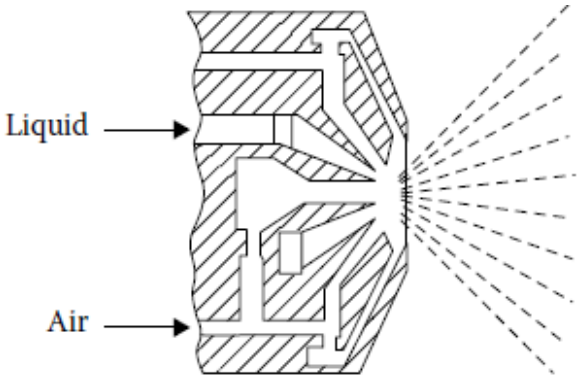

Figure 1.12 Parker Hannifin slurry nozzle (Lefebvre and Mcdonell, 2017)

Air-blast atomizers

The Air-blast atomizers use an identical principal with Air-assist atomizers but, in this configuration larger quantities of air that flow at much lower velocities <100 m/s in order to achieve good atomization are deployed. This type of atomizer is ideal when liquid fuels are to be atomized in combustions systems such as gas turbines and that's a reason why they are extensively used in the aviation industry. The excess amount of air that is used though is not wasted as enter the combustion chamber and mixes with the additional air that is necessary to properly complete the combustion. In addition, the main objective of Air-blast atomizer is to effectively deploy the available air to achieve good atomization quality within the combustion zone.

The Air-blast atomizers have many advantages over the pressure atomizers, mostly in combustion systems that operate at high pressures. Moreover, a lower fuel pump pressure is required and the sprays produced are finer. Additionally, the Air-blast atomizers guarantee that the mixture that enters the combustion chamber, which consists of air and fuel are properly mixed.

During combustion process, this results in reduced soot formation and the blue flame of low luminosity is likely to be promoted, therefore, minimum exhaust smoke is produced and lower flame radiation is achieved. Generally, the advantages of Air-blast atomizers have led to their installation in gas turbines applications such as aircraft, marine and industrial applications. Nowadays, the most common type that is extensively used in gas turbines applications is the pre-filming Air-blast atomizer Figure 1.13 which has higher atomization performance over the Plain-jet Air-blast nozzle. In the pre-filming-type which has a quite complicated design, the liquid is initially spread out as a thin conical sheet and then is exposed to two separate airstreams of high velocity that impact on its both sides. The fuel flows through a number of tangential ports on a pre-filming surface before being discharged

at the atomizing lip. The first airflow is deflected radially outwards by a swirler which is contained in the central circular passage and this causes the airflow to impinge the inner surface of the continuous sheet. The second annular passage surrounds the main body of the atomizer which also contains a swirler that arranges to the airflow impact on the outer surface of the fuel sheet instead of the inner. The two airflows coalesce at the exit of the atomizer and the atomized fuel enters the combustion zone. The flow within the atomizer of Plain-jet Air-blast and the Plain-orifice atomizers are almost the same, while for Pre-filming Air-blast nozzle the internal hydrodynamics are quite complex.

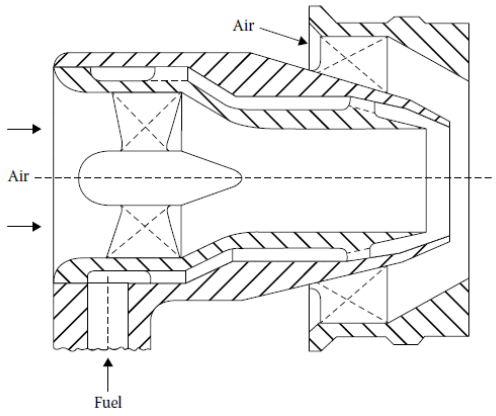

Figure 1.13 Pre-filming air-blast atomizer (Lefebvre and Mcdonell, 2017) (Courtesy of Parker Hannifin Corp.)

1.3 Factors that affect atomization

1.3.1 Generally

Factors that affect the performance of an atomizer regardless of type are not only its size and geometry, but also the physical properties of the liquid to be atomized and the surrounding medium in which the droplets are discharged. For instance, the governing dimension of Plain-orifice and plain-jet Air-blast atomizers, is the diameter of the outer orifice while for pressure-swirl, rotary and pre-filming Air-blast atomizers is the thickness of the sheet that is produced as soon as it leaves the atomizer.

Liquid Properties

The properties that have a strong impact on the flow and spray characteristics are density, viscosity and surface tension of the liquid or fuel. The density doesn't easily change without affecting any other property of the liquid. Most liquids have small differences in density, so their contribution to the atomization performance is not of prime importance, while the mean drop size is almost uninfluenced in density variations.

When a liquid is atomized, it results in a spray that has larger liquid surface area over a plain liquid jet column. The liquid surface area of a spray can be considered as the sum of surface areas of every single drop, thus, this indicates the atomization level that can be achieved. This, can be very handy in applications such as evaporation or absorption, in which the surface phenomena are considered significant. The surface tension can be defined as a force which resists to new area formation. The minimum energy that is required for atomization is the product of the surface tension to the liquid surface area increase. On whatever occasion, if the surface tension forces are assumed important, then the Weber number has a key role in the correlation of the size of the drop. Usually, the surface tension ranges from $0.073\frac{N}{m}$ for water to $0.027\frac{N}{m}$ for petroleum products. Surface tension is decreased if there is a rise in the liquid temperature Figure 1.14.

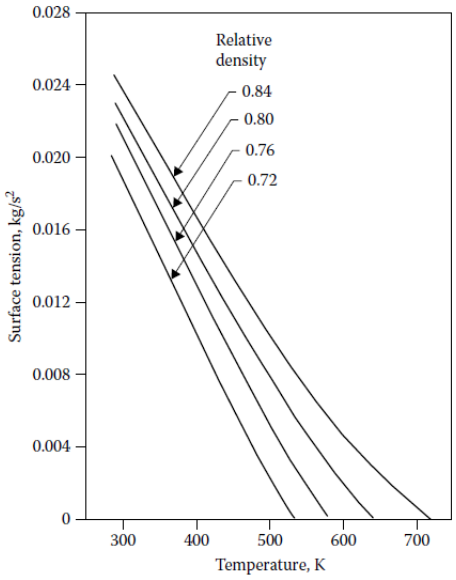

Figure 1.14 Surface tension as a function of temperature for hydrocarbons fuels with different relative density (Lefebvre and Mcdonell, 2017)

An important property of the liquid can be considered its viscosity. This property can influence the resulting spray characteristics, such as the drop size distribution, the spray pattern or even the nozzle flowrate. An increase in the liquid viscosity implies lower Reynolds number and the natural instability of a jet can be prevented, thus, disintegration is delayed and the drop size in the resulting spray grows. The flow within a nozzle can be very complicated by any viscosity variations. For example, in hollow-cone atomizers, if viscosity is slightly increased, then the flowrate is increased because the liquid film in the discharge orifice thickens, therefore results in a higher effective flow area but at high viscosities, the flowrate is reduced. Respectively, in pressure-swirl atomizers, an increase in viscosity leads to a narrower spray angle, or even if viscosity is extremely high, then the conical spray pattern is likely to

collapse. In a more general way, viscosity has a strong impact on the atomization quality because if viscous losses are large enough, then the available energy for atomization is less, thus the spray obtained is coarser. Thus, as water and diesel have low viscosity, this makes them suitable fluids in atomization as they are capable enough to produce fine sprays. The viscosity of a liquid is affected by the temperature. More specifically, a rise in temperature decreases liquid viscosity which can be very useful in many applications. For instance, heavy fuel oils can be heated up to improve the quality of atomization or even reduce the pumping power requirements.

Ambient Conditions

When a spray is injected into a combustion chamber, the properties of the surrounding medium such as pressure and temperature are extensively changed. For example, in gas turbines applications the spray is injected into a turbulent flow field, swirling recirculating streams of the gases that reacted or even in industrial furnaces, the fuel is sprayed in an environment that has high temperature. The spray angle in a pressure-swirl atomizer is noticeably reduced if the density of the ambient gas is increased. Actually, the spray angle is reduced down to a minimum value, where at this point, any further increase of the density of the surrounding medium doesn't affect the angle of the spray anymore. As well, the mean drop size is greatly influenced by any changes of the ambient gas density in the pressure-swirl atomizers. In fact, the mean drop size depends on the gas ambient pressure. If the pressure increases, then the drop size grows until a maximum value is reached, whilst, any further increase beyond that value will cause the drop size to decrease steadily.

Generally, the spray pattern is affected by any variations in the ambient gas density. For instance, the spray angle of a Plain-orifice atomizer widens as the surrounding medium density is increased. As density rises, the aerodynamic drag on the drops is increased, thus, the drops in the axial direction experience more deceleration over the drops that are in the radial direction. However, in the Air-blast atomizers, the spray pattern seems to be uninfluenced by any density variations. The largest drops in size of the spray have the tendency to follow the streamlines of the flow field which is unaffected by the density variations. In fact, if the density is increased, then the spray pattern tends to stick to the streamlines of the atomizing air more closely.

1.4 Basic Processes in Atomization

1.4.1 Generally

During the atomization process, a liquid bulk is converted into drops while the action of internal and external forces greatly affect it. Internal forces are considered the surface tension forces and the latter the aerodynamic forces. When the disruptive forces are absent, surface tension has the tendency to

make the liquid having a spherical shape and opposes to any changes in the geometry of the system. Aerodynamic forces can be considered as an external distorting force which apply on the liquid bulk. The disruption process is promoted when the aerodynamic forces are acting on the surface of the liquid and the breakup occurs when the magnitude of this force equals the surface tension force. The initial disintegration process produces quite large drops that are unstable and disintegrate more in drops of smaller size. Therefore, both primary and secondary atomization processes have a significant influence on the final range of drop sizes in a spray.

1.4.2 Static formation of Drops and Drop break-up

Static formation of Drops

The simplest form of atomization can be considered the quasi-static case of a hanging drop. The most common example of this form of atomization is that which corresponds to a dripping faucet Figure 1.15. The drop is formed at the end of the faucet when the gravity forces are greater in magnitude than surface tension forces. The mass of the drop can be determined by the equation of surface tension forces to the forces of gravity on the drop as given Equation 2 while the drop size by Equation 3(d_o corresponds to the diameter of a thin circular tube).

$$m_D g = \pi d_o \sigma \text{ Equation 2}$$

$$D = \left(\frac{6 d_o \sigma}{\rho_l g}\right)^{\frac{1}{3}} \text{ Equation 3}$$

Figure 1.15 Dripping faucet (Munson *et al.*, 2009)

The dripping mechanism unavoidably leads to the formation of large drops at very low flowrates. However, when it comes to practical applications this mechanism cannot provide any handy results, as most of them require high flowrates and fine quality of atomization.

Break-up of Drops

The break-up of drops and the secondary atomization are related directly. Several interacting mechanisms are involved in the overall atomization process such as the splitting of large drops during the final stages of disintegration. Therefore, it is of prime importance to understand the various ways that a single drop can break-up when aerodynamic forces are acting on the drop. When equilibrium conditions are reached, the pressures that are involved are: the internal pressure p_I, the aerodynamic pressure p_a and the surface tension pressure p_σ. The internal pressure is able enough to balance the aerodynamic and surface tension pressures, thus, by equating them, the Equation 4 can be obtained. The Equation 5 corresponds to a drop of spherical shape and indicates the higher value of surface tension pressure that can be attained.

$$p_I = p_a + p_\sigma = constant \quad \text{Equation 4}$$

$$p_\sigma = \frac{4\sigma}{D} \quad \text{Equation 5}$$

As long as the surface tension pressure is able enough to compensate any changes of air pressure at any point on the surface of the drop, the drop remains stable. When aerodynamic pressure is large enough compared to the surface tension pressure, then the drop is deformed and breaks further to smaller drops. Also, Equation 5 shows that the surface tension pressure is inversely proportional to the drop diameter. Therefore, the smaller drops may be able enough to compensate the aerodynamic pressure variations, thus, they remain stable and further drop break-up is eliminated.

Drops in Flowing Air

Drops in the flowing air is a break-up process that has been considered in detail both theoretically and experimentally. The three basic types of deformation have been identified from (Hinze, 1955) and are the following Figure 1.16:

1. During Lenticular deformation, the drop shape changes from spherical to oval. The subsequent deformation is related to the magnitude of internal forces that cause the deformation of the drop
2. The spherical drop lengthens until a long cylindrical thread shape is reached which breaks-up to small drops. This deformation type is called cigar-shaped deformation
3. Bulges and protuberances are generated on the surface of the drop and when they are detached from the main drop, smaller drops are formed. This type is known as bulgy deformation

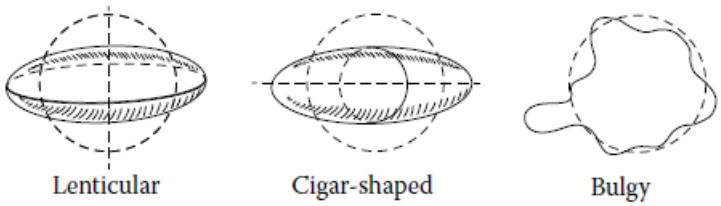

Figure 1.16 Basic types of spherical deformation (Hinze, 1955; Lefebvre and Mcdonell, 2017, p. 18)

The lenticular deformation occurs under the action of aerodynamic pressures or viscous stresses that are produced by parallel and rotating flows on the drop. The cigar-shaped deformation is observed when the drop is exposed to plane hyperbolic and Couette flows and the bulgy deformation occurs when the flow is of irregular pattern.

The dominant parameters that control the drop break-up in flowing air are the dynamic pressure, surface tension, and viscous forces. The initial condition of break-up is satisfied when the aerodynamic drag equals the surface tension force as indicated by Equation 6, which is valid for any given liquid. In this equation, C_D corresponds for the drag coefficient, ρ_a for the density of the flowing air, U_R for the relative velocity of the air and D refers to the drop size. If the terms are rearranged, the dimensionless Equation 7 is extracted, which defines the critical Weber number.

The Weber number is a dimensionless number that is used when there is an interface between two different fluids. This number can be defined as the ratio of Drag to Cohesion forces (proportional to the external pressure forces). If Weber number is increased, the external forces are larger than surface tension forces and they have the tendency to deform the drop, while the surface tension forces tend to oppose the deformation that is caused. The maximum diameter of a drop that can be obtained for a given relative velocity is indicated by Equation 8.

$$\frac{1}{2}C_D\rho_a U_R^2\frac{\pi D^2}{4} = \pi D\sigma \quad \text{Equation 6}$$

$$We_{crit} = \left(\frac{\rho_a U_R^2 D}{\sigma}\right)_{crit} = \frac{8}{C_D} \quad \text{Equation 7}$$

$$D_{max} = \frac{8\sigma}{\rho_a U_R^2 C_D} \quad \text{Equation 8}$$

Experimental and theoretical investigations have shown that the disintegration of a drop mainly consists of two modes, which the first considers that the drop is subjected to steady acceleration while the second, if it's exposed to a high-velocity airstream. When the drop is subjected to steady acceleration, the drop gradually flattens. If a critical velocity is reached during the steady acceleration,

the drop blows up into the form of a hollow bag that disintegrates further to fine drops, which are attached to a circular rim. However, the disintegration of drop that is exposed to a high-velocity airstream differs significantly. In this mode, the drop is deformed in the opposite direction and a convex surface is composed which is parallel with the airflow, thus, the drop obtains a saucer-shape. The edges of the deformed drop are drawn out into fine ligaments which finally break to drops.

1.4.3 Liquid Jet Disintegration

Generally

As a liquid jet emerges from a nozzle, it has a form of a continuous cylindrical column. As the liquid moves away from the orifice and when certain conditions are reached, oscillations and perturbations rise, thus, disintegration of the liquid jet is promoted and the first drops are formed. Occasionally, the disintegration of the jet is a process that can be named as primary atomization. Further disintegration occurs when the size of the drop outstrips the critical value of. This process can be referred though as secondary atomization in which drop break-up is considered.

The jet disintegration is a process that has been examined by many researches (Tyler, 2009; Rajendran, 2012), both experimentally and theoretically for over 100 years. During this process, it is considered that the liquid is the dispersed phase and the air or gas is the continuous phase. In other words, a liquid jet is injected into a gaseous atmosphere and it is of interest to examine its properties. For example, the length of the continuous jet and the drop size, are properties of prime importance that need to be examined or how the jet is disrupted. In addition, the length of the continuous jet is able enough to provide a measure of the disturbance growth rate while, the drop size provides a measure of the wave number of the most unstable disturbance. Investigations (Mccarthy and Molloy, 1974; Martinon, 1983; Clanet, 2003)showed that for constant diameter of the jet, the continuous length of the cylindrical column increases as the velocity of the jet increases and vice versa. Also, these investigations have revealed that, if the jet velocity is kept constant, the length of the jet changes proportionally to its diameter.

In order to predict under which conditions the liquid jet collapses when it emerges at low velocity, (Strutt, 1878) used the small disturbances method as a part of a mathematical analysis. By comparing the surface energy of the jet that is undisturbed with that which is disturbed, he obtained very useful results. For instance, during the break-up of non-viscous liquid jet that exits the nozzle at laminar flow conditions, it was found that all the disturbances on a jet will grow if they have wavelengths greater than its circumference. In addition, another result that obtained is that, the disturbance class which grows faster than the other controls the jet break-up process. Even though, if a viscous liquid jet under turbulent conditions which is exposed to a surrounding medium is considered, the conclusions

obtained are generally valid as first approximations. Generally, Rayleigh showed that if exponential disturbance growth rate is considered, after the break-up spherical drops can be formed which have an average size almost twice the undisturbed jet diameter. The Rayleigh ideal break-up and the actual break-up are showed in Figure 1.17. The ideal break-up theory considers that when the break-up occurs, the drops that are formed have uniform size and spacing between each another, while the actual break-up indicates that the forming drops have large size and small drops between their spaces. It is obvious that, as axisymmetric disturbances grow, the cylindrical column becomes unstable especially at its end where it disintegrates to drops.

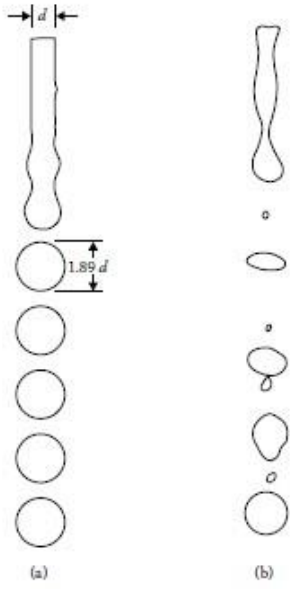

Figure 1.17 (a) Rayleigh ideal break-up (b) Actual break-up (Lefebvre and Mcdonell, 2017)

Break-up regimes

During the disintegration of a liquid jet there are four main regimes of break-up Figure 1.18.

1. The mechanism that Rayleigh studied, considers the formation of a drop without any air effects. The primary disturbances in the liquid and surface tension forces, results in the formation of radial symmetric waves. In this regime, the break-up length is affected linearly by any changes in the velocity of the jet.
2. When the air influence is considered in the drop formation process, the aerodynamic forces of the surrounding medium should be also evaluated as the velocity of the jet is increased. The waves that are formed, are similar to those in the first regime but are more intense.
3. The aerodynamic forces become more effective while the surface tension influence weakens. The drops that are formed in this sinuous regime are on account of the jet waviness.

4. The jet is completely disintegrated; therefore, the liquid is atomized in a chaotic and irregular manner within a short distance from the nozzle.

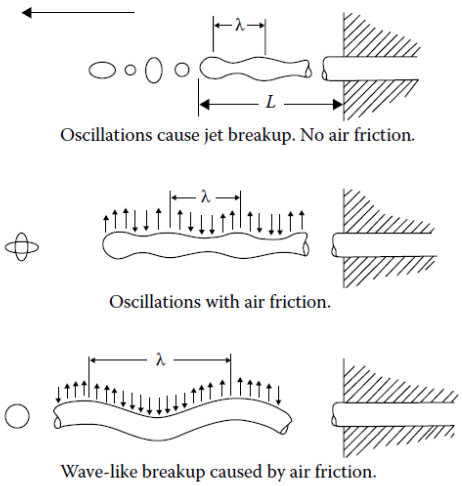

Figure 1.18 Main regimes of break-up (Lefebvre and Mcdonell, 2017)

However, the four regimes may be different, but it's quite difficult to distinguish them. The work of (Ohnesorge, 1936) showed the importance of each parameter during the jet break-up mechanism. Parameters that affect the disintegration of the jet are: gravitational, inertial, surface tension and viscous forces. These parameters constitute a dimensional number known as the Ohnesorge number stability number which is defined by Equation 9. This equation, actually comprises that this dimensionless number is defined as the ratio of the viscous forces to the square root of the product of inertia and surface tension forces. Ohnesorge presented that the jet break-up can be described in three stages by the dimensionless stability number and the magnitude of Reynolds number Figure 1.19. The liquid Reynolds number is defined by Equation 10 as the ratio of the inertial to viscous forces and is able to describe the flow state of the emerging jet. In a more general way, the flow state of jet can be laminar or turbulent. The laminar flow is promoted by the following: the flow disturbances are absent, the atomizer has a well-rounded entrance to the tube and when the viscosity of the liquid is high. On other the hand, the turbulent flow is promoted by the following: the jet emerges at high velocity, the surface roughness, any rapid changes in the cross-sectional area and any protuberances projecting in the flowing stream.

$$Oh = \frac{\mu_L}{\sqrt{\rho_L \sigma d_o}} \quad \text{Equation 9}$$

$$Re_L = \frac{\rho_L \, d_o U_L}{\mu_L} \quad \text{Equation 10}$$

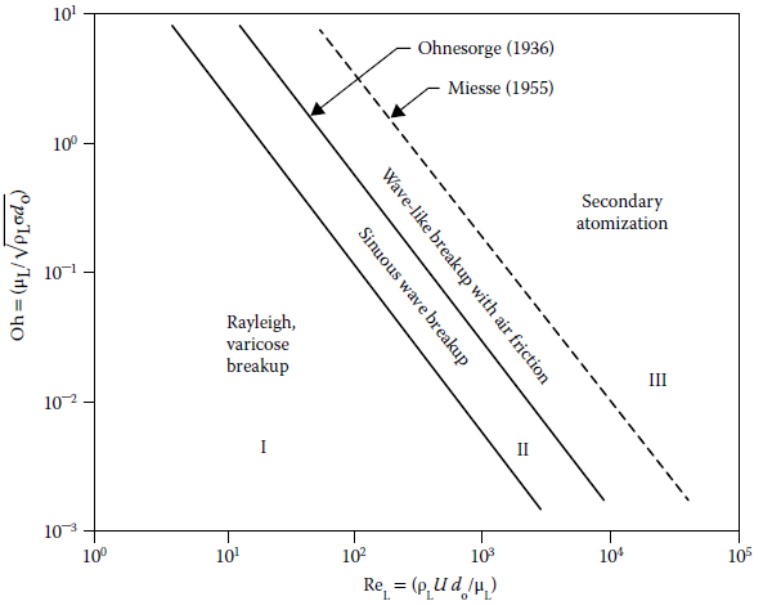

Figure 1.19 Disintegration modes (Ohnesorge, 1936; Lefebvre and Mcdonell, 2017)

The categorization of jet break-up stages is actually based on the formation speed of drops.

1. Stage one refers to the Rayleigh break-up mechanism, in which the jet is disintegrated in large drops of uniform size at low Re number
2. In mid-range Re, jet oscillations begin to occur and their magnitude grows with the resistance of air until the jet is completely disintegrated. The drops that are produced have a wide range of size
3. At high Re, the jet is entirely disintegrated and atomization is completed as soon as the jet emerges from the nozzle

Plain Jet in Crossflow

The injection of a liquid jet in a high-velocity gaseous medium is considered to be useful in numerous fuel injection applications such as gas turbines or afterburners. The fuel atomization quality is likely to be improved by the radial fuel injection in a crossflow airstream. Many theoretical, experimental and numerical studies have been carried out in order to predict or correlate the various characteristics of a liquid jet in a cross-stream for many practical applications. The experimental studies that have been accomplished, mainly focus on the trajectory of the jet in the flowing stream, the break-up processes that are involved and the characteristics of the spray such as penetration, patternation, dispersion, cone angle, mean drop size and drop size distribution mainly.

When a liquid jet is perpendicularly injected in a uniform crossflow airstream, the aerodynamic forces act on the jet's surface and tend to deflect it in the airflow direction. This is one of the simplest forms

of liquid jet injection in a crossflow airstream. The relative momentum ratio of the gas to the liquid phase is of prime importance as the final trajectory of the jet is considerably influenced. High values of this parameter have the tendency to bend the jet and make it follow and crossflow airstream. Also, the cross-sectional shape of the jet is deformed when the aerodynamic forces act on its surface. At lower values, the general behaviour of the jet is similar to that of jet break-up in still air. Respectively, as the instabilities of the jet grow, they result in the jet break-up at a certain distance downstream from the center of the liquid column (Shen, Li and Columbia, 1996). Moreover, the stability curve of a plain jet is shown in Figure 1.20. As it is indicated by this figure, the length of the jet increases proportionally with the jet velocity when the jet is in the laminar region. Any increase of the jet velocity beyond that point causes the break-up point to occur at a lower distance from the outer orifice. As the jet enters the turbulent region, the length of the jet increases.

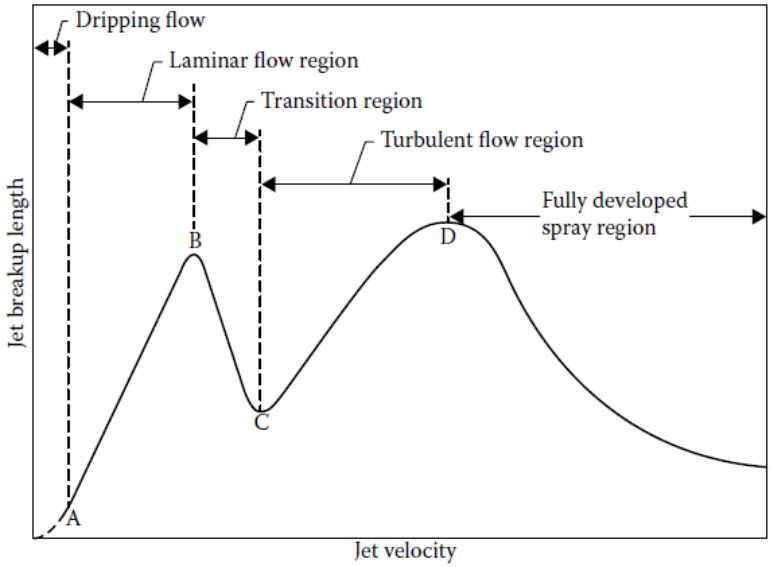

Figure 1.20 Jet break-up length as a function of velocity (Lefebvre and Mcdonell, 2017)

To sum up, the main trajectory of the jet and to the point where the jet breaks-up is a function of the magnitude of the aerodynamic forces that act on the surface of the emerging jet. The point where the break-up of the jet occurs, is frequently referred as the column break-up location. The trajectory of a jet can be effectively described by power law functions which is a result of many experimental and numerical investigations (Sallam, Aalburg and Faeth, 2004; Ashgriz, 2011; No, 2015). Further disintegration of the jet at this point leads to the formation of large drops that are likely to experience secondary break-up and split up to smaller drops. In addition, liquid ligaments or drops may be also detached from the jet before the column break-up location point is reached when the cross-stream relative velocity is sufficiently high. In this occasion, the early detached ligaments and drops may also experience secondary break-up. Finally, a spray plume is formed that consists of liquid particles that

are early detached and those which are formed at the column break-up location point. Also, the penetration of a spray has strong impact on the design of a combustion chamber because its size it is limited. When the penetration length of a jet is long enough, then there is a longer distance for the liquid particles to be pulled off from the main jet column by the cross-stream and as a result, the drop size distribution of the resulting spray is significantly affected. The particle separation at the jet's surface is another important feature that needs to be characterized as they possess an important role in the advection and secondary break-up process.

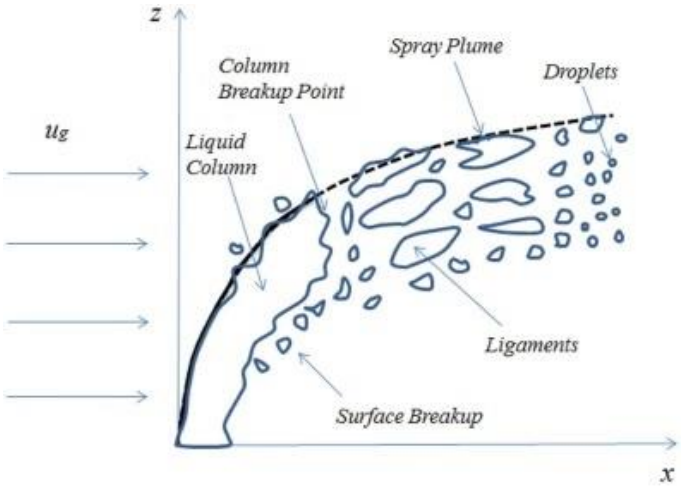

Figure 1.21 Penetration of a jet in a crossflow airstream (Broumand and Birouk, 2016)

1.4.4 Dimensionless Numbers that characterize atomization

Generally, the variables that possess important role in the atomization process of a liquid jet in crossflow are the following:

1. the liquid related parameters are: the jet velocity U_L , the liquid density ρ_L , its surface tension σ, its dynamic viscosity μ_L
2. the gas phase parameters which are: crossflow velocity U_g , the gas density ρ_g and its dynamic viscosity μ_g
3. The diameter of the outer orifice d_o

The parameters and dimensionless numbers that are discussed below, are able enough to help understanding the basic physics of the atomization process

- The Mass Flux is defined by Equation 11 as the ratio of mass flow rate to the unit area or can be also defined as the product of density to the average flow velocity

$$G = \frac{\dot{m}}{A} = \rho U \quad \text{Equation 11}$$

- The liquid momentum to the gas phase ratio expressed by Equation 12

$$Q = \frac{\rho_L U_L^2}{\rho_G U_G^2}$$ Equation 12

This dimensionless number indicates the momentum inflow ratio of the jet to the gas. This parameter has a key role in order to predict the trajectory of the jet. When this parameter is high enough, the jet penetrates downstream at a further distance from the outer orifice and the liquid column bends less, while if it is lower, then the slope of the jet trajectory increases.

- The mass flow ratio of gas to the liquid phase expressed by Equation 13

$$q = \frac{\dot{m}_G}{\dot{m}_L}$$ Equation 13

This parameter indicates the mass flow ratio of gas to liquid. When this value is high, means that the gas mass flow is higher than the liquid jet mass flow. Thus, the jet is rapidly disintegrated and a spray is formed and its dispersion is increased. Low values of this parameter, indicate that the liquid jet is almost uninfluenced and is discharged as a liquid column.

- The Weber number expressed by Equation 14

$$We_i = \frac{\rho_i d_j U_i^2}{\sigma}$$ Equation 14

The Weber number is capable of providing a measure of the relative importance of the gas inertia to the liquid surface tension. The number has a key-role which helps understanding the sizes of the drops that are produced by the different break-up mechanisms. This parameter has secondary effect on the trajectory of the jet but, when it comes to high-pressure flows this parameter becomes more important.

- The Reynolds number of a fluid that is expressed by Equation15

$$Re_i = \frac{\rho_i d_i U_i}{\mu_i}$$ Equation 15

The Reynolds number is of great significance in the characterization of drop sizes, velocities and the break-up locations. It can determine the flow state of the liquid jet or the gas flow, which is either laminar or turbulent.

1.5 External Spray Characteristics

1.5.1 Generally

In the most applications, the main target of the atomizer is not only to disintegrate a liquid in small drops, but also to produce a spray pattern which is uniform and symmetrical. For instance, the Plain-

orifice atomizers produce a spray which can be described as solid, as they tend to produce a narrow spray cone angle that is constituted by an equal dispersion of drops. Solid sprays, can be also produced by pressure-swirl atomizers but, they form a spray that has a hollow cone spray pattern of wide angle with the drop distribution to be concentrated mainly at its periphery. The drops that are formed in the two types of atomizers have the tendency to preserve the initial direction of motion of the emerging jet. The main body of the spray that is formed, due to the air resistance, it is surrounded by fine drops that lost their initial momentum and their further dispersion is mainly depended on the airflow pattern that are exposed to. The spray that is produced by Plain-orifice atomizers has a small proportion of drops that are experiencing air resistance effects due to their narrow spray angle, thus, the whole spray distribution follows the direction of motion that is given to it initially. On the other hand, with twin fluid atomizers, Air-assist or Air-blast, the drops are transported away at their inception by the internal airflows of the configuration of the nozzle, therefore, the trajectory of the final spray is affected. A common feature between twin-fluid and Plain-orifice atomizers is that they have low sensitivity control of the spray geometry characteristics to the physical properties of both phases. However, in the pressure-swirl atomizers the situation is totally different. The initial spray cone angle that is formed is strongly influenced by various factors such as the design features of the nozzle, the operating conditions and the liquid properties. Also, even if the liquid is discharged into still air, the core of air that is generated within the atomizer, has a major impact on the spray structure that is formed. The initial conical sheet is produced by the exposure of the liquid to the surrounding medium, thus, any further exposure of the liquid to the air augments the atomization quality. This is one reason that makes the spray cone angle to be such a significant characteristic of the pressure-swirl atomizers.

1.5.2 Main Characteristics of the Spray

The main characteristics of the spray are presented below:

Dispersion

Dispersion of a spray can be defined in many ways. If the liquid volume within the spray is known, then the degree of Dispersion can be expressed as the ratio of the spray volume to the liquid volume which is contained in it. When the dispersion is sufficient enough, the liquid is rapidly mixed with the surrounding medium, which subsequently leads to higher evaporation rates. For example, with Plain-orifice atomizers, the dispersion is not much as the spray angle is narrow. With Pressure-swirl atomizers, the dispersion is mainly affected by the spray characteristics such as the mean drop size and drop size distribution and the spray cone angle while the physical properties of the two phases

have less impact on it. To sum up, the dispersion is promoted by the factors that increase the spray cone angle.

Penetration

The spray penetration can be defined as the maximum distance that can be reached when a spray is injected into quiescent air or a crossflow airstream. When a spray is injected into a gaseous medium, the relative magnitudes of the initial kinetic energy of the liquid jet and the aerodynamic drag, govern the penetration. At the nozzle exit, the jet has quite high velocity but as the liquid moves to a further distance from the outer orifice, the surface area of the spray is increased and the kinetic energy of liquid is continuously decreased by the gas aerodynamic friction. When the kinetic energy of the drops is completely dissipated, then their trajectory is mainly depended on the flow state of the surrounding medium. For example, if the drops are exposed to quiescent air, then gravity controls their trajectory, but, if the spray is injected into a flowing stream, then their trajectory is mainly depended on the airflow pattern. On the other hand, if the spray is injected into a crossflow air stream, then, the spray will follow the flow stream direction and a curved trajectory will be formed. Generally, penetration is promoted by a compact, narrow spray while, a wide cone angle well-atomized spray, experiences more aerodynamic resistance thus, its penetration is sufficiently lower.

Cone Angle

The spray cone angle is an important characteristic that describes the external spray behaviour. When a spray interacts with the air, its boundaries become curved, therefore, this makes the cone angle measurement quite difficult to be determined. There are many ways that a spray cone angle can be determined. Firstly, one method comprises that the spray cone angle can be evaluated by drawing two straight lines from the outer orifice to the cut the spray contours to a determinated distance from the face of the atomizer. Moreover, by recording images of the spray silhouette in proper magnification, the spray cone angle can be measured. Alternatively, the spray measurements can be made at specified axial locations, therefore the spray profile is to be defined. One technique relies on the contact of two probes to the spray edges. The two probes are evenly spaced to the centreline of the nozzle and they move until they contact the spray edges. In another technique with Pressure-swirl atomizers, the probe positions are determined by linear variable displacement transducers, which calculate the spray cone angle and the skewness about the its axis. However, it is quite difficult to determine the spray cone angle, thus, significant efforts of creating a standard measuring protocols have been made. Thus, when measuring the value of the spray cone angle, the exact descriptions of how these values were determined should be stated.

Patternation

The symmetry of a spray pattern that is produced from each atomizer is considered to be a significant parameter in many practical applications. For instance, in spray drying applications, if the spray pattern is asymmetric, then the gas and liquid aren't properly mixed, therefore, this leads to reduced process efficiency and the lower product quality. Applications that definitely require a uniform spray pattern are not only painting and coating of surfaces but also combustion applications. For example, combustion systems such as oil burners, demand uniform fuel distribution to achieve higher combustion efficiency and reduced emissions. The spray asymmetry is visually detected only when the problem is severe, otherwards quantitative determination of the spray pattern should be imposed to improve the nozzle design and therefore higher quality control in certain applications.

Liquid Distribution

The liquid distribution within a spray can be determined by measuring the radial and circumferential direction of its patternation. A typical patternation apparatus has some collection tubes which are equally distanced and are oriented in the radial direction of the spray. Typical patternator device is illustrated in Figure 1.22. Before taking any samples, the device should be drained without any liquid left in the sampling tubes. When the flow rate is adjusted and the desired conditions are reached, then the patternator is rotated to an upright position and the sampling tubes are filled with the liquid. Then, when one of the tubes is about 75% filled, the liquid supply is turned off and the device is rotated for about 30° until a thin metal plate which is a part of the patternator, to block the spray and avoid any liquid dribbling. The volume of the liquid is measured by visual inspection usually with the location of the meniscus between the lines, thus the radial distribution curves are plotted as a function of the liquid volume collected the angular location of the sampling tubes. This type of plot, indicates of how the operating conditions affect the collected liquid volume in every single location of the spray. Nevertheless, comparisons between flowrates at different angular positions on the same curve are not feasible, because all sampling tubes have the same size to measure specific volumes. A drawback of this method is that, the sampling tubes that aren't oriented in the center of the spray, tend to collect less liquid than those which are in the middle. Therefore, area weighting factors are used, which, represent the required total sampling tubes to measure the liquid at specified distances from the center of the spray. Thereafter, the corrected liquid volumes are added and the total liquid amount is calculated. If the corrected volume is divided by the total volume, then the percentage of the total spray volume is calculated at each angular position, consequently, a corrected liquid distribution curve is obtained.

Also, the equivalent spray angle is introduced, to describe more precisely the influence of the operating parameters on the liquid distribution. This is useful because the radial distribution curve is

reduced to only one numerical value, which is the equivalent spray angle. The equivalent spray angle ϕ_k can be calculated by as the sum of the two angles, the left and right hand of the liquid distribution curve Equation 16. In fact, the actual meaning of the ϕ_k, is that the θ value reflects to the mass center position of a material system for each side, left or right, of the liquid distribution curve. Moreover, the quantitative measurement of the circumferential liquid distribution is an important parameter that should be evaluated as well. A method of measuring the symmetry of a hollow-cone spray pattern that originally came from the gas turbines applications many years ago, comprises that a vessel is placed under the atomizer, where the spray is collected into a cylindrical tray. This tray is separated into a certain number of pie-shaped sectors which, each one of these sectors ends up to separate sampling tubes. In addition, the patternator should be properly adjusted to make sure that the spray is entirely collected. The sampling measurement is completed when one of the sampling tubes is almost full. When the liquid collection procedure is accomplished, the tubes are separately measured and recorded. Additionally, the statistical properties of the sampling tubes are extracted, where any spray circumferential irregularities can be detected by the normalized standard deviation. Nowadays, modern optical techniques have been developed such as the extinction tomography. This method is very handy because is able enough to provide quite reliable results, as a mechanical device would do.

$$\varphi_k = \frac{\sum y\theta \sin(\theta)}{\sum y \sin(\theta)} \quad \text{Equation 16}$$

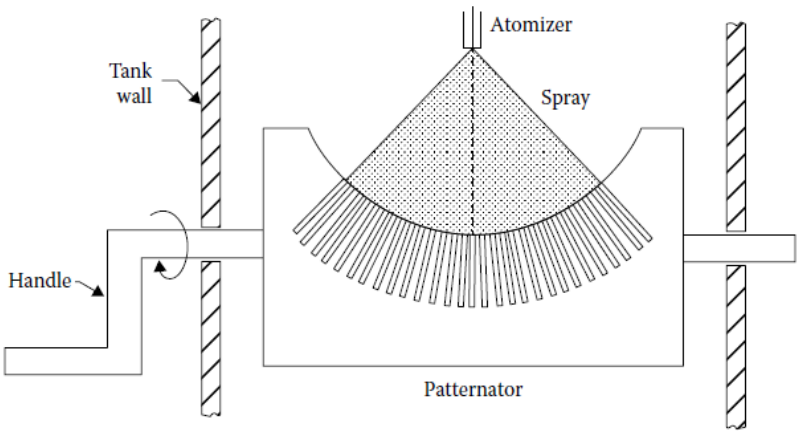

Figure 1.22 Patternator device (Lefebvre and Mcdonell, 2017)

Factors that affect Spray Patternation

Generally, the causes of poor patternation are mainly caused either by the apparatus or the sampling method used. For example, the nozzle must be exactly placed to the center of the collecting tubes and to have proper distance from it, as the entire spray have to be collected. In addition, when the liquid flowrate is high or even with Air-Blast atomizers when the air velocity is sufficiently high, then, the splashing effect in the collecting tube may affect and counterfeit the obtained results. This difficulty

can be overcome by using a patternator that has deep enough collection tubes. Sometimes, it was observed that extremely low liquid flowrates also affect the symmetry of the pattern as the spray was not fully developed. In addition, the circumferential patternation is easily affected in some specific atomizer types. For instance, the patternation of Simplex atomizers has a correlation with the eccentricity degree between the inner swirl chamber and the outer orifice. Moreover, the quality of the nozzle has prime importance as the spray patternation is considerably decreased by factors such as poor surface finish, the imperfections of the orifice and the plugged flow passages mostly.

1.6 Hot-wire anemometry

Hot-wire anemometry is a technique that is used for measuring velocity. This technique can be very effective in a wide speed ranges which also includes both, subsonic and supersonic flows. This technique possesses some good features such as flows with high turbulence can be detected effectively with a fair spatial and time resolution. The basic operating principle of the hot-wire is that the sensor relies on heat transfer changes when is exposed to a flow. Moreover, the electric resistivity of the (5μm diameter and about 0.5–2mm long.) sensor material used is a function of temperature. The hot-wire usually has a cylindrical shape which has extremely small thermal inertia, thus high dynamic response is achieved. The most popular operating methods of hot-wire anemometry are: the constant current (CCA), constant temperature (CTA) and constant voltage (CVA) (Tropea, Yarin and Foss, 2007). The CTA method can be also inferred as constant resistance method as it tries to maintain the resistance of the sensor constant by adjusting the voltage at the edges of the sensor when it is exposed to a flow. Also, with this method temperature changes in turbulent flows can be measured. In this case, a feedback loop tries to keep constant the temperature of the sensor and so the thermal inertia which is automatically compensated (Tavoularis, 2005). The heat that is introduced in the sensor is cooled down mainly by the forced convection mechanism. The heating rate at the sensor is equal with the product of the sensor resistance to the square of the current intensity that passes within it. Thus, the cooling rate of the sensor is a function of the form of $(T_w-T_a)\phi_{conv}$ (U). The T_w refers for the sensor temperature, T_a for the unheated sensor temperature which is the ambient temperature. The term ϕ_{conv}(U) refers for the forced convention effect which is primarily depended on the fluid velocity normal to the wire. The temperatures that correspond to the heating rate are: the sensor temperature when the wire is heated and at the same location when the wire is unheated. Actually, the unheated wire temperature is equal with that of the surrounding medium temperature. Furthermore, a parameter that is worth mentioning is the overheat ratio. This ratio has for numerator the difference between the heated and the unheated resistance and as a denominator the unheated resistance. For practical applications, this ratio is recommended to be in a range of 0.05-1 for air or

other gases, otherwise the sensor can be permanently oxidized or deformed. More generally, the greater the overheat ratio is, the higher frequency response is but the life of the wire shortens. However, for air, most of the manufactures recommend a value of overheat ratio 0.8. The mean flow velocity and the velocity fluctuations that are in the axial direction of the flow can be detected, as any fluctuations in the other directions are considered neglected because they behave as second order terms Figure 1.23.

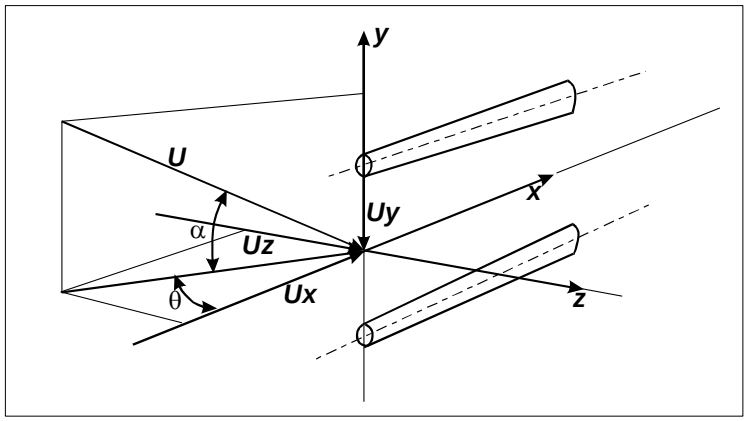

Figure 1.23 Single hot wire (Dantec, 2002)

The main components of a CTA circuit are a Wheatstone bridge and the feedback amplifier Figure 1.24. The probe is connected on the one arm of the bridge and any differences in voltage are instantly measured. More specifically, any resistance variations of the wire due to the velocity fluctuations corresponds to voltage differences which are the input to the operational amplifier. The top bridge voltage is increased when the flow velocity is increased or when the temperature of the fluid is decreased, thus the intensity of the current that passes through the wire is increased. There is also an output current feedback to the top of the bridge, to restore the resistance of the wire. The current that returns back from the feedback amplifier passes through several stages of voltage gain and a unity-gain current booster. Another parameter that has an important role in such circuit is the bridge ratio $\frac{R_2}{R_1}$. Usually, a ratio above one is chosen, for example 5,10,20 and the R_1 is frequently selected to be quite large 10Ω,20Ω. In this way, the current that passes through the amplifier enters the active arm which is the one that the probe is connected. Therefore, the voltage at the top of the bridge is increased and the voltage acquisition is easier. The overheat ratio can be regulated by properly adjusting the resistance R_3.

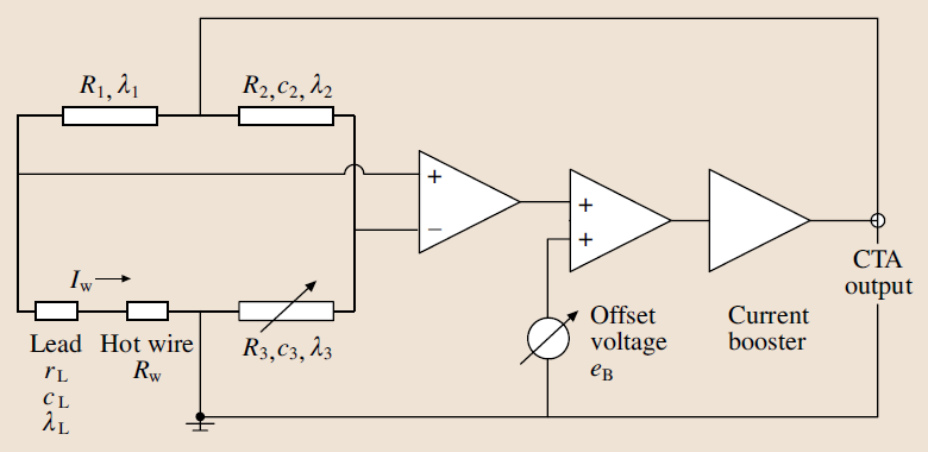

Figure 1.24 CTA block diagram (Tropea, Yarin and Foss, 2007)

1.7 Direct Shadowgraphy

1.7.1 Generally

Generally, the rays of light that are emitted from a source remain unbent or do not cross each other unless they are disturbed. To begin with, shadowgraphy is a technique that is used to visualize phenomena such as the spatial density variation in transparent media. Most common transparent medium can considered the air (Emberson *et al.*, 2016). The shadowgraph method has some essential features such as a point shaped source of light, a schlieren object that is exposed to the light rays and a reflective screen where the exposed to light object is casting a shadow. In this way, the emitted light is transmitted through the schlieren object and a shadow pattern can be observed at a certain distance behind the object Figure 1.25. Nowadays, shadowgraphy is based on precise lens and high-speed cameras in order to capture the refractive disturbances in the transparent medium (Settles and Hargather, 2017).The shadow of the schlieren object can be recorded with a camera instead of being showed on a screen. The camera lens is focused on the recording plane which is at a certain distance from the schlieren object, therefore, in the shadow picture the object is not in focus. If the object was absent, then, the light would be uniformly illuminated on the screen (Settles, 2001). However, if the object is present, some of the light rays are refracted, bent and deflected to another path than their original. The light that has suffered refraction through an angle, reaches the reflective screen at a new displaced position. The new displaced position is being illuminated with extra light, while the previous point is being illuminated with less light. Therefore, optical inhomogeneities redistribute the illuminance of the screen and the shadow of the schlieren object is different than the shadow of the solid object.

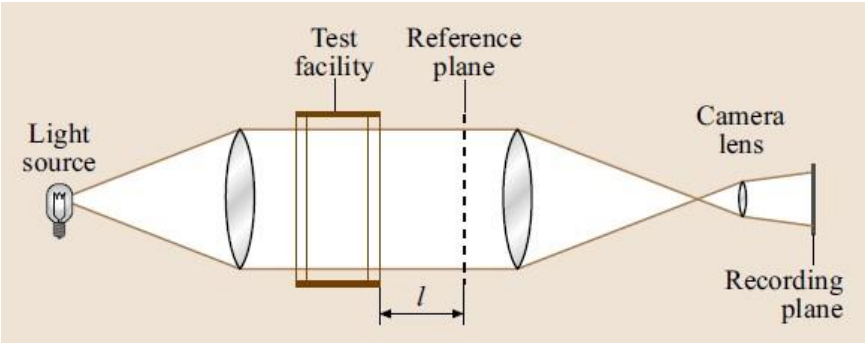

Figure 1.25 Shadowgraphy typical setup (Tropea, Yarin and Foss, 2007)

To avoid the optical inhomogeneities, a lens that aligns the emitted light can be added. As a result, the light rays have the same parallel direction until the schlieren object is reached (Rasenat, G. Hartung and Rehberg, 1989). Even more, the light is evenly illuminated on the screen or camera when the schlieren object is absent. Any relocation of the light source further or closer to the lens, has the same effect with the added lens because the light diversion is avoided. Moreover, not only in the lab but also in the daily life a shadow picture of a flow can be noticed. For example, the most common shadow is that of a heat source that is projected by a lamp on a window or on a wall such as the shadow of a candle. Another example that is mainly observed during winter is when the emitted heat from a radiator is projected on the wall by the sunlight.

1.7.2 Shadowgraphy in Atomization Process

The shadowgraphy as explained above, is a great tool that many researches (Watanawanyoo and Hirahara, 2011; Stevenin *et al.*, 2012; Crua, 2014) have used in order to observe the characteristics of the atomization process. Generally, this method is quite reliable when it comes to the observation of liquid structures, obtain particle sizes and droplet distribution, jet or spray penetration, jet trajectory, column break-up and many other characteristics of the atomization process. By recording a great number of instantaneous images, results in a more reliable averaged values of the acquired data. This may be quite useful because it provides a better understanding of how the process is evolved.

1.8 Thesis Aim

Since the atomization process in general has a fundamental role in combustion applications such as fuel injection in gas turbines, the exact knowledge of how this process evolves under certain conditions is of prime importance. Nowadays, the planet mainly suffers from the excess amount of pollutant combustion products that are emitted in the atmosphere. By increasing the combustion efficiency and improving the atomization quality can reduce the environmental effects. As far as concerning the current investigation, the goal is to examine the behaviour of a liquid jet and a spray

for a range of different flowrates when injected into a uniform crossflow airstream. An effort is made to conduct a parametric investigation of the jet and spray behaviour with dominant parameters the aerodynamic Weber We, the air to liquid momentum ratio Q and the mass flow ratio q. The range of the examined flowrates consists of different liquid flowrates, different crossflow velocities and different amounts of atomizing air that are expressed with the above dimensionless numbers. Moreover, an attempt is made to extract empirical correlations that are based on the experimental data. The characteristics of the jet that are of interest are the trajectory of a jet, the penetration in the flowing stream and the column break-up location. In the current investigation, the spray characteristics that have been examined are the spray cone angle. In general, water as the dispersed phase has similar properties with the light aviation fuels so it can be considered as a reasonable alternative (Lefebvre and Ballal, 1988; Lefebvre and Mcdonell, 2017, p. 8). Thus, the examined range will provide a better view of how each variable affects the spray characteristics and provide insight of the behaviour of injection in gas turbine applications under variable conditions.

2. Experimental Apparatus, Methods and Procedures

2.1 Generally

In this chapter, the experimental apparatus, the equipment and techniques that are used for the measurements are described by the following sub-sections. The experiments were conducted in the Fluids and Turbomachinery Lab of Mechanical Engineering Department of University of Thessaly. In this experimental investigation, an Air-assist atomizer is used to produce a spray in a crossflow airstream. First and foremost, the initial crossflow flow profile had significant flow fluctuations than the accepted (Hancock and Bradshaw, 1980) (initial turbulence within the flow was about 5%), so an effort is made in order to reach a straight smooth profile without any intense fluctuations within the circular duct. Hot-wire anemometry is used to precisely detect the crossflow flow profile and measure the flow fluctuations. The flowrate of the emerging liquid jet is measured and then it is calibrated with a pressure sensor in order to extract a relation between flowrate and liquid injection pressure in this configuration. Shadowgraphy is also used in order to process the obtained data and detect the characteristics of the spray. The characteristics that are of interest are the column break-up location, the jet trajectory and the spray cone angle of the average spray.

2.2 Test Conditions

The properties liquid properties and the experimental test conditions of the current investigation will be presented in Table 2.1. The experiments were carried out in atmospheric conditions. Instead of using kerosene or other hydrocarbon fuels, purified water is used as a safe alternative.

Table 2.1 Properties

Property	Purified Water	Ambient Air
ρ ($\frac{kg}{m^3}$)	1000	1.204
μ ($Pa\ s$)	0.001	$1.83 \cdot 10^{-5}$
σ ($\frac{N}{m}$)	0.072	
T (°C)	20	
P_{atm} (Bar)	1.01	

The examined flow conditions of the current investigation are shown below Table 2.2. The geometrical configuration and the working fluids were kept constant, while the fluid flowrates varied. The Ohnesorge number is 0.0058 which indicates that the viscous effects are low.

Table 2.2 Test Conditions

Blower Frequency Hz	0,15,30,45
Crossflow Velocity $\frac{m}{s}$	0-9.79
Liquid Pressure Diff Bar	Atomizing Air flowrate $\frac{L}{min}$
0.06	0,8
0.085	0,8,9
0.15	0,8,11
0.22	0,8,11
Q (momentum flux ratio-gas to liquid)	$4.24 \cdot 10^{-4}$-$163 \cdot 10^{-4}$
q (mass flow ratio-gas to liquid)	0.22-0.51
Jet Velocity ($\frac{m}{s}$)	2.46-5.52

The dimensionless numbers of the flow conditions are presented below Table 2.3,Table 2.4.

Table 2.3 Crossflow Conditions

$U_g \frac{m}{s}$	Re_g	We_g
0.00	0.00E+00	0.00
3.26	2.54E+04	0.07
6.53	5.08E+04	0.29
9.79	7.62E+04	0.66

Table 2.4 Liquid Flow Conditions

Mean Pressure differential bar	U jet $\frac{m}{s}$	Re_l	We_l
0.061	2.52	1031	36.0
0.086	3.08	1262	54.0
0.160	4.40	1803	110.2
0.231	5.44	2232	168.7

2.3 Experimental Arrangement

2.3.1 Circular duct and Blower

The experimental apparatus is shown in Figure 2.1. The diameter of the circular duct is about 12cm and its total length of 1.5 meters. Within the duct, 7 screens in total and 1 honeycomb are placed to straighten the flow profile to reduce velocity fluctuations. A triple screen is placed at a distance of $30cm$ from the exit of the centrifugal blower and the honeycomb at a distance of about 70cm from the triple screen. The honeycomb length is 6cm and the cells within the honeycomb are of cylindrical shape with a diameter of 5.5mm. After the honeycomb a distance of about 12cm is left and the four successively screens are followed with a distance of about 3.5cm between them. The four successively screens within the duct are being supported by a 3D-printed object Figure 2.2 and a piece of PVC duct of about 3.45cm is cut in order to piece together each screen. The size of the screens is 16x16. Then, a distance of 30cm after the last screen follows. A honeycomb within the flow is useful because it contributes to straighten the flow, reduce the large-scale turbulence and to remove any swirl of the flowing air. Therefore, the swirling motion produced by the centrifugal blower is almost eliminated which leads to a reduced lateral velocity (Bradshaw and Pankhurst, 1964; Mehta and Bradshaw, 1979). The screens within the flow can also reduce the amount and scale of turbulence and decrease any non-uniformities (Santos *et al.*, 2016). Moreover, a honeycomb is found to be effective in reducing the lateral turbulence more than the axial turbulence, while, the screens promote the reduction of the axial turbulence. The screens are less effective than a honeycomb in reducing the lateral turbulence (Bradshaw and Pankhurst, 1964). The distance among screens was chosen to be about 3.5cm which is a bit above the minimum 20% of the hydraulic flow diameter which is recommended by the investigators (R.D. Mehta, 1977; Welsh, 2013). The blower is a Siemens D-97615. The rotational velocity of the motor is controlled by a Siemens Micromaster 420 inverter. Using hot-wire anemometry the crossflow profile is measured and will be presented within the next sections.

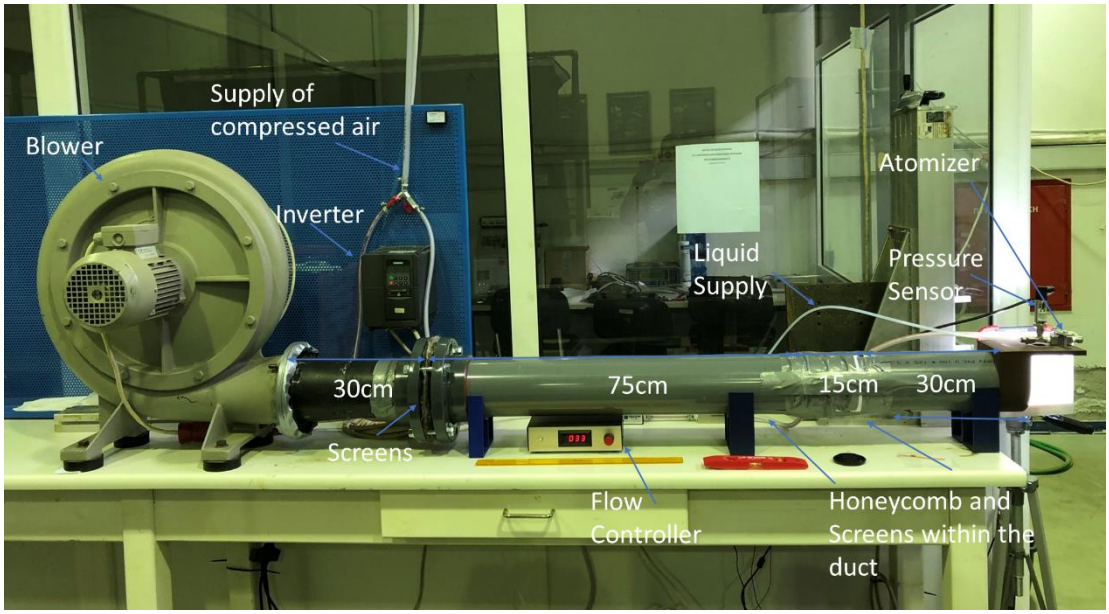

Figure 2.1 Experimental Setup

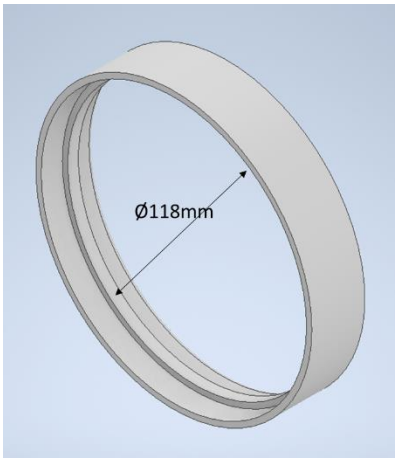

Figure 2.2 Screens Support

2.3.2 Atomizer

In the current experimental investigation, an external mixing air assist atomizer of Spraying Systems B1/4J-316SS is used Figure 2.3. The nozzle diameter is 0.41mm. The atomizer is placed on a 3D-printed custom base which is fitted on the circular duct. The atomizer is mounted on the custom base at a distance of 8cm from the exit tip of the main duct and the tip of the atomizer is exposed in the crossflow airstream at a distance of 1.5cm. Moreover, a pressure tank Figure 2.4 is used to have constant liquid pressure supply which for the current experiment is set at 2Bar. The model of the pressure tank is a Spraying Systems 22140 which is connected to the main pressure supply of the lab. The pressure within the tank can be controlled with a pressure regulator and the liquid flowrate of the emerging jet can be controlled with a flow controller. The pressure regulator used is an R27 Precision

Pressure Regulator while the liquid flow controller used is an Entegris 6500-T2-F02-B06-M-P2-U1. Also, an Omega XM319-3.5A10V pressure transducer is used to measure the exact injection pressure of the liquid. Another pressure regulator is used in order to control the amount of air that is used in order to produce the spray. More specifically, a Cole-Parmer Digital Pressure gauge is used in order to have exact knowledge of the air flowrate that passes through the outer orifices of the atomizer. This instrument is able enough to measure with high precision the air flowrate at standard litres per minute.

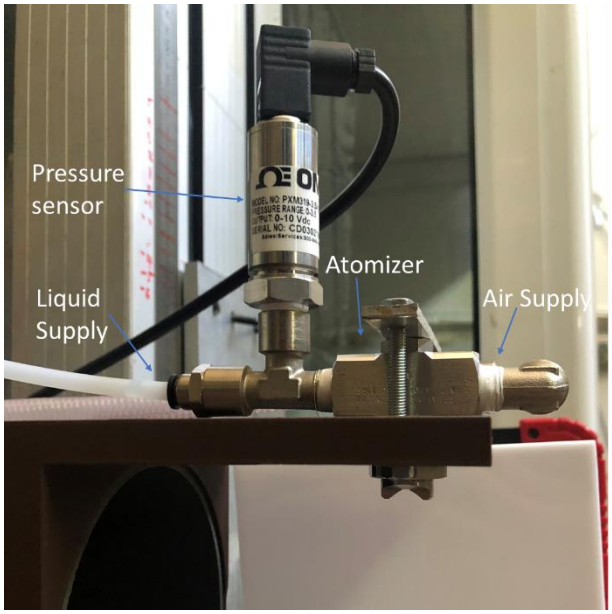

Figure 2.3 Atomizer

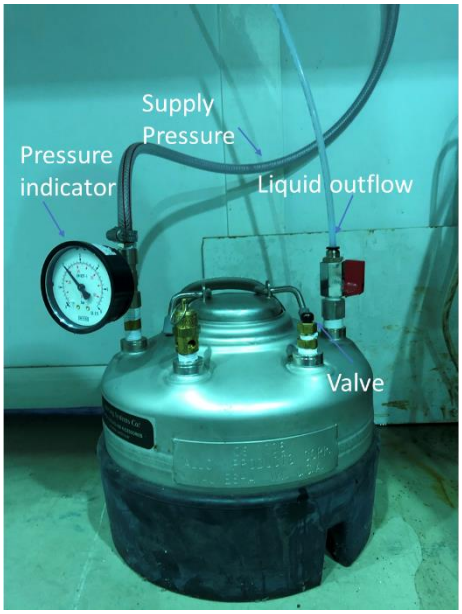

Figure 2.4 Pressure Tank

2.3.3 Camera and Illumination

The CCD Camera in a solid-state electrical device while the letters correspond for ‘charged coupled device’. The CCD camera is actually an integrated circuit that is etched onto a silicon surface and forms elements that are sensitive to light. The name of ‘charged couple device’ is given because of the conjugation of electrical potentials that are in the chemical structure of the silicon material. These elements are called pixels which comprise the chip layers. When this surface is sufficiently illuminated, the electrons can be captured successfully. The electronics of the can convert the light input to an electronic signal (L’Annunziata, 2003). The liquid jet injection is a phenomenon that requires a camera to capture it. The CCD camera used here was a TSI Powerview plus HS-200. The camera is mounted on a tripod and the camera has a SIGMA 70-200mm F.2.8 APO lens attached. The camera was controlled with the TSI Insight 3D program using a computer. The resolution of the camera is 2048x2048 with a resolution of 12-bit intensity dynamic range. However, a 512x512 resolution is used in order to minimize the size of the image and increase the illumination of image. The camera was operated at 6fps. To capture this phenomenon the ideal exposure time was about 1µs but the minimum the camera can take is 80 µs. The illumination source was a LED light of 450 lumens XW 750 Dekton that was mounted on a tripod that was behind the liquid jet so the shadow of the jet was captured by the camera. Moreover, a square light diffusing background was used in order to provide a uniform light distribution and to eliminate the excess illumination near the LED source. The diffusing screen was mounted on a 3D printed support which was placed on a tripod. The camera and illumination arrangement are shown below Figure 2.5, Figure 2.6.

Figure 2.5 CCD Camera with Lens

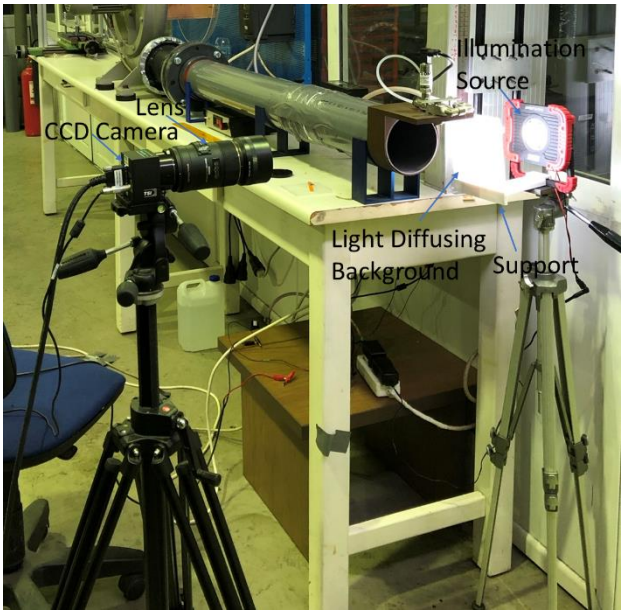

Figure 2.6 CCD Camera and Illumination source

The camera was aligned in order to capture the structures that are of interest. Before and after each data acquiring procedure, a number of 200 images of the focused area without any liquid injection were recorded to obtain the background. Furthermore, in order to correlate the pixels of the captured image with physical dimensions of the imaged area, a ruler with a scale was exposed in the background image. For each flow condition, 2000 images were captured. As mentioned above, the shadowgraphy technique is employed. The captured images showed that the atomization of a liquid jet in a gaseous medium is a complex process in general. Thus, using Octave, an image processing algorithm was developed to extract some of the main statistical properties of the captured images. Each image consists of 512x512 pixels, with each pixel to have a specific value. Thus, an image can be represented as a matrix. An area of about 6cm in total is of interest as the camera focuses on the phenomena that take place near the atomizer Figure 2.7. Through image the calibration procedure, a correlation is made between pixels and real dimensions Figure 2.8.

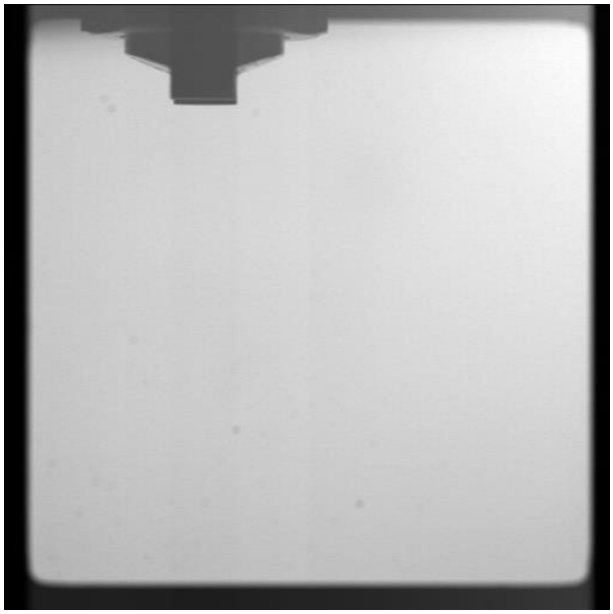

Figure 2.7 Background image of the atomizer

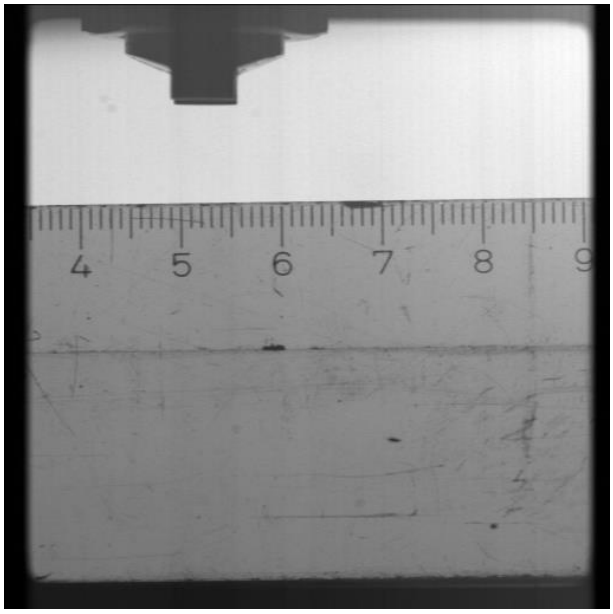

Figure 2.8 Image Calibration

2.3.4 Hot-wire

In the current experimental investigation, a Dantec 55P11 single probe sensor is used and a CTA AA lab systems AN-1005 anemometer Figure 2.9. The sensor that is used, was repaired using new 5µm wire made of Gold-plated Tungsten. To fulfil the need of data acquisition, a National Instruments NI USB-6009 acquisition card is used. The acquisition card was directly connected with a USB port to a PC Figure 2.10.The flow characteristics that are of interest are the mean velocity, the standard deviation of the velocity and the turbulence intensity of the flowing stream. The acquisition card has

an output voltage signal that varied between ±10 V and the AA lab anemometer is capable of having 1 output channel.

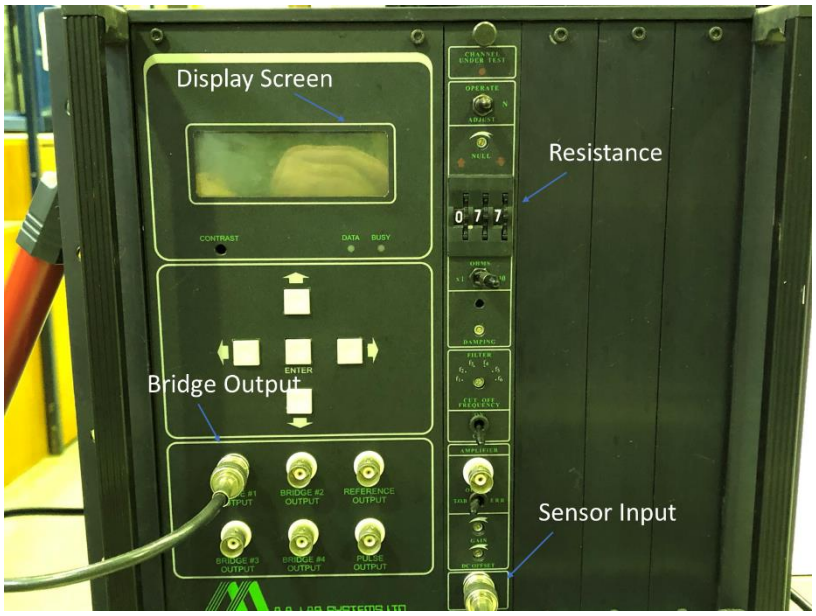

Figure 2.9 AA Lab AN-1005 anemometer

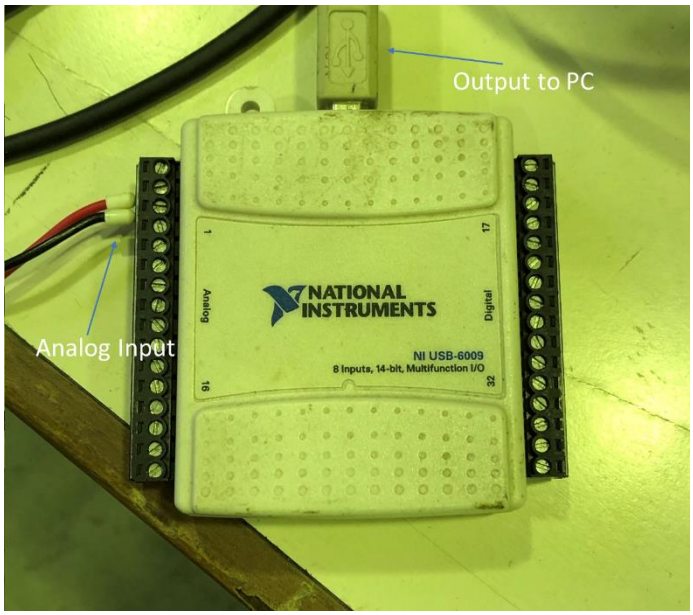

Figure 2.10 Acquisition Card NI 6009

First, the cable resistance was measured using a shorting probe 55H30 Figure 2.11 and then the hotwire was connected to adjust the parameters such as the overheat ratio, damping, gain and DC offset.

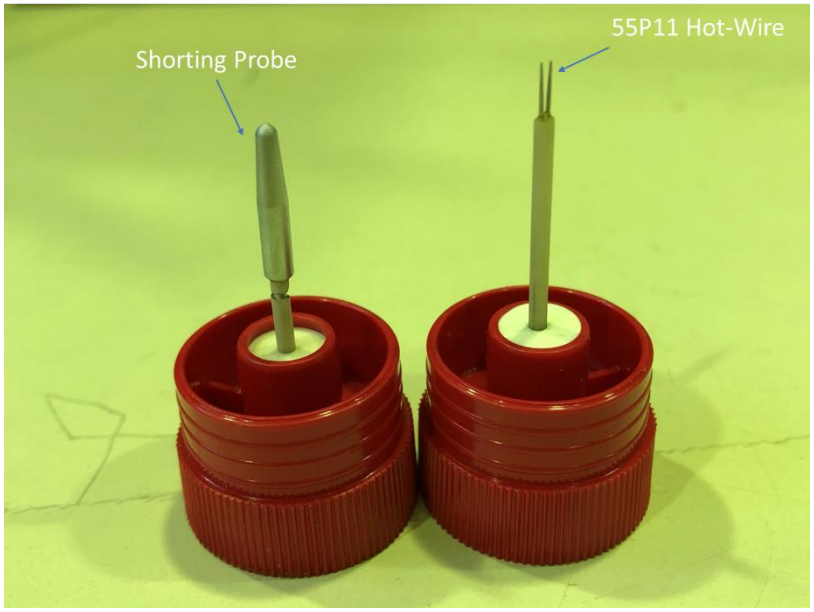

Figure 2.11 Probes

The overheat ratio was chosen to be 1.8 as most of the manufactures recommend (A.A.LabSystems, 2000; Dantec, 2002; Tavoularis, 2005; Tropea, Yarin and Foss, 2007). The gain value was set to 101.54 and the DC offset to -4.5V. During the calibration, the hotwire was exposed to the maximum velocity of the wind tunnel in order to test the dynamic response of the current channel. Using an oscilloscope, the damping of the hot wire was adjusted in order to match the ideal square wave response Figure 2.12. Thus, the maximum frequency response obtained with the current probe and anemometer is about 50kHz. However, the maximum sampling rate of the acquisition card is 48kHz. Next, the hotwire was calibrated in the freestream flow of the wind tunnel in order to extract a function that relates the output amplifier voltage with the flow speed. Usually, power relationships such as King's law or polynomial fits can describe effectively the relation between voltage and velocity (Dantec, 2002; Tropea, Yarin and Foss, 2007). In this investigation, a polynomial of 4^{th} degree is used. The measurements consisted of 11 different velocities which were repeated three times in order to check the validity of the results. The freestream velocity was measured using a pitot-static tube which was connected with a Wohler DM2000 manometer. During calibration, the hot-wire probe and the pitot-static tube were mounted on a traverse and were placed next to each other in order to measure identical velocity magnitude.

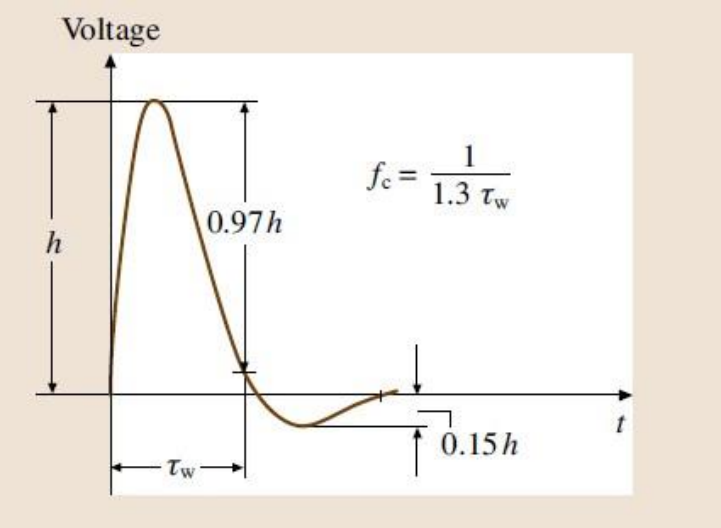

Figure 2.12 Ideal Square Wave test (Tropea, Yarin and Foss, 2007)

After calibrating the hot-wire the calibration curve can be extracted Figure 2.13. The function returns directly the velocity to m/s from the volts measured during calibration. During the calibration procedure, the volt fluctuations measured were below 5mVolts, thus, their contribution can be considered negligible.

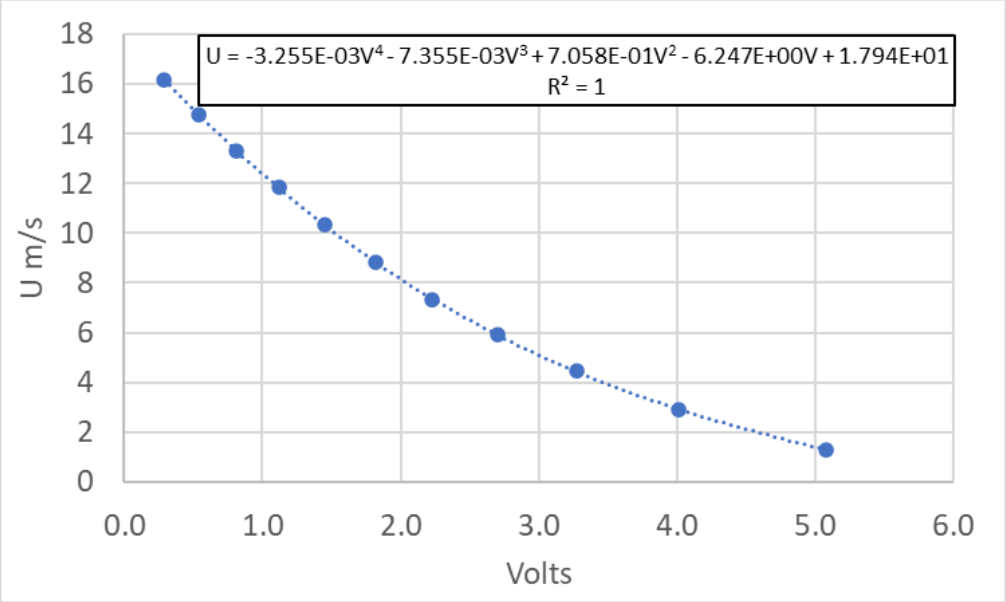

Figure 2.13 Hot-wire Calibration Curve

2.3.5 Calibration of the Centrifugal Blower

Since the hot-wire is calibrated, then it was mounted on another traverse in order to measure the fluctuations within the circular duct. The turbulence measured within the circular duct was about 5% and it cannot be considered as accepted for such experiments (Hancock and Bradshaw, 1980; Selig

and McGranahan, 2004; Santos *et al.*, 2016). Then, after some tests, honeycombs and screens were placed within the flow as described above to minimize the turbulence intensity. The mean velocity of the new profile is illustrated in Figure 2.14, its standard deviation in Figure 2.15 while the turbulence intensity Figure 2.16. The sampling time of the measurements was 20s at a frequency of 100Hz. Moreover, 5 different frequencies of the inverter at height 12 points at each frequency have been examined. Each point has a difference of the previous of 1cm, thus, the point zero refers to the centre of the circular duct. This procedure was repeated twice, and the same results were acquired.

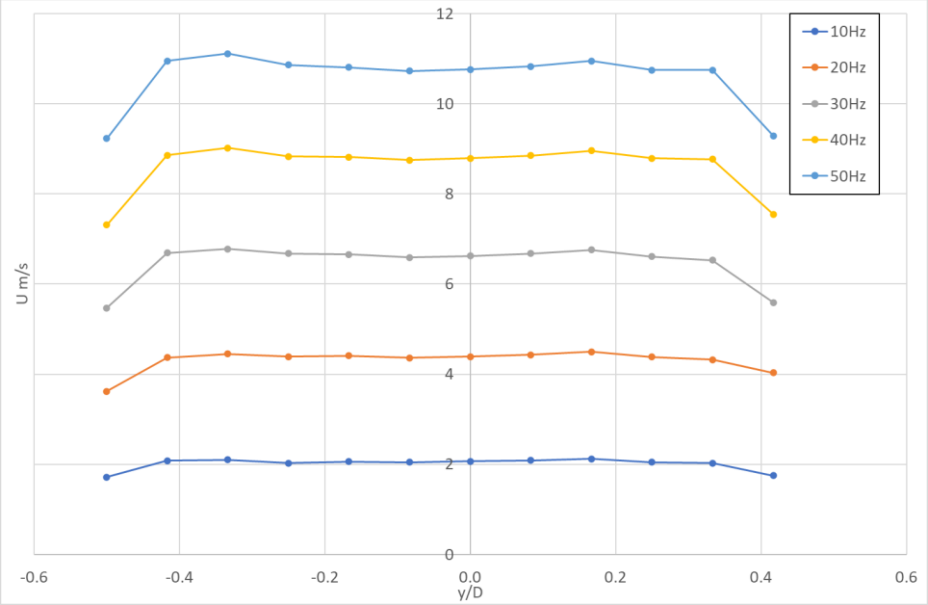

Figure 2.14 Mean Velocity Profile at the exit of the Circular Duct

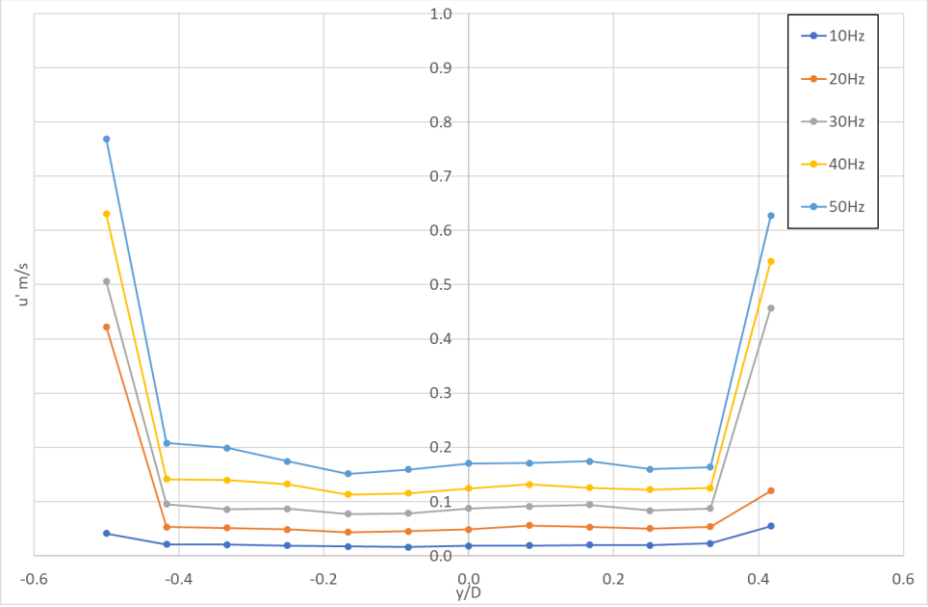

Figure 2.15 Standard Deviation at the exit of the Circular Duct

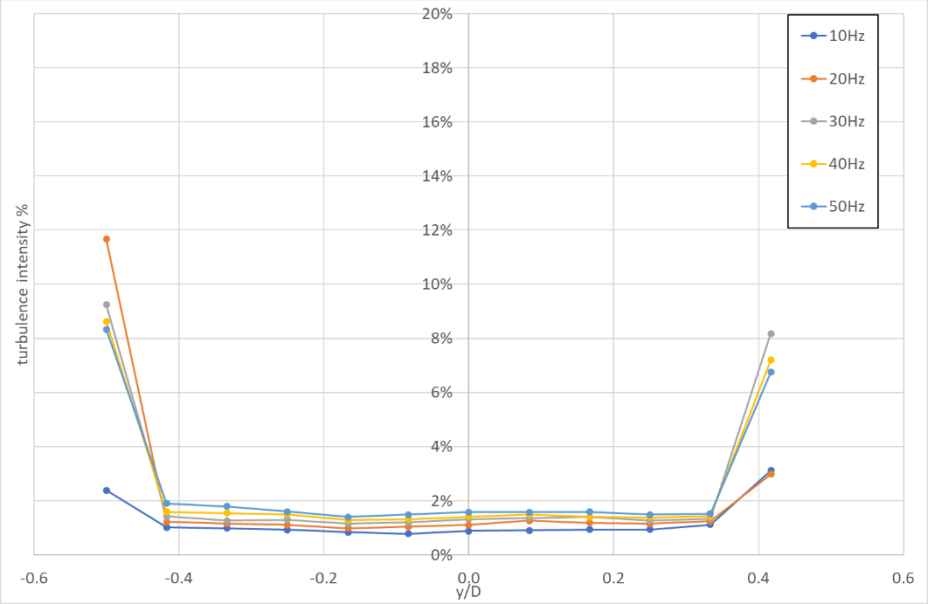

Figure 2.16 Turbulence Intensity at the exit of the Circular Duct

The vertical axes of the first two figures refer to the average velocity and its standard deviation in m/s respectively. The vertical axis of the last figure refers to the turbulence intensity percentage. The turbulence intensity is defined as the ratio of the standard deviation of the velocity u' to mean velocity U. The horizontal axis refers to the height of each point divided by the duct diameter for all the figures. The turbulence in the flow has sufficiently reduced except near the boundaries. In general, the flow profile seems to be quite uniform for all the frequencies of the inverter. In fact, the region of the flow profile that is of interest is the upper region of 5cm. More specifically, the atomizer extends about 2cm in the flow, which means that the spray is injected to a uniform low turbulence cross-stream. The maximum turbulence intensity percentage at the higher inverter frequency is about 1.6% and it can be considered as acceptable (Welsh, 2013; Santos *et al.*, 2016). For lower inverter frequencies such as 30Hz inverter frequency, the maximum turbulence intensity is lower than 1%. Thus, there is exact knowledge of the flow conditions that take part at each inverter frequency. Moreover, the average volumetric flowrate is calculated. Since the crossflow velocity is known, and the air flowrate is proportional to the rotating frequency of the inverter, then a correlation between flowrate and the inverter rotating frequency can be extracted as shown in Figure 2.17.

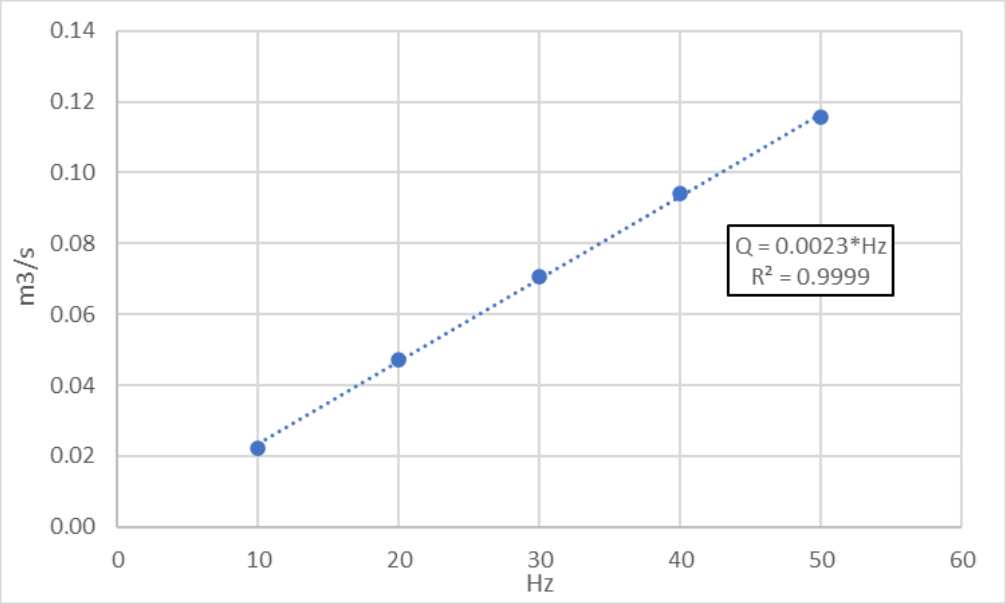

Figure 2.17 Blower Flowrate vs Inverter frequency

2.3.6 Liquid Flowrate Calibration

The flowrate calibration was achieved by using a pressure transducer instead of using the flow controller. This is because desired liquid flow rates were outside the flow controller's normal range of operation and uncertainty was significant. The function between the volts measured with the corresponding injection pressure is known as it is provided by the manufacturer. The function is the following p(bar)=0.3497V. The flowrate calibration procedure was carried out three times in order to check the validity and the repeatability of the results. A volumetric tube was used in order to collect the mass of the emerging jet. The volumetric tube was initially measured using an electrical scale (KERN EMS) and then it was tared Figure 2.18. The pressure transducer was calibrated in terms of pressure differential, by meaning that the atmospheric pressure was measured with the pressure transducer for a minute and then the flowrate was measured. The flowrate was measured by collecting the liquid in a volumetric tube for at least 100s and until at least 100g of liquid mass to be collected. Thus, for each flow condition, there was always a precision of three significant digits. The pressure transducer was arranged to measure the pressure differential until the mass collection procedure was finished. The pressure sampling frequency at each flow condition was kept constant at 100Hz while the acquired samples were properly adjusted until the procedure to come to an end.

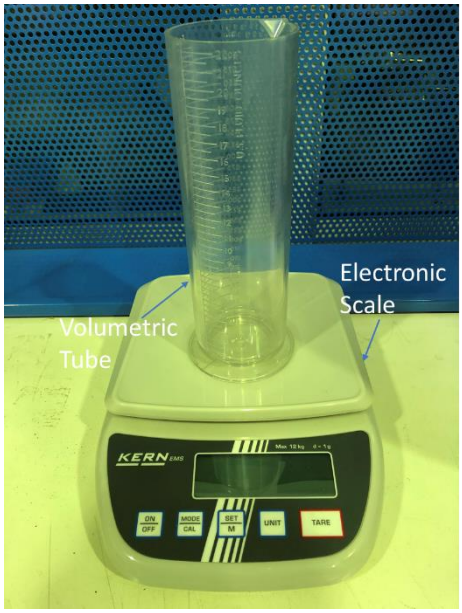

Figure 2.18 Volumetric tube and electrical scale

It is worth mentioning that the results obtained were almost the same for all the three times. Moreover, by measuring the collected liquid mass, a function can be extracted that precisely describes the relation between the injection pressure differential and the actual flowrate. For the examined flowrate conditions, the discharge coefficient has also been evaluated. For the current points, the discharge coefficient ranges from 0.71 to 0.78 for the range of Reynolds numbers from 980 to 2226. The discharge coefficient behaviour is illustrated in Figure 2.19 while the Figure 2.20 describes the relation between the actual flowrate and the pressure differential. The function that relates the pressure differential with the actual flowrate is a power law function. The corresponding units of this function is bar for the pressure differential while cc/min for the flowrate. The discharge coefficient slightly changes for the examined flowrate conditions. For Reynolds numbers that exceed 1700 the discharge coefficient remains unchanged at a value of 0.78 which means that the flow conditions are entering the turbulent region.

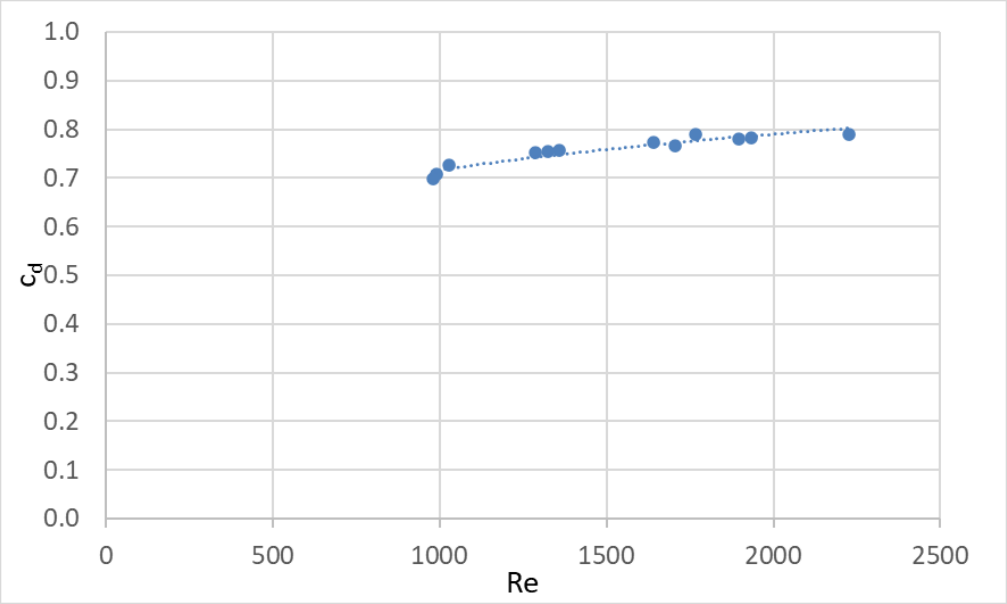

Figure 2.19 Discharge coefficient vs Reynolds number

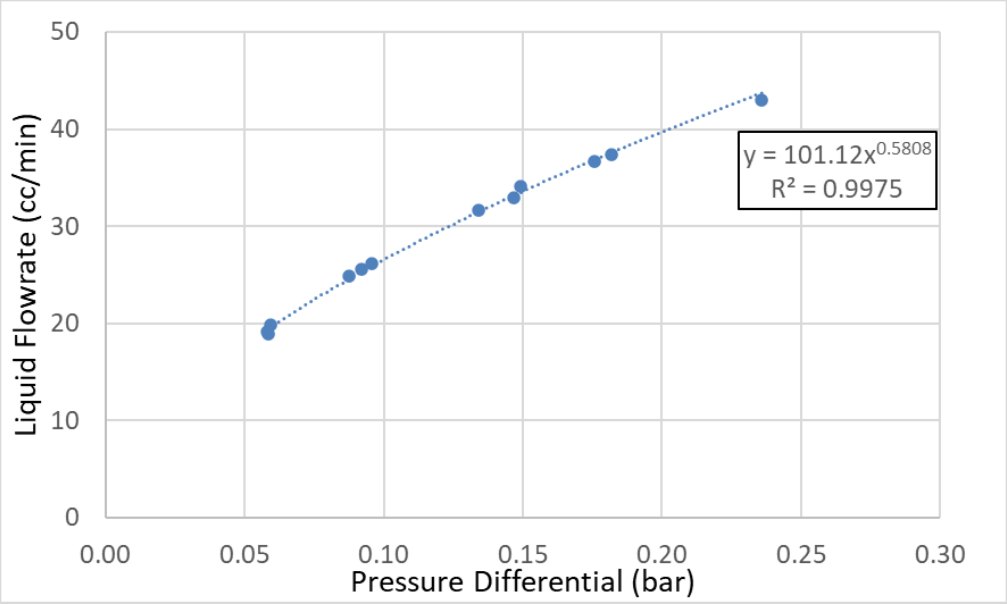

Figure 2.20 Liquid Flowrate Calibration

3. Results and Discussion

In this chapter, the experimental results are presented. Firstly, the jet trajectory and the column break-up location are presented and discussed. Next, the spray cone angles and the coefficients that describe their behaviour are introduced.

3.1 Jet Trajectories and Column break-up location

To begin with, the trajectory and the coefficients of the average jet are presented. There are four different liquid flowrates in which the jet is exposed and range from Re=1082 to Re=2230. Moreover, the four different liquid flowrates are exposed in three different aerodynamic Weber numbers that range from We=0 to We=0.66. The gas to liquid momentum ratio ranges from $4.24 \cdot 10^{-4}$-$163 \cdot 10^{-4}$. There are 16 different cases and a total number of 4 cases that are not presented because the jet is injected into still air and the trajectory is a straight line. The trajectory of each jet starts from the point (0,0) which is actually the outer orifice of the atomizer. The y-axis refers to the vertical direction of the jet injection while the x-axis for the horizontal direction which is parallel to the crossflow airstream. The trajectories of each jet were first calculated in pixels and then in normalized with the jet diameter. The normalized parameter refers to ratio of each variable x or y to the jet diameter. The function that is used to describe the trajectory of the jet has the form of $y = a_1 + a_2 x^{a_3}$. Thus, the resulting function with the dimensionless parameters is $\frac{y}{d_j} = a_1 + a_2(\frac{x}{d_j})^{a_3}$.

3.1.1 Jet trajectories

Case: Re=1082, We=0.07,0.29,0.66

In this case, the flow conditions for Re=1082 correspond for a jet velocity of about 2.6m/s. The crossflow velocity at these conditions corresponds to 3.26,6.53,9.79m/s and the aerodynamic Weber for this range is We=0.07,0.29,0.66. In Figure 3.2, the average trajectory of the jet and the predicted jet trajectory at different aerodynamic Weber numbers is illustrated. Each colour represents a unique Weber number. The different Weber numbers are shown in the figure with a continuous line while the power law function with a dashedline. The x and y axis refer to the normalized parameter of y/d and x/d respectively. As it seems, the trajectory of the jet is influenced by the increase of the aerodynamic Weber number. In the current case, a power law function can describe the trajectory of the jet. In general, when the aerodynamic Weber is increased, then the average trajectory of the jet abruptly inclines. In bibliography (No, 2015; Broumand and Birouk, 2016), the trajectory of a jet is frequently described by power law functions in the most flowing conditions. When We=0.07 and

We=0.29, for both configurations the fitted trajectory can be considered identical to the trajectory of the jet. When We=0.66, there is a small divergence to the predicted trajectory because in this case, the liquid flowrate is the lowest and the crossflow velocity is maximum. In general, in this case, the gas to liquid momentum ratio is the weakest of all cases and as a result, the trajectories diverge the most from the vertical direction. Furthermore, at the edge of the trajectory at the higher Weber number, it is very obvious that strong disturbances take place and the jet is being deflected. As it seems, when the crossflow velocity is not high-enough, the average jet trajectory at its edge is smoother and the fitting power law function can describe more accurately the average trajectory of the jet. In Figure 3.1 the original trajectories of the jet for each case are illustrated. These images were captured during the experiment. The Reynolds number is constant in this case and the aerodynamic Weber is increased from 0.07 to 0.66. Starting from the left image, the aerodynamic Weber that corresponds in this case is We=0.07, the middle corresponds for We=0.29 and the right image for We=0.66.

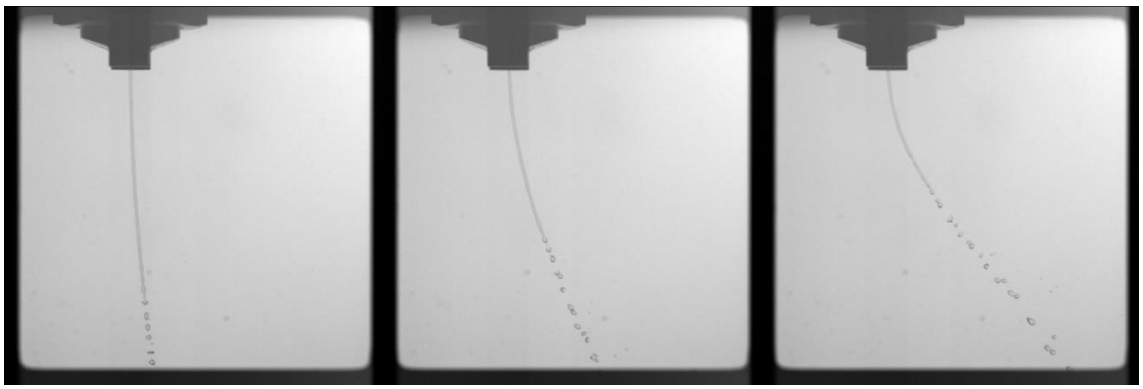

Figure 3.1 Jet Trajectories Re=1082, We=0.07,0.29,0.66

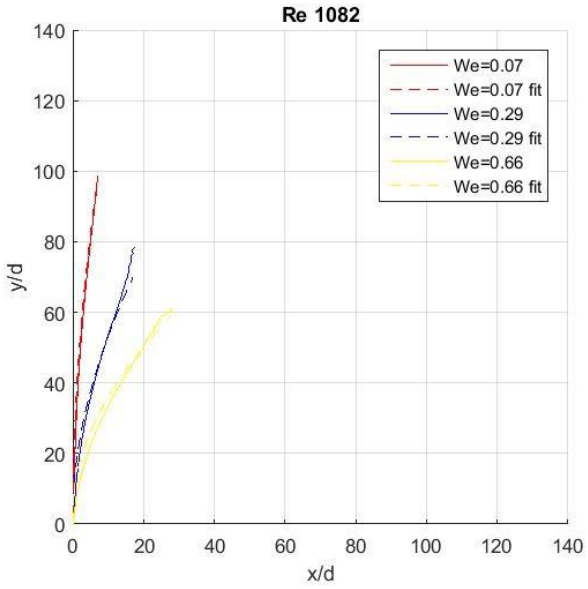

Figure 3.2 Average Jet trajectories Re=1082, We=0.07,0.29,0.66

Case: Re=1290, We=0.07,0.29,0.66

For the next case, the jet velocity was about 3.2m/s. As the liquid Reynolds number is increased, the jet is able to penetrate more into the flowing gaseous medium as indicated by Figure 3.4.The average trajectories of all jets are closer to the vertical axis than the previous case. The accuracy of the fitted trajectories is improved as well in this case. Also, at the higher aerodynamic Weber, the average jet trajectory and the power law fit is better than the previous case of Re=1082, We=0.66 because the liquid flowrate is increased and the air to liquid momentum ratio is lower in this case, thus, the jet is smoother. In Figure 3.3 the example images of the jet for each case are presented. The Reynolds number in these images is Re=1290 and the aerodynamic Weber is increased from 0.07 to 0.66. Starting from the left image, the aerodynamic Weber that corresponds in this case is We=0.07, the middle corresponds for We=0.29 and the right image for We=0.66.

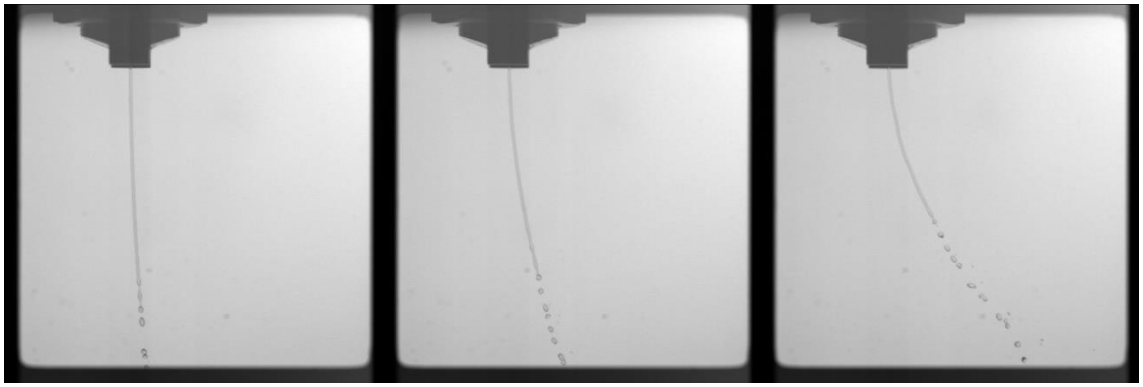

Figure 3.3 Jet trajectories Re=1290 We=0.07,0.29,0.66

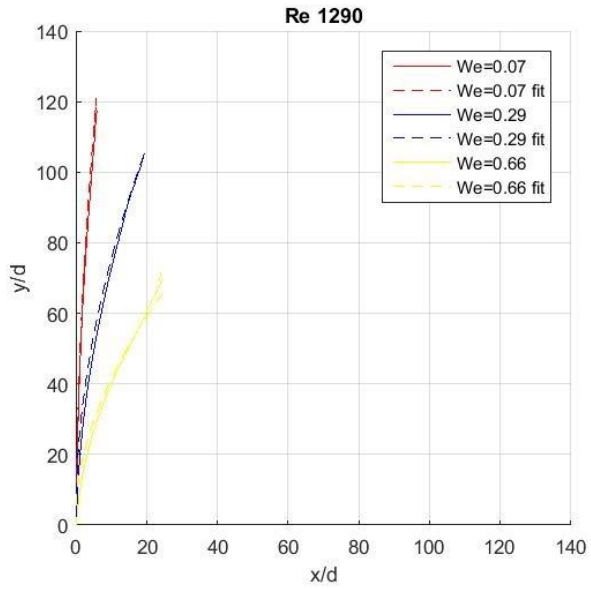

Figure 3.4 Average Jet trajectories Re=1290 We=0.07,0.29,0.66

Case: Re=1790, We=0.07,0.29,0.66

In this case, the jet velocity was about 4.4m/s. The trajectories of the jets are not only getting closer to the vertical axis but also to each other Figure 3.6. The average trajectories are smoother than all the previous cases. By progressively increasing the liquid flowrate results in a better fit which can precisely describe the jet behaviour for all the aerodynamic Weber numbers. Moreover, at higher the liquid flowrate, the distance between of the three jets is decreasing and they are getting closer to each other. In general, if the flowrate is high enough and the aerodynamic Weber is low, the prediction of trajectories gets more accurate with the power law fit. In this case, the power law fit can describe with high accuracy the average trajectory of the jets at all crossflow flow conditions. In Figure 3.5 the original trajectories of the jet for each case are illustrated. The Reynolds number in these images is Re=1790 and the aerodynamic Weber is increased from 0.07 to 0.66. Starting from the left image, the aerodynamic Weber that corresponds in this case is We=0.07, the middle corresponds for We=0.29 and the right image for We=0.66. Even from the unprocessed images of Figure 3.5, it can be inferred that the trajectories are getting closer to each other.

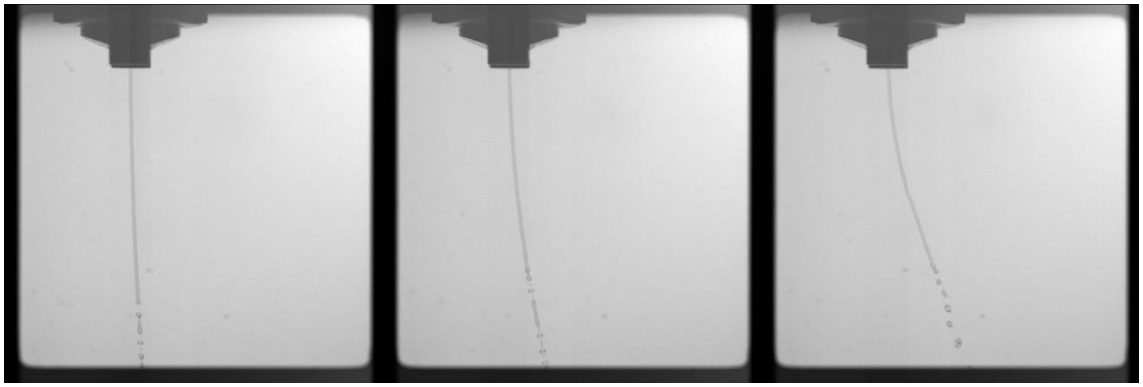

Figure 3.5 Jet trajectories Re=1790, We=0.07,0.29,0.66

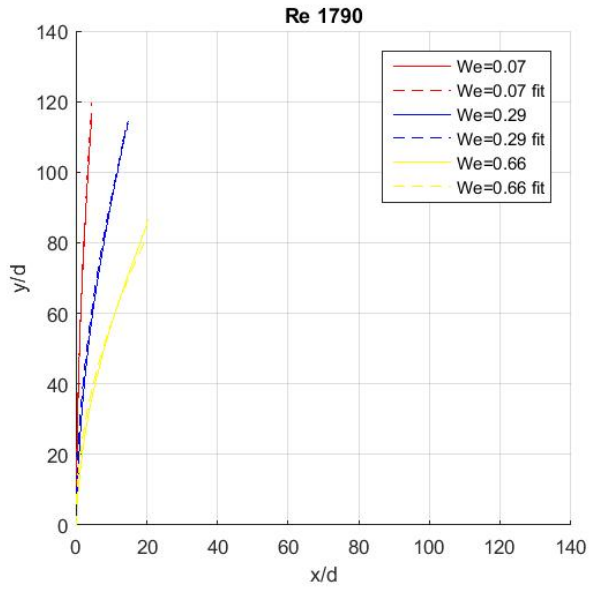

Figure 3.6 Average Jet trajectories Re=1790, We=0.07,0.29,0.66

Case: Re=2230, We=0.07,0.29,0.66

In this case, the jet velocity was about 5.5m/s. The average trajectory of each jet is getting closer to each other and even closer to the vertical axis. The gradient of the average jet trajectories as illustrated in Figure 3.8 seems to be smoother than the other cases because the gas to liquid momentum ratio is the higher at this occasion. Moreover, the average trajectories for all three cases have the tendency to follow their initial path and slightly diverge from the vertical direction. The average jets in this case are closer than before to each other and to the vertical axis because the liquid flux momentum ratio is the lower. Therefore, the jets are able to penetrate further into the gaseous medium. At the edges of the average jet the dislocation has sufficiently reduced and the fitting trajectories are exactly identical to the average jet trajectories. In Figure 3.7 the original trajectories of the jet for each case are illustrated. The Reynolds number in these images is Re=1790 and the aerodynamic Weber is increased from 0.07 to 0.66. Starting from the left image, the aerodynamic Weber that corresponds

in this case is We=0.07, the middle corresponds for We=0.29 and the right image for We=0.66. It is obvious that the three jets slightly diverge from the vertical direction, especially when We=0.07 and We=0.29.

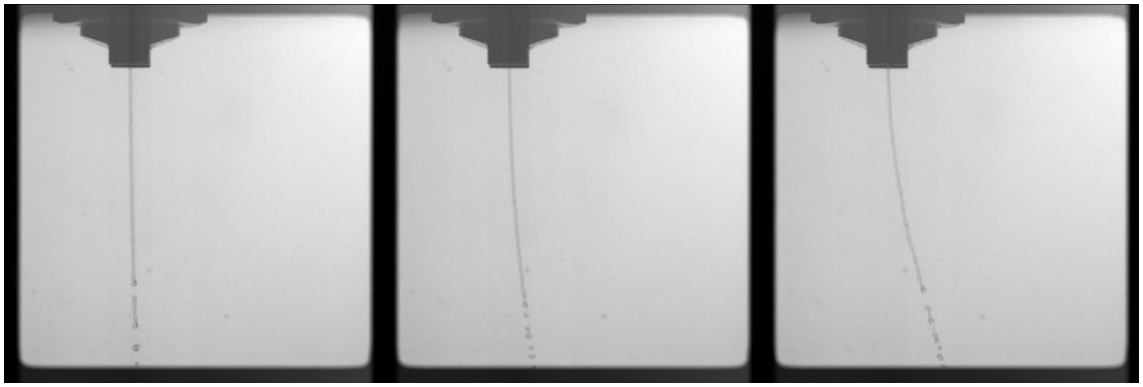

Figure 3.7 Jet trajectories Re=2230, We=0.07,0.29,0.66

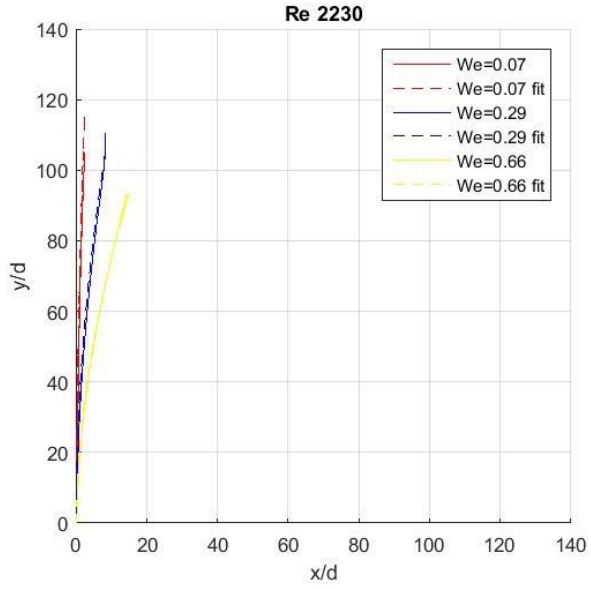

Figure 3.8 Average Jet trajectories Re=2230, We=0.07,0.29,0.66

3.1.2 Fitting power law for jet trajectories

The power law coefficients of the proposed function $\frac{y}{d_j} = a_1 + a_2(\frac{x}{d_j})^{a_3}$ are presented in this section. Each trajectory has its unique coefficients but one of the most important coefficients is the exponential coefficient a_3. In all figures, the x-axis corresponds to the aerodynamic Weber number while the vertical axis to the magnitude of each coefficient.

a_1 coefficient

Firstly, the coefficient a_1 is shown in Figure 3.9. The coefficient a_1 range is 0.32 to 8.46. It seems that there is no obvious correlation between each flow condition. When the aerodynamic Weber is 0.07 all the liquid Reynolds numbers are close to each other except from Re=1082 which is quite larger than the others. With a further increase of the aerodynamic Weber, the coefficients are having identical magnitudes that range from 4.5 to 7.6. At the highest aerodynamic Weber, the magnitude of the coefficient a_1 when Re=1082 and Re=1290 is very close to each other. When Re=1790 the a_1 coefficient has slightly smaller magnitude that the other case while when Re=2230 this magnitude is almost zero. In general, the most values of this coefficient are somewhere between 4 and 8. In fact, the coefficient a_1 stands for an offset in the power law fit function and that's why it has the same units as the y/d and x/d which are normalised to the jet's diameter.

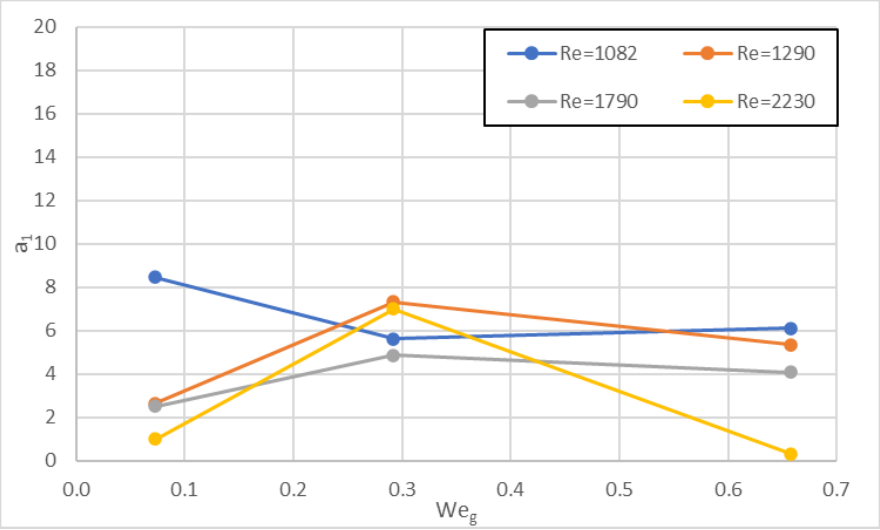

Figure 3.9 Coefficient a_1 of the power law fitting

a_2 coefficient

The a_2 coefficient of the power law fitting is shown in Figure 3.10. It seems that there is a correlation between the different flow conditions. The coefficient a_2 of the power law fitting follows similar declining trends of a different magnitude at each liquid Reynolds number. This coefficient ranges from 8 to 73. In each individual Reynolds number, the magnitude of this coefficient starts from a high value when We=0.07 and then rapidly decreases when We=0.29. With a further increase of the aerodynamic Weber, this coefficient still decreases but in a milder way than We=0.29. In general, when We=0.07 the coefficient a_2 of the power law fitting has large differences in magnitude between each liquid Reynolds number. As the aerodynamic Weber number is increased, not only the magnitude of this coefficient is decreased but also the difference in magnitude of each individual jet. Furthermore, it is worth mentioning that for each aerodynamic Weber the ratio of the magnitude of each Reynolds

number with the lowest Reynolds number Re=1082 remains almost constant for all the range of aerodynamic Weber numbers. This ratio can be defined by the magnitude of the a_2 coefficient of the power fitting divided by the same coefficient at each Reynolds number. This ratio is shown in Figure 3.11. Except from the point Re1290/Re1082, We=0.66 and Re1790/Re1082, We=0.07 that diverge a little, all the other cases remain on the same straight line.

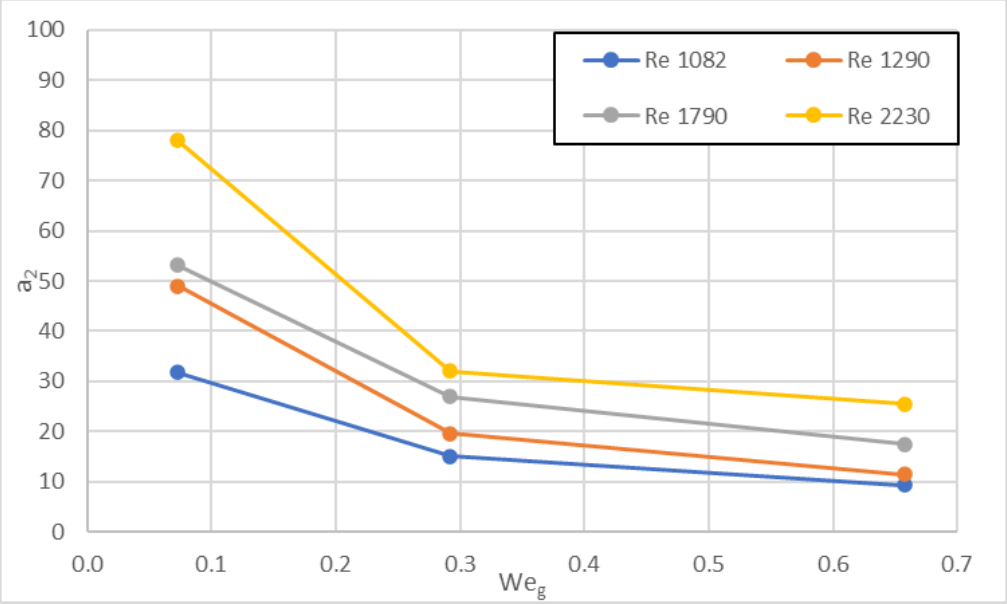

Figure 3.10 Coefficient a_2 of the power law fitting

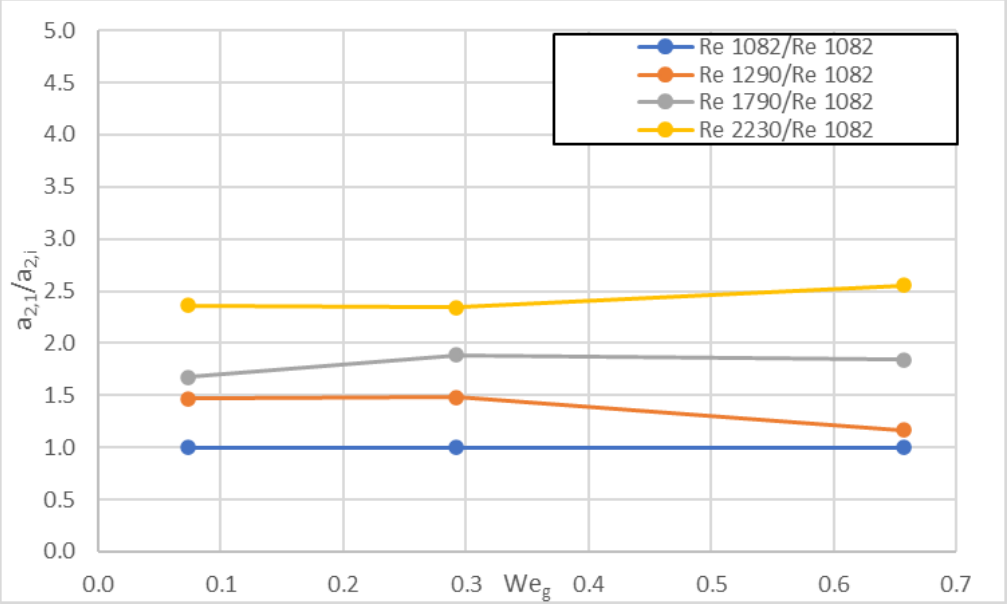

Figure 3.11 a_2 magnitude ratio of each Reynolds number vs aerodynamic Weber

a_3 coefficient

The a_3 coefficient is one of the most important parameters as it can describe the trajectory of each jet. As far as the physical meaning of this coefficient is concerned, it shows that if this parameter is sufficiently low, then the jet experiences high aerodynamic forces and it is deflected more easily into the crossflow airstream. On the other hand, if this parameter is not very low, it means that the jet has high inertia compared to the crossflow airstream and it is not easily deflected away. This means that the average trajectory of the jet is able to penetrate at a further distance from the outer orifice of the nozzle. In fact, this parameter shows the slope of the emerging jet into the gaseous crossflow airstream. The a_3 power law coefficient for a jet into a crossflow airstream is usually around 0.5 for similar flow conditions (Pei-Kuan Wu, Kevin A. Kirkendall, 1997; Broumand and Birouk, 2016). A simple model that is able to predict the jet trajectory is to assume that only y-direction aerodynamic forces are acting on the liquid jet column and viscous forces are neglected. Thus, the liquid jet is deflected on the x-direction. The aerodynamic forces that are acting on the liquid jet are equal with $F=0.5\cdot\rho_g\cdot U_g\cdot A\cdot C_D$. By equating the aerodynamic forces equal with the acceleration forces, the following relation can be obtained $0.5\cdot\rho_g\cdot U_g\cdot A_F\cdot C_D=\rho_l\cdot A_c\cdot h\cdot\ddot{x}$. The term A_F refers to the frontal area of the jet which is equal to the product of jet's diameter to its thickness h while the term A_c refers to the cross-sectional area of $0.25\cdot\pi d^2$. The term $\ddot{x}$ refers to the acceleration at the x-direction. By integrating this differential equation, the following relation is obtained $\frac{x}{d}=\frac{1}{\pi}C_D\frac{\rho_g}{\rho_l}U_g^2\frac{t^2}{d_j{}^2}$. Setting the $t=y\cdot U_j$ and the relation becomes $\frac{x}{d}=\frac{1}{\pi}C_D\frac{\rho_g}{\rho_l}\left(\frac{U_g}{U_l}\right)^2\left(\frac{y}{d_j}\right)^2$. Rearranging this equation yields to $\frac{y}{d_j}=\sqrt{\frac{\pi}{C_D}q(\frac{x}{d_j})}$. Thus, the theoretical a_3 power law coefficient is 0.5 which means that the term $\frac{y}{d_j}$ is proportional to the square root of $\frac{x}{d_j}$.

In this investigation, the coefficients range from 0.51 to 0.57. Generally, when the aerodynamic Weber is low, the coefficients tend to be close or higher than 0.5 because the jet doesn't bend as much as at higher aerodynamic Weber numbers. The higher the jet bends, the lower the coefficient would be because the average jet trajectory behaves as a concave down increasing curve. In general, this coefficient remains almost constant and slightly diverges in the most cases. The cases where Re=1290, Re=2230 for the same aerodynamic Weber We=0.07 are an exception of the above statement because the coefficient is 0.51.

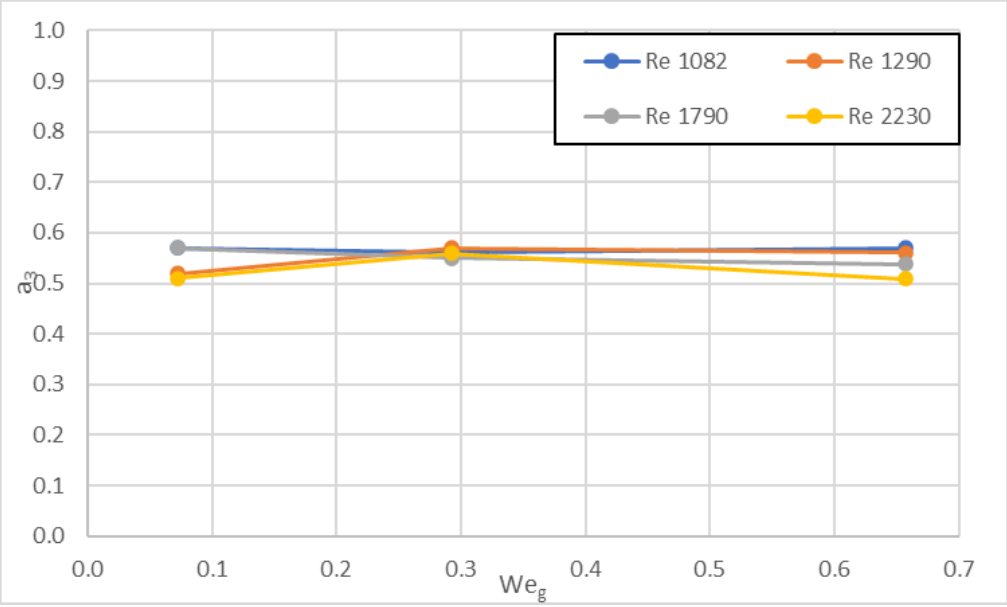

Figure 3.12 Coefficient a_3 of the power law fitting

3.1.3 Column Break-up Location

In this section the trajectories of average jet at a constant aerodynamic Weber number are presented. In each graph, not only the jet trajectories of the various Reynolds numbers are shown but also the several break-up points that have been detected by the algorithm. The results rely on a sample of 256 images at each case. The trajectory of each jet is presented as a solid line while the break-up points as dots on that line. Each colour on the graph corresponds to a unique Reynolds number. Each jet trajectory and its break-up points have the same colour. The vertical axis refers to the vertical direction of the jet injection while the x-axis for the horizontal direction which is parallel to the crossflow airstream. The units of each axis are expressed as the ratio of each point to the jet's diameter. There are three cases at which each case corresponds to a unique Weber number that ranges from 0.07 to 0.66. The average crossflow velocity at each case was 3.26m/s 6.53m/s and 9.79m/s.

Case We=0.07

In this case, the average trajectories are presented in Figure 3.13. The trajectories of all jets are close to the vertical axis because the liquid columns do not experience high momentum. In this case the gas to liquid momentum ranges from $4.24 \cdot 10^{-4}$-$1.94 \cdot 10^{-3}$ and the crossflow velocity is about 3.3m/s. Furthermore, most of the trajectories coincide with each other. Each scatter point at each trajectory indicates the instantaneous break-up point as it was captured by the camera. Taking a closer look into the Figure 3.13, it is obvious that there is a range of coordinates that the liquid column has broken-up. Thus, the average values of each jet are extracted in order to have an estimation of this location. The average values x/d refers to the penetration that is parallel with the crossflow airstream while the

average values y/d refer to the vertical penetration. In this next subsection the average coordinates of each jet will be further discussed. Taking a look at Figure 3.13, the maximum penetration x/d along the horizontal axis happens when the Reynolds number is at its minimum while the minimum penetration at the highest Reynolds number. It was expected that the maximum vertical penetration to occur when the liquid Reynolds number is the highest. However, the maximum penetration occurs when the Reynolds number is Re=1790. This happens because the Reynolds number Re=2230 has passed in the transitional region. Therefore, the break-up of the jet occurs at a lower distance from the break-up point Re=1790 and is validated by the bibliography (Ohnesorge, 1936; Lefebvre and Mcdonell, 2017). Also, the minimum vertical penetration would be expected at the lowest Reynolds number but happens when the Reynolds number is the maximum.

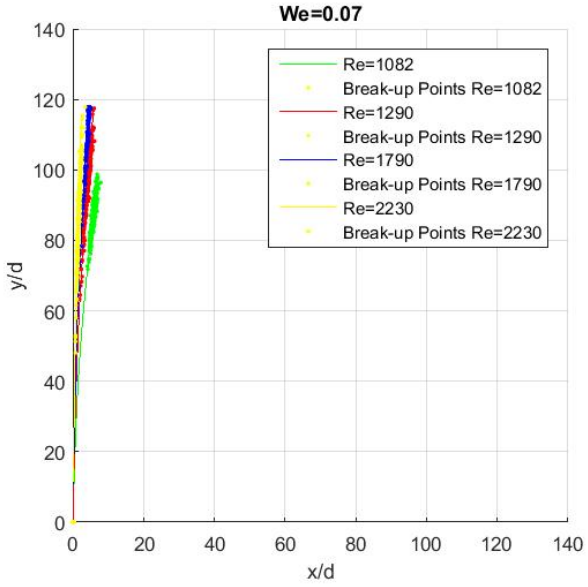

Figure 3.13 Jet trajectories for We=0.07

Case We=0.29

Next case and the aerodynamic Weber is increased to We=0.29. The corresponding crossflow velocity is 6.5m/s and the the gas to liquid momentum ranges from$1.73\cdot10^{-3}$-$1.17\cdot10^{-2}$. The jet trajectories for this case are presented in Figure 3.14. The trajectories of each jet started to separate from each other, and this is a result of the increased momentum. For the lowest liquid flowrate, the dispersion of the break-up points is more intense than the others. In general, the break-up point dispersion of the rest trajectories is higher than the previous case. This is a result of the low liquid flowrate, therefore the liquid column breaks to various coordinates. As the liquid flowrate increases, the dispersion of the break-up points becomes smoother. In this case, the maximum penetration along the horizontal axis happens when Re=1082 and the minimum x/d penetration occurs when the Reynolds number is the

highest as expected. The maximum y/d penetration happens at the moderate Reynolds number which is Re=1790 while the minimum y/d penetration happens at the lowest Reynolds number.

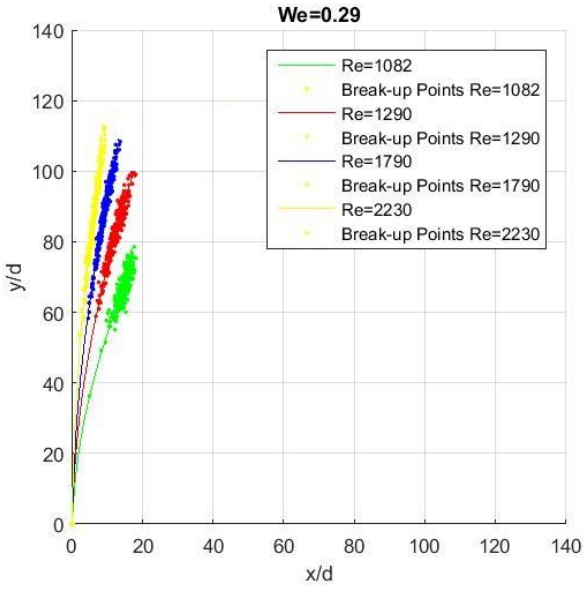

Figure 3.14 Jet trajectories for We=0.29 normal orientation

Case We=0.66

In the final case, the Weber number is We=0.66 and the corresponding crossflow velocity is 9.79m/s. The gas to liquid momentum ratio in this case ranges from $3.58 \cdot 10^{-3}$-$2.21 \cdot 10^{-2}$. In this case, the lower Reynolds number experiences the highest momentum. The jet trajectories for this case and the instantaneous break-up point location are presented in Figure 3.15. The trajectories of each jet have a large distance between them and the jets with low liquid flowrate bend more than the others. The break-up points dispersion has reached a peak in this case especially at the lowest liquid flowrate. At the higher liquid flowrates, the break-up point dispersion is smoother than the others but still it can't go unnoticed. The horizontal penetration is maximum when Re=1290 and minimum for the highest Reynolds number. In this case, it was expected that the maximum horizontal penetration would be at the lowest Reynolds numbers. In fact, the horizontal penetration can be considered identical in the cases where Re=1082 Re=1290 because they don't have significant differences. The minimum vertical penetration is achieved at the lowest Reynolds numbers while the maximum vertical penetration is achieved at the moderate Reynolds numbers where Re=1790.

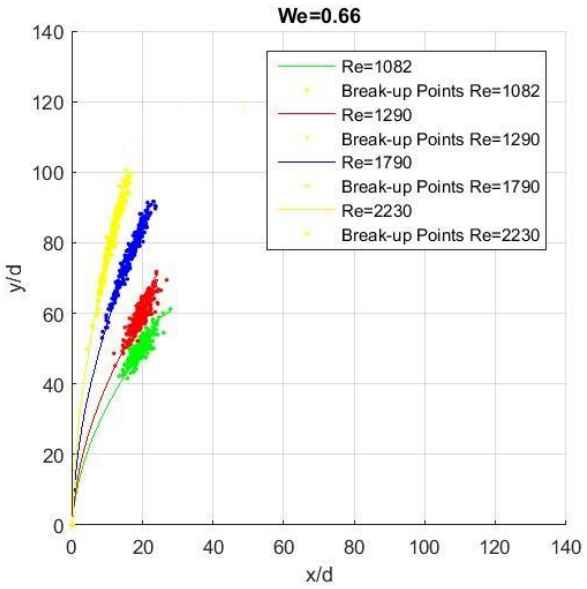

Figure 3.15 Jet trajectories for We=0.66

Column Break-up Location (CBL) trends

In this sub-section the trends of each penetration vertical or horizontal is presented. Apart from the range of We=0.07-0.66, the column break-up location for still air is also presented. In the following figures, the x-axis refers to aerodynamic Weber number in all figures while the vertical axis for the penetration at each direction, axial or lateral respectively. The units of the vertical-axis are normalised to the jet diameter. The horizontal penetration is presented in Figure 3.16. There is an upward trend in this figure because the aerodynamic Weber number is increased. Thus, the x/d jet penetration is displaced at a further distance from the horizontal axis origin into the flowing stream. In general, it is expected that the liquid jet with the lowest flowrate would penetrate more along the horizontal axis at the highest crossflow velocity while the jet with the highest flowrate would have the least penetration at that direction. At the lowest aerodynamic Weber number, when Re=2230 the break-up point occurs at about 2 x/d while when Re=1082 the break-up point is about 6 x/d. At the highest aerodynamic Weber number, the minimum horizontal penetration occurs at about 9 x/d when Re=2230 while the maximum penetration when Re=1290. The break-up point of Re=1082 and Re=1290 can be considered as identical because their difference is insignificant. When Re=2230, the break-up points are closer to the vertical axis for all crossflow conditions as expected. When Re=1082 the x/d break-up point has penetrated further than the other cases except from the case discussed above. It was expected that at the lowest Reynolds number, the break-up point would be at a further distance than the other cases.

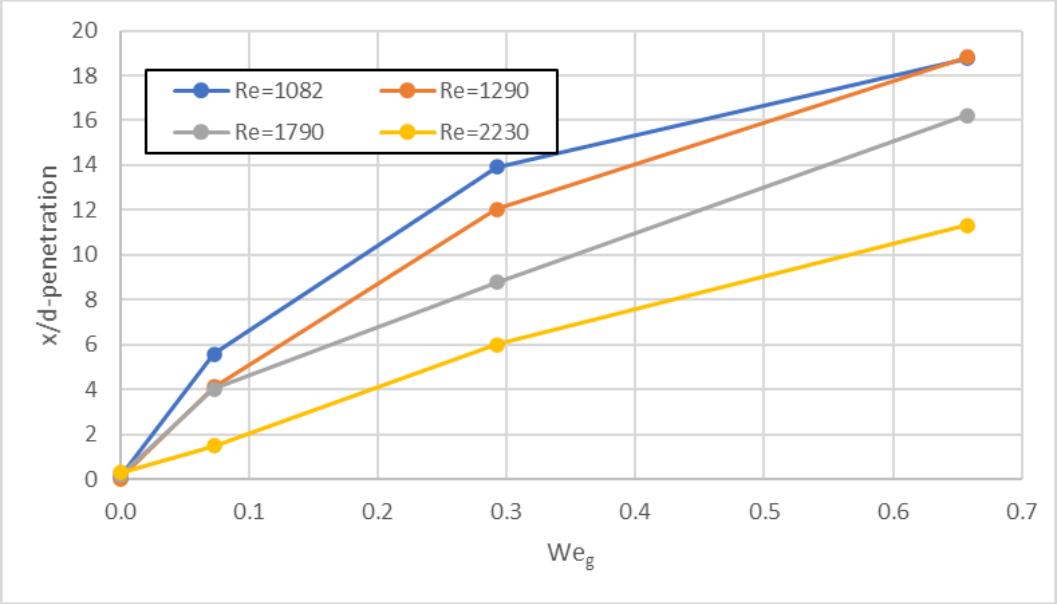

Figure 3.16 Horizontal penetration trends

In Figure 3.17 the vertical penetration of each jet is presented. It is expected that the jet with the highest flowrate would penetrate more into the crossflow stream and the lowest would penetrate less as far as the Reynolds number remains in the laminar region. When the jet is injected into still air, the results are of about the same magnitude except from the case of Re=1290 which is a bit higher than the others. As the aerodynamic Weber is increased it would be expected that the liquid with the highest flowrate would have penetrated at a further distance from the discharge orifice. In this case, when We=0.07 the maximum penetration is reached when Re=1790 and the minimum when Re=2230. The break-up points in this occasion are 110 y/d and 86 y/d respectively. At the highest aerodynamic Weber, the lowest vertical penetration is 48.17 y/d and corresponds for the case where Re=1082 while the highest vertical penetration occurs when Re=1790 and the corresponding break-up point is about 78 y/d. In general, by the increase of the aerodynamic Weber number, the vertical penetration of each jet in the crossflow airstream is reduced as indicated by Figure 3.17.

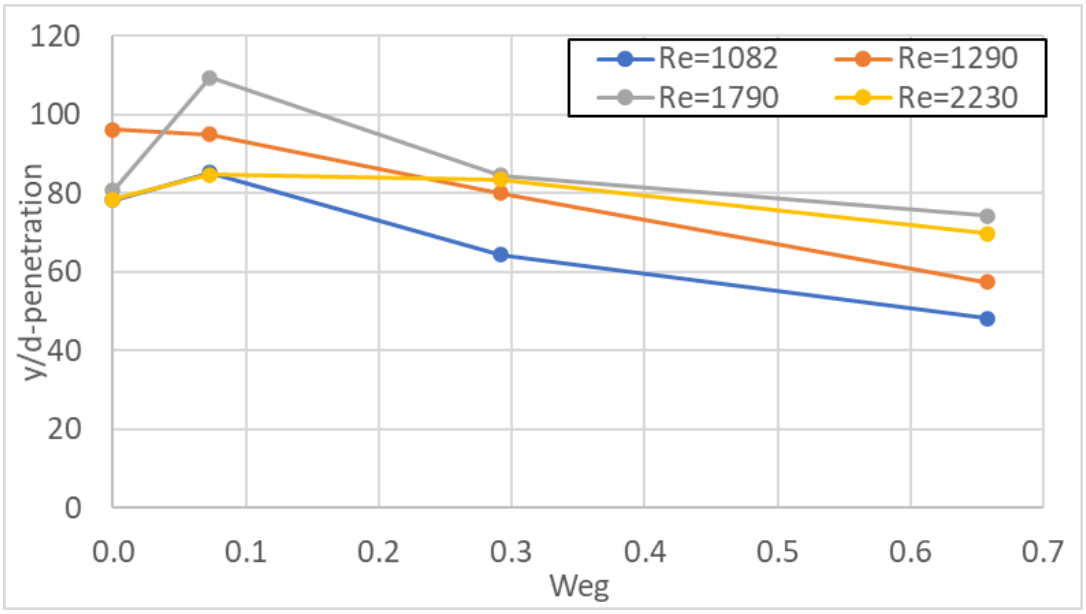

Figure 3.17 Vertical penetration trend

3.2 Spray Angles

The exact evaluation of the spray cone angle as mentioned in the above sections is quite difficult to be determined. The spray cone angles were determined by considering the outer contours of the resulting spray by using ImageJ software Figure 3.19. The current estimations have an uncertainty of about ±1.5° . As soon as the spray cone angles were evaluated, then a power law function is proposed in order to correlate the mass flow ratio q with the resulting spray cone angle. The proposed correlation is the following $\theta=a\cdot(q-b)^c$ (a, b, c constants, θ in degrees). Moreover, the sprays that were captured during the experiment are presented in Figure 3.18. In this figure, the spray is injected into still air. The mass flow ratio that corresponds for each image is a) q=0.51 b) q=0.39 c) q=0.45 d) q=0.27 e) q=0.38 f) q=0.22 g) q=0.30. It is obvious that the higher the mass flow ratio is, the spray cone angle is wider.

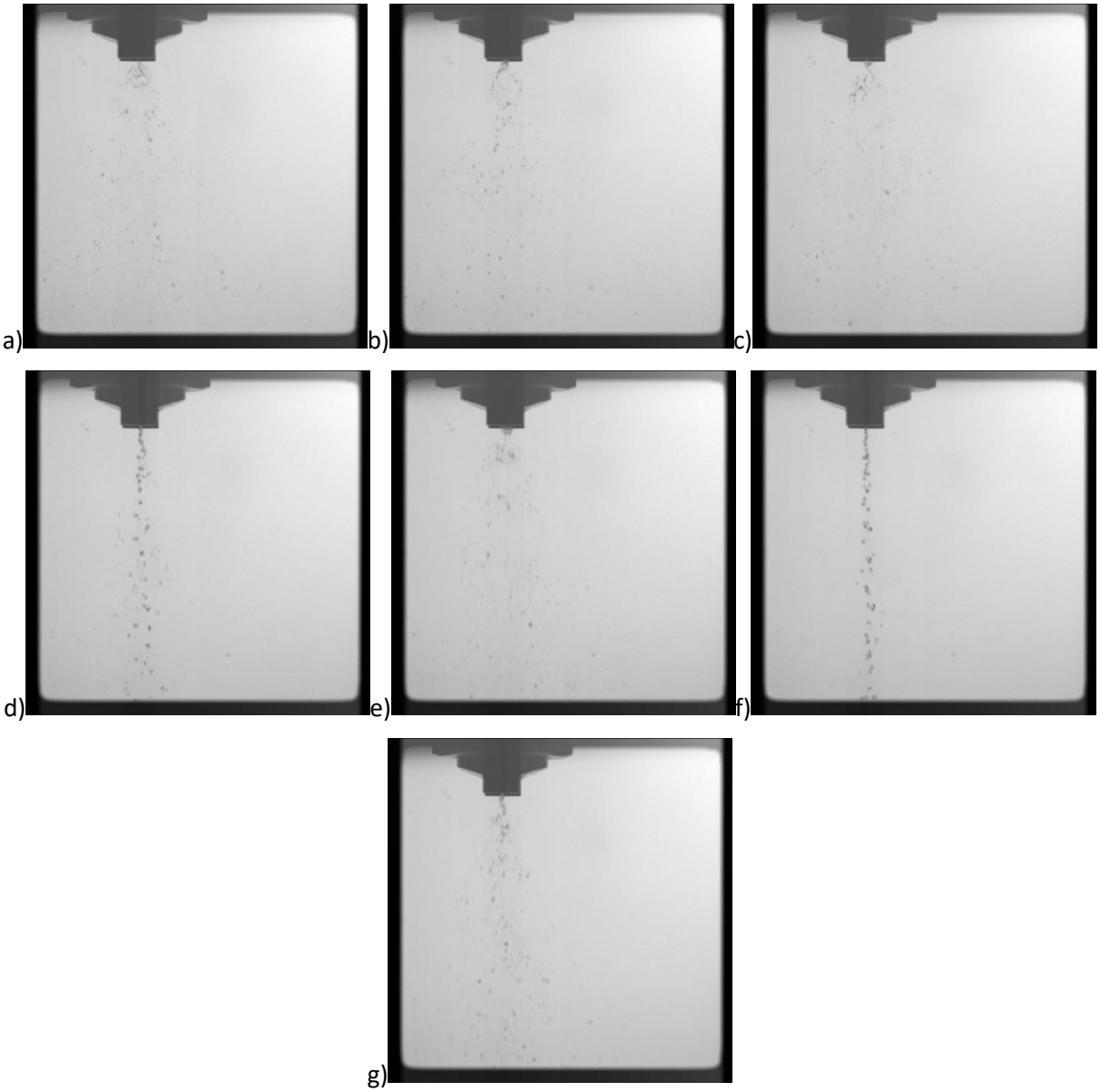

Figure 3.18 Spray injection in still air for different mass flow ratios a) q=0.51 b) q=0.39 c) q=0.45 d) q=0.27 e) q=0.38 f) q=0.22 g) q=0.30

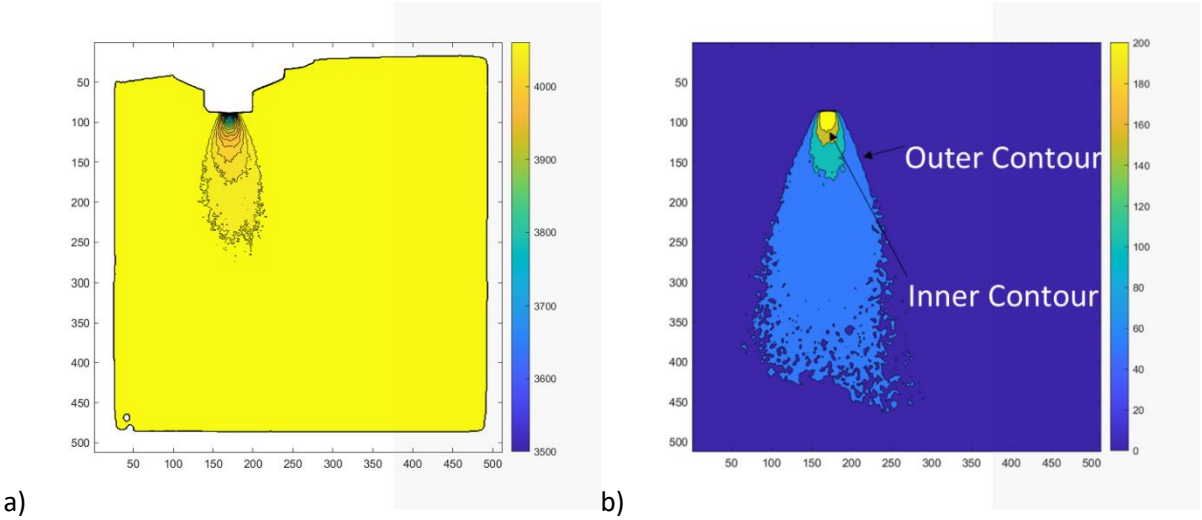

a) b)

Figure 3.19 a) Mean processed image of a spray at q=0.51, We=0 b) Standard Deviation of the processed image of a spray at q=0.51, We=0

The measures spray cone angles are shown in the following figures. Each figure is representing the measured spray cone angle in degrees as a function of the mass flow ratio for each aerodynamic Weber. The mass flow ratio ranged from 0.22 to 0.51 while the aerodynamic Weber from 0 to 0.66. The liquid flowrates range from 18.8cc/min to 45.0 cc/min while the air flowrate from 8L/min to 11L/min. The mass flow ratio q is defined as the ratio of gas mass flow to the liquid mass flow. Thus, the higher the gas mass flow is, the higher the spray cone angle which is supported by the experimental results. At each figure, the measured spray cone angle is presented with a blue dot while the predicted spray cone angle with the other colour and this applies to all figures. The measure spray cone angle is presented in Figure 3.20. The measured spray cone angles range from 12° to 46°. The estimations of the spray cone angle from the proposed empirical correlation seems to have a good accuracy as the predicted spray angle is close to the measured angle.

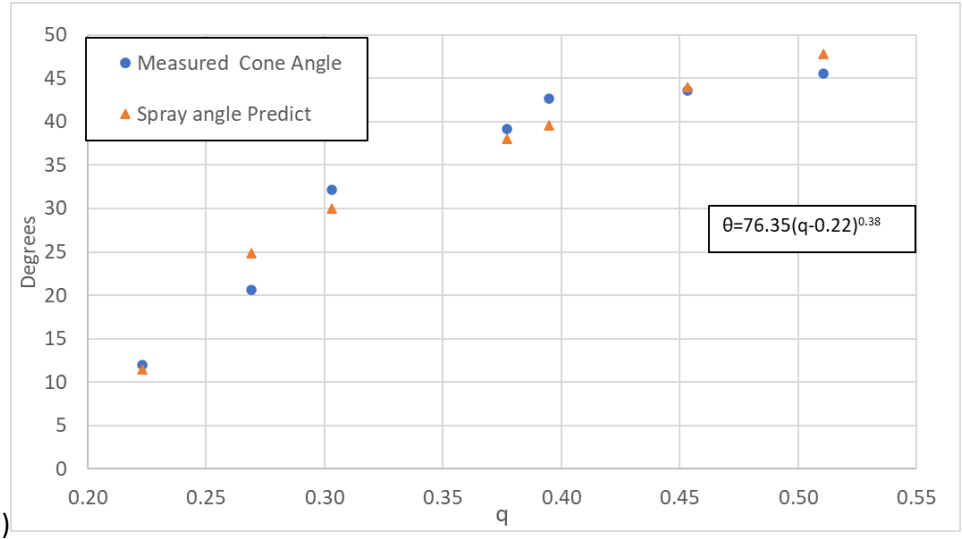

a)

b)

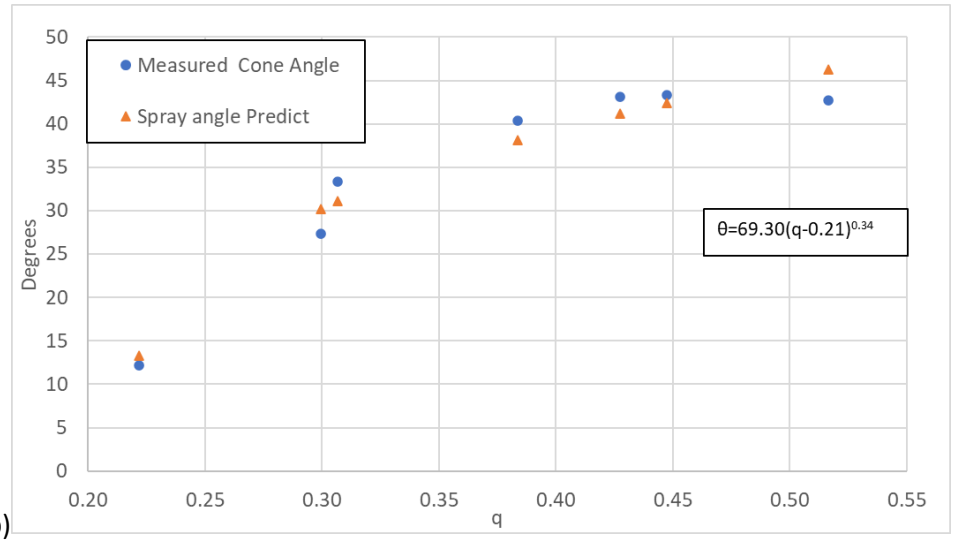

c)

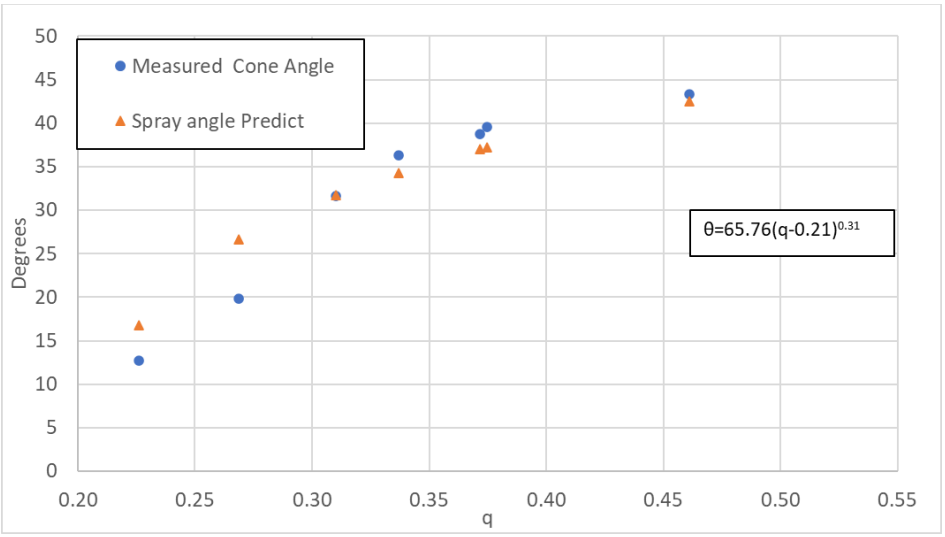

d)

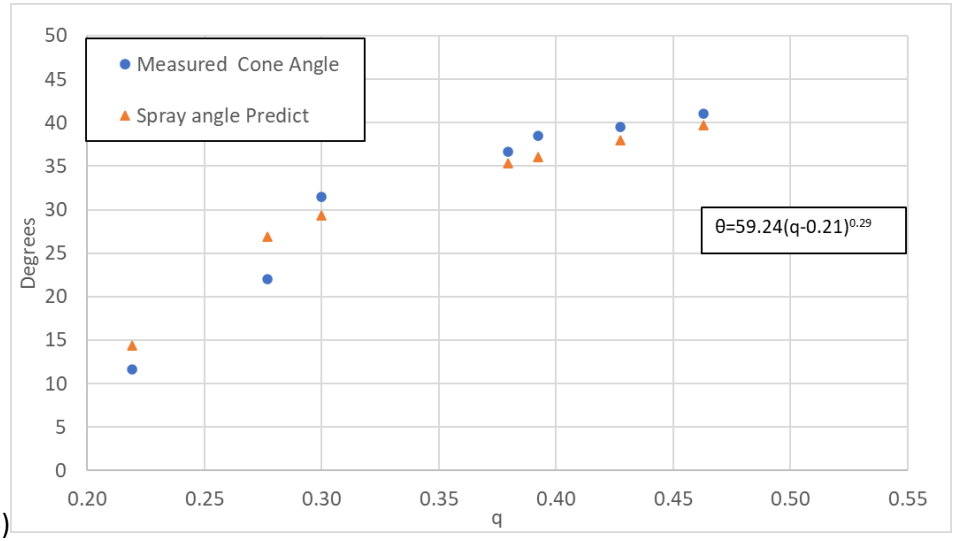

Figure 3.20 Spray Cone Angles for specific aerodynamic Weber a) We=0 b) We=0.07 c) We=0.29 d) We=0.67

Fitting power law for spray cone angles

The figures below represent the calculated coefficients of the proposed correlation as a function of the aerodynamic Weber. The Figure 3.21 shows the behaviour of the coefficient (a) of the power law function. When the liquid is atomized in still air, the coefficient is high. As the aerodynamic Weber is increased the coefficient (a) of the power law function starts to decrease in almost with a constant rate. The range of this coefficients is 59 to 77.

Furthermore, the (b) coefficient is illustrated in Figure 3.22. This coefficient corresponds to the minimum mass flow ratio q at each aerodynamic Weber number and that's the reason why it remains constant because the spray was exposed in identical flow conditions. In Figure 3.23 the coefficient (c) of the power law function is presented. The coefficient (c) of the power law function ranges from 0.28-0.38. By the increase of the aerodynamic Weber, this coefficient is decreasing.

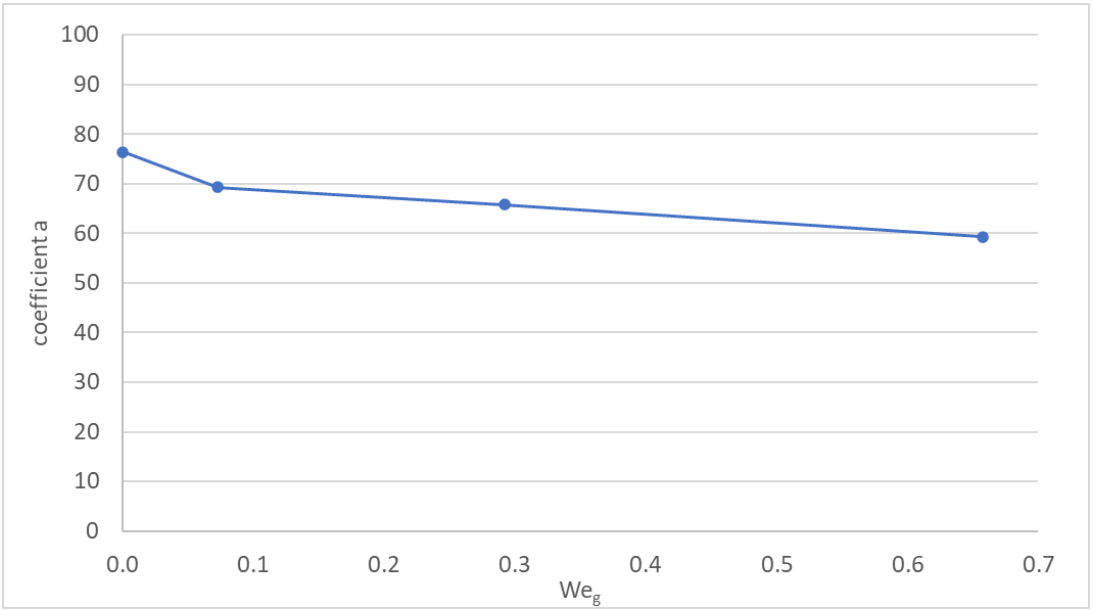

Figure 3.21 (a) Coefficient of power law function for spray cone angle

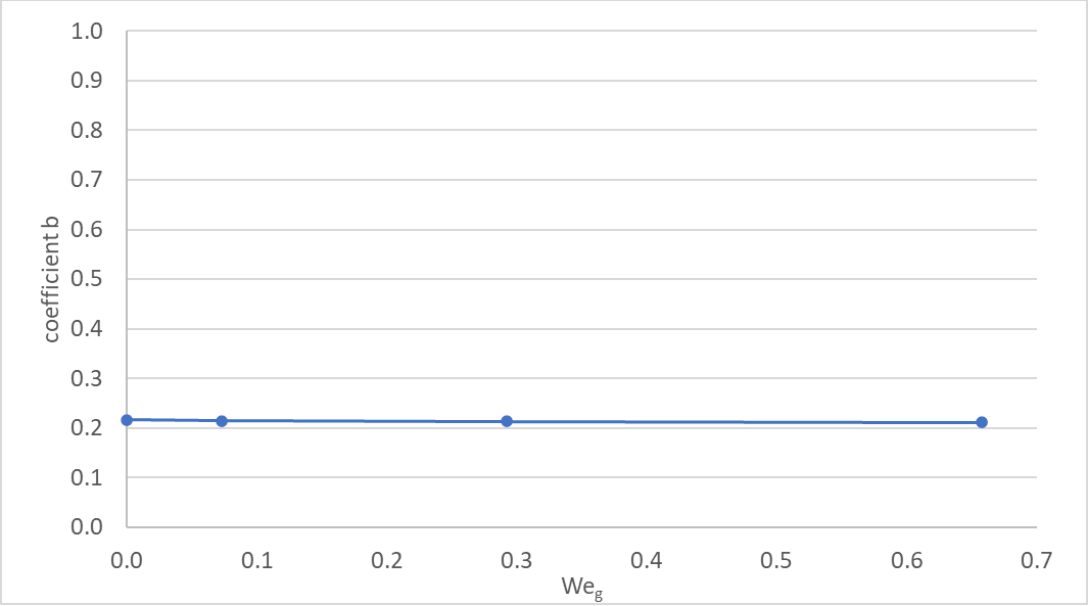

Figure 3.22 (b) Coefficient of power law function for spray cone angle

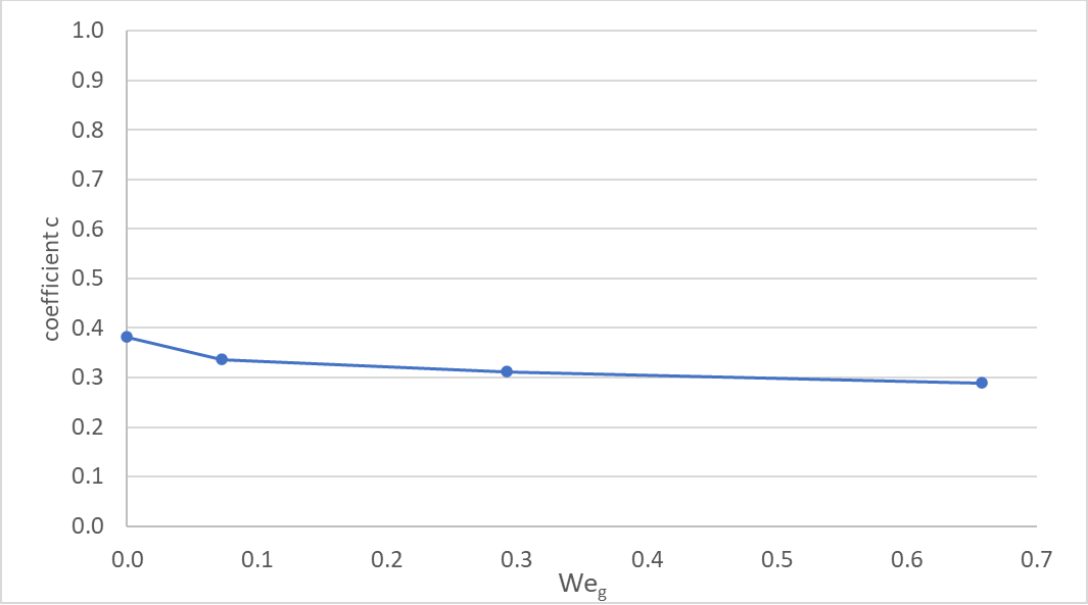

Figure 3.23 (c) Coefficient of power law function for spray cone angle

4. Conclusions

In the current experimental investigation, the injection of a liquid jet/spray into a crossflow airstream is examined. The dominant parameters of this investigation are the liquid Reynolds, the aerodynamic Weber, the gas to liquid momentum ratio and the gas to liquid mass flow ratio. These parameters ranged Re=1349-2993, We=0.04–1.34 and $Q=4.24\cdot10^{-4}$-$163\cdot10^{-4}$ and q=0.22-0.51. The jet was visualised with the technique of shadowgraphy and captured by a camera. In the current investigation it was found that:

1. The higher the aerodynamic Weber is, the liquid jet diverges increasingly from the vertical direction
2. The vertical penetration is reduced with the increase of the aerodynamic Weber while the horizontal penetration increases.
3. As the liquid Reynolds number is increased, the jet gets closer to the vertical axis and it is not easily deflected.
4. When the Reynolds number is lowest, the jet experiences the highest gas to liquid momentum when the aerodynamic Weber is the highest. Therefore, the edges of trajectory in these cases are intensively dislocated and in general the jet is deflected away more easily.
5. The trajectory of the average jet can be described by the power law function with good accuracy.
6. The a_2 power law coefficient is correlated with the flow conditions. The ratio of the magnitude of the a_2 power law coefficient in each Reynolds number divided with the lowest Reynolds number remains almost constant in the most cases.
7. The power law coefficient a_3 remains almost steady at about 0.54-0.57 in the most cases. However, it should be mentioned that in the cases where Re=1290, Re=2230 and We=0.07 the coefficient is 0.51 which is slightly lower from the other coefficients.
8. The higher the mass flow ratio, the wider spray cone angle.
9. The maximum spray cone angle occurs when the spray has the minimum liquid flowrate and the highest gas flowrate. The maximum spray cone angle is achieved when the spray is injected into still air. This case refers at that which q=0.51 and We=0 and the measured spray cone angle is 46°.
10. At the highest aerodynamic Weber and the lowest mass flow ratio, the spray cone angle is the minimum. The case refers to that when q=0.22 and We=0.66 and the measured spray cone angle is 12°.

11. The spray cone angle is slightly reduced by the increase of the aerodynamic Weber
12. The fitting power law for predicting the spray cone angle can be considered as a good approach. However, it should be noted that there is a little divergence between the measured spray cone angle and the predicted spray cone angle at the lowest mass flow ratio.

As far as the future suggestions are concerned, many things can be done. The suggestions are presented in the following:

1. In the current investigation, the jet was exposed into a uniform crossflow profile with low turbulence. Alternatively, the jet can be exposed into various turbulent crossflow profiles that match the flow conditions of an actual application.
2. The turbulence within the crossflow was about 1.5%. This percentage is preferred to be lower than 1% to be fully considered as a low turbulence crossflow profile. Fine screens can be added to decrease more the turbulence within the circular duct. Nevertheless, it should be also considered that by adding more screens in the flow results in lower crossflow velocities due to excess pressure drop.
3. The injected liquid here was purified water. Different liquids with different properties can be used too, in order to further examine of how the break-up of the jet or the spray cone angle of the spray are affected. Moreover, high-viscosity liquids such as glycerine can be used to direct compare the obtained results between high and low viscosity liquids.
4. Instead of using pure different liquids, blends of aviation fuels such as Jet A-1 can be used or even alternative fuels.
5. Instead of using the current power law function, an alternative is proposed which has the form of $\frac{y}{d_j} = a_1 Q^{a_2} (\frac{x}{d_j})^{a_3}$.

5. References

A.A.LabSystems (2000) 'AA Lab Systems Manual'.

Ashgriz, N. (2011) *Atomization Hand Book*.

Bradshaw, P. and Pankhurst, R. C. (1964) 'The design of low speed wind tunnels', *Progress in Aerospace Sciences*, 1–69(5), p. 46.

Broumand, M. and Birouk, M. (2016) 'Liquid jet in a subsonic gaseous crossflow: Recent progress and remaining challenges', *Progress in Energy and Combustion Science*, 57, pp. 1–29. doi: 10.1016/j.pecs.2016.08.003.

Clanet, C. (2003) 'Les nappes d ' eau de Felix Savart .'

Crua, C. (2014) 'Direct imaging of primary atomisation in the near-nozzle region of diesel sprays Direct imaging of primary atomisation in the near-nozzle region of diesel sprays', (September). doi: 10.13140/2.1.1817.0244.

Dantec (2002) 'How to measure turbulence with hot-wire anemometers - a practical guide'.

Dombrowski, N., Hasson, D. and Ward, D. E. (1960) 'Some aspects of liquid flow through fan spray nozzles', *Chemical Engineering Science*, 12(1), pp. 35–50. doi: 10.1016/0009-2509(60)90004-X.

Dumouchel, C. (2008) 'On the experimental investigation on primary atomization of liquid streams', *Experiments in Fluids*, 45(3), pp. 371–422. doi: 10.1007/s00348-008-0526-0.

Emberson, D. R. *et al.* (2016) 'Optical characterization of Diesel and water emulsion fuel injection sprays using shadowgraphy', *Fuel*, 172(x), pp. 253–262. doi: 10.1016/j.fuel.2016.01.015.

Gelalles, A. . (1931) 'EFFECT OF ORIFICE LENGTE-DIAMETER RATIO ON FUEL SPRAYS FOR COMPRESSION-IGNITION ENGINES', (402), pp. 79–90.

Hancock, P. E. and Bradshaw, P. (1980) 'THE EFFECT OF FREE-STREAM TURBULENCE ON TURBULENT BOUNDARY LAYERS'. doi: 10.1115/1.3240989.

Hinze, J. O. (1955) 'Fundamentals of the hydrodynamic mechanism of splitting in dispersion processes', *AIChE Journal*, 1(3), pp. 289–295. doi: 10.1002/aic.690010303.

Hiroyasu, H., Arai, M. and Shimizu, M. (1991) 'Break-up length of a liquid jet and internal flow in a

nozzle', *NIST Special Publication*, (813), pp. 275–282.

L'Annunziata, M. F. (2003) *Handbook of Radioactivity Analysis*.

Lefebvre, A. H. and Ballal, D. R. (1988) *Gas Turbine Combustion Alternative Fuels and Emissions*, *The Tohoku Journal of Experimental Medicine*. CRC Press.

Lefebvre, A. and Mcdonell, V. (2017) *Atomization and Sprays, Second Edition.* 2nd edn, *Boca Raton: CRC Press*. 2nd edn. CRC Press. doi: 10.1016/0009-2509(90)87140-N.

Martinon, J. (1983) 'Stability of capillary cylindrical jeMartinon, By Jean Dynamique, Laboratoire De Racteurs, Centrets in external flow', 34(September).

Mccarthy, M. J. and Molloy, N. A. (1974) 'Review of Stability of Liquid Jets and the Influence of Nozzle Design', 7.

Mehta, R. D. and Bradshaw, P. (1979) 'DESIGN RULES FOR SMALL LOW SPEED WIND TUNNELS.', *Aeronautical Journal*, 83(827), pp. 443–449.

Munson, B. R. *et al.* (2009) *Fundamentals of Fluid Mechanics 6th - Munson, young, Okiishi, Huebsch.pdf*. Wiley.

No, S. Y. (2015) 'A review on empirical correlations for jet/spray trajectory of liquid jet in uniform cross flow', *International Journal of Spray and Combustion Dynamics*, 7(4), pp. 283–314. doi: 10.1260/1756-8277.7.4.283.

Ohnesorge, W. V. (1936) 'Formation of Drops by Nozzles and the Breakup of Liquid Jets', *Applied Mathematics and Mechanics*, 16, pp. 355–358. doi: 10.26153/tsw/3371.2.

Pei-Kuan Wu, Kevin A. Kirkendall, R. P. F. and A. S. N. (1997) 'Breakup Processes of Liquid Jets in Subsonic Crossflows', pp. 64–73. doi: https://doi.org/10.2514/2.5151.

R.D. Mehta (1977) 'The Aerodynamic Design of Blower Tunnels With Wide-angle Diffusers', *Prog. Aerospace Sci*, 18, pp. 59–120.

Rajendran, S. (2012) 'EXPERIMENTAL INVESTIGATION OF JET BREAKUP AT LOW WEBER NUMBER'.

Rasenat, S., G. Hartung, B. L. W. and Rehberg, I. (1989) 'The shadowgraph method in convection experiments', *Symposium A Quarterly Journal In Modern Foreign Literatures*, 262, pp. 412–420.

Sallam, K. A., Aalburg, C. and Faeth, G. M. (2004) 'Breakup of round nonturbulent liquid jets in gaseous crossflow', *AIAA Journal*, 42(12), pp. 2529–2540. doi: 10.2514/1.3749.

Santos, A. M. *et al.* (2016) 'Effects of screens set characteristics on the flow field in a wind tunnel', *Journal of Physics: Conference Series*, 733(1). doi: 10.1088/1742-6596/733/1/012001.

Schweitzer, P. H. (1937) 'Mechanism of disintegration of liquid jets', *Journal of Applied Physics*, 8(8), pp. 513–521. doi: 10.1063/1.1710333.

Selig, M. S. and McGranahan, B. D. (2004) *Wind Tunnel Aerodynamic Tests of Six Airfoils for Use on Small Wind Turbines*, *Journal of Solar Energy Engineering*. doi: 10.1115/1.1793208.

Settles, G. S. (2001) *Schlieren und shadowgraph techniques: visualizing phenomena in transparent media - Experimental Fluid Mechanics*.

Settles, G. S. and Hargather, M. J. (2017) 'A review of recent developments in schlieren and shadowgraph techniques', *Measurement Science and Technology*, 28(4). doi: 10.1088/1361-6501/aa5748.

Sharma, N., Bachalo, W. D. and Agarwal, A. K. (2020) 'Spray droplet size distribution and droplet velocity measurements in a firing optical engine', *Physics of Fluids*, 32(2). doi: 10.1063/1.5126498.

Shen, J., Li, X. and Columbia, B. (1996) 'Instability of an annular viscous liquid jet', 183, pp. 167–183.

Stevenin, C. *et al.* (2012) 'Shadowgraphy investigations of high speed water jet atomization into still air HAL Id : hal-00782164', (September).

Strutt, J. W. (1878) 'On the instability of jets.', *Proc. London Math. Soc.*, pp. 4–13.

Sun, Y., Guan, Z. and Hooman, K. (2019) 'Cavitation in Diesel Fuel Injector Nozzles and its Influence on Atomization and Spray', *Chemical Engineering and Technology*, 42(1), pp. 6–29. doi: 10.1002/ceat.201800323.

Tavoularis, S. (2005) *Measurement in fluid mechanics*. 1st edn. Cambridge University Press; 1 edition (August 24, 2009).

Tropea, C., Yarin, A. L. and Foss, J. F. (2007) *Spinger Handbook of experimental Fluid Mechanics*.

Tyler, E. (2009) 'Instability of liquid jets', 5982. doi: 10.1080/14786443309462302.

Watanawanyoo, P. and Hirahara, H. (2011) 'Experimental Investigations on Spray Characteristics in Twin-Fluid Atomizer', 24, pp. 866–872. doi: 10.1016/j.proeng.2011.12.416.

Welsh, A. (2013) 'Low Turbulence Wind Tunnel Design and Wind Turbine Wake Characterization', *Modelling, Measurement and Control B*, (May), p. 56.

https://spray-imaging.com/spray-description.html